Deliverable 4.6: Final report describing improvement and implementation of scale transition methods to model coupled processes

Work Package DONUT

The project leading to this application has received funding from the European Union's Horizon 2020 research and innovation programme under grant agreement No 847593.

Document information

Project Acronym	**EURAD**
Project Title	**European Joint Programme on Radioactive Waste Management**
Project Type	**European Joint Programme (EJP)**
EC grant agreement No.	**847593**
Project starting / end date	**1st June 2019 – 30 May 2024**
Work Package No.	**4**
Work Package Title	**Development and Improvement Of Numerical methods and Tools for modelling coupled processes**
Work Package Acronym	**DONUT**
Deliverable No.	**D4.6**
Deliverable Title	**Final report describing improvement and implementation of scale transition methods to model coupled processes**
Lead Beneficiary	**ANDRA**
Contractual Delivery Date	**M52**
Actual Delivery Date	**17/04/2024**
Type	**Report**
Dissemination level	**Public**
Editors	**Olaf Kolditz (UFZ), Nikos Prasianakis (PSI) and Francis Claret (BRGM) compiled a multi authors contribution. For each contribution compiled in this document an author list is associated**

To be cited as:

Kolditz, O. Prasianakis, N, Claret, F. (2024). Final report describing improvement and implementation of scale transition methods to model coupled processes. Final version as of xx.xx.xxxx of deliverable D4.6 of the HORIZON 2020 project EURAD. EC Grant agreement no: 847593.

Disclaimer

Acknowledgement

This document is a deliverable of the European Joint Programme on Radioactive Waste Management (EURAD). EURAD has received funding from the European Union's Horizon 2020 research and innovation programme under grant agreement No 847593.

Status of deliverable		
	By	Date
Delivered (Lead Beneficiary)	Andra	18.04.024
Verified (WP Leader)	F. Claret	15.032024
Reviewed (Reviewers)	D. Jacques	22.03.2024
Approved (PMO)	B. Grambow	17.04.204
Submitted to EC (Coordinator)	Andra	19.04.2024

Executive Summary

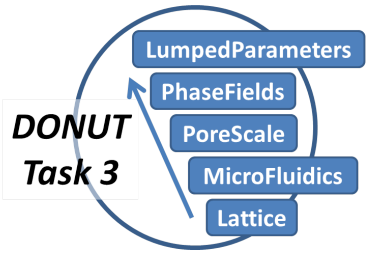

. Deliverable 4.6: Final report describing improvement and implementation of scale transition methods to model coupled processes

Executive Summary

Task 3 of DONUT focuses on upscaling methods for Thermo-Hydrological-Mechanical-Chemical (THMC) processes in both the near and far fields of nuclear repositories. The emphasis is on the multi-barrier concept of safe waste isolation, which is based on combined geotechnical and geological barrier elements. Upscaling fully coupled THMC models remains a significant challenge. DONUT provides methods and results for flow and transport, reactive transport processes (RTP) as well as thermo-hydro-mechanical (THM) processes. The diagram in the top right corner outlines the main methods that were developed and used during scale transitions. Coupled process modelling still requires a trade-off between scale and complexity: at smaller scales, greater complexity can be considered, whereas at larger scales, reduced complexity is often required. These methods will be summarised below and described in more detail in the report. The report is structured according to scale, starting from small (pores and interfaces), moving to meso (REV), and ending with larger scales (near and far fields). It includes citations of main publications that are recommended for further reading.

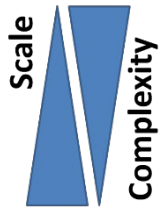

The PSI/FZJ team (Paul-Scherrer-Institute and Research Centre Jülich) is working on **chemically processes at perturbed interfaces in the near field** (Section 1).

Reactive transport modeling is crucial for assessing the chemical/physical evolution of nuclear geological repositories, with great relevance to the safety and performance. However the accurate representation of chemical processes and the time evolution of the transport parameters is still challenging. Existing empirical relationships like Archie's law are insufficient to universally describe the evolution of diffusivity in the presence of strong geochemical gradients, since in such cases the microstructural evolution leads to non-linear change of diffusivity depending not only on the initial porosity but also on the chemial composition and saturation levels of the reactants. This signifies the need for process-based models integrating microstructural details. Pore-scale modeling studies have introduced an extended law addressing Archie's limitations by incorporating the concept of critical porosity and diffusivity. Investigations relevant to the applicability of such a concept when mineral reactions take place were conducted at FJZ. Experimental micromodels (Poonoosamy at al. 2020) and follow-up pore-scale modeling was employed, revealing insights into mineral impacts on pore architecture and deriving constitutive equations with upscaled transport parameters. At the same time, the pore-size dependency of mineral nucleation by using a microfluidic approach was investigated in (Poonoosamy et al. 2023, Lönartz et al. 2023)

After closure, the foreseen waste repositories are expected to remain at partial saturation for a long period. Partial saturated conditions affect the solute transport in a non-linear way. Pore level models have been developed by FZJ/PSI to simulate such phenomena in microporous (e.g. sandy soils) and nano porous media (e.g. clay). Effective diffusion coefficients by considering also the electrostatic interactions have been calculated and compared with experimental observations (Yang et al. 2024).

Another topic addressed by PSI was the development of methodologies for efficient communication between different codes and different scales using machine learning techniques using neural networks. A pore-level lattice Boltzmann solver was interfaced with a random walk based macroscopic solver for the study of dissolution (Prasianakis et al. 2020). On the same front FZJ and OGS team created a prototype multiscale coupling by interfacing a Lattice Boltzmann code with OpenGeoSys finite element code. The hybrid approach was also validated using analytical solutions.

ISTO/BRGM team (Institut des Sciences de la Terre Orléans et le Bureau de recherches géologiques et minières and Lawrence Berkeley Laboratory) developped porousMedia4Foam, **a multi-scale open-source platform for hydro-geochemical simulations** (Section 2). porousMedia4Foam is an open-source package with included benefits to account for reactive transport processes occurring at various scales—pore, hybrid, and Darcy scales. While the flow and transport part is solved using OpenFOAM® one of the most popular open-source numerical toolbox, chemistry is solved using one of the state of the art geochemical solver as to said Phreeqc-RM. The coupling across the scale has been benchmarked considering complex and well-established cases available in the reactive transport modeling community. A unique formulation can handle pore-scale, hybrid-scale and continuum-scale simulations for hydro-geochemical processes. This hybrid-scale approach relies on the Darcy-Brinkman-Stokes (DBS) equation that allows for the modelling of flow and transport in regions free of solid and porous regions in a single framework. In a logic of cascade of scales nested within each other, fractured porous media can be modelled by: i) pore-scale approaches, ii) discrete fracture networks, iii) dual porosity models. The hybrid-scale approach that was proposed here is intermediate between a full pore-scale description in which the fracture and the pores in the matrix are fully resolved and a discrete fracture network in which the matrix is modelled as a porous medium and the fractures as discrete elements that exchange matter with the matrix. The hybrid-scale approach is therefore crucial to characterize and improve the effective parameters (e.g. transfer functions between the porous matrix and the fracture) used in discrete fracture networks and larger-scale models

The OpenGeoSys team is focusing on **fracture mechanics and scale transition schemes for coupled THM processes** (Section 3). The OGS team consists of the Helmholtz Center for Environmental Research (UFZ) Technische Universität Bergakademie Freiberg (TUBAF), Montanuniversität Leoben (MUL), and Dresden University of Technology (TUDD).

The OGS team is concentrating on the Variational Phase Field (VPF) method for multiscale simulation of fracture nucleation and propagation processes. The VPF method offers two advantages: it can be seamlessly integrated into the finite element method for multiphysics simulations, namely thermo-hydro-mechanical-chemical (THMC) processes, and fracture propagation processes are not affected by meshing effects. However, mesh density is crucial for accuracy. We describe the calculation of fracture aperture using two evaluated methods: line integral and level-set approaches. Fracture aperture is a crucial factor in determining fracture permeability, which affects flow and transport processes in both near and far fields. Accurate determination of fractures and crack sizes is crucial for understanding multi-scale processes in subsurface systems. The VPF method has been successfully applied for both laboratory and field scale applications (Kolditz et al. 2023).

Concerning experimental analysis on laboratory scales, the VPF methods has successfully applied for the analyses of various experiments in Task G of DECOVALEX 2023. Various experiments with the GREAT cell apparatus at University of Edinburgh using brittle samples of crystalline rocks have provided an excellent data basis for model verification (McDermott et al. 2). Moreover, a comprehensive set of fracture mechanics benchmarks have been developed andintroduced into the model comparison of DECOVALEX (Mollaali et al. 2023).

The scaling method was successfully applied to experimental data from the underground research laboratory Mont Terri (Switzerland) (CD-A experiment) (Cajuhi et al. 2023). Methods for the quantification of uncertainties for coupled THM processes were developed and also successfully applied to an experiment in Mont Terri (FE experiment). Methods of scaling numerical methods for fracture mechanics processes from the laboratory to the field scale were developed (Buchwald et al. 2024).

OGS team's work is founded on the open-source OpenGeoSys platform and contributes to its further development using the VPF method (see software development below)

Technical University of Liberec (TUL) team is dealing with **integral postprocessing of a 3D flow and transport model into a lumped-parameter model as an upscaling method** (Section 4)

The TUL team is developing Lumped Parameter Models (LPM) for performance assessment (PA) purposes. LPM is computationally efficient and allows for upscaling across multiple scales. The models are used for integral post-processing of travel time distributions, including decay and sorption processes, based on a realistic numerical flow model that represents specific hydrogeological site conditions. Thanks to its computational efficiency, LPM allows for stochastic Monte-Carlo simulations (momentum analyses over cross-sections), making it a beneficial PA tool that covers various scenarios. Despite its advantages, LPM suffers from a lack of physical meaning of parameters, particularly in their quantification, which can be partly compensated for by statistical analysis. TUL is combining the in-house code Flow123d with the Goldsim software for pipeline modelling of reactive transport processes. For evaluation and selection of a suitable location of a potential repository, TUL have developed a criteria concept based on specific parameters (depending on priorities of the evaluation process). The LPM concept is being applied for PA of a candidate site in Czechia.

Software development

The following open source software platforms have been further developed with EURAD DONUT:

- Flow123d (TUL): https://flow123d.github.io
- GeoML (PSI): https://geoml.eu and https://geoml.ai/
- OpenGeoSys (UFZ): https://www.opengeosys.org/ and https://gitlab.opengeosys.org/
- porousMedia4Foam (BRGM): https://github.com/csoulain/porousMedia4Foam

Lönartz, M. I., Yang, Y., Deissmann, G., Bosbach, D., & Poonoosamy, J. (2023). Capturing the dynamic processes of porosity clogging. *Water Resources Research*, *59*(11), e2023WR034722.

Poonoosamy, J., Obaied, A., Deissmann, G., Prasianakis, N. I., Kindelmann, M., Wollenhaupt, B., ... & Curti, E. (2023). Microfluidic investigation of pore-size dependency of Barite nucleation. *Communications Chemistry*, *6*(1), 250.

Yang, Y., Churakov, S. V., Patel, R. A., Prasianakis, N., Deissmann, G., Bosbach, D., & Poonoosamy, J. (2024). Pore-Scale Modeling of Water and Ion Diffusion in Partially Saturated Clays. *Water Resources Research*, *60*(1), e2023WR035595.

Table of Content

Table of figures

List of Tables

Part A: Upscaling diffusivity in chemically evolving and partially saturated porous media

[1]Poonoosamy J., [1]Yang, Y., [1]Lönartz M., [2]Renchao L., [3]Prasianakis N.

[1]Institute of Energy and Climate Research, Nuclear Waste Management (IEK-6), Forschungszentrum Juelich, Germany

[2]Helmholtz Centre for Environmental Research - UFZ, 04318 Leipzig, Germany

[3]Laboratory for Waste Management (LES), Paul Scherrer Institute, Switzerland

The project leading to this application has received funding from the European Union's Horizon 2020 research and innovation programme under grant agreement No 84759

Abstract

Understanding the mechanisms of radionuclide transport at perturbed interfaces in the near field is critical for the evaluation of the long-term safety of geological repositories for radioactive wastes. Upscaling, i.e., accounting for pore-scale heterogeneities into larger-scale analyses, remains one of the biggest challenges of reactive transport modelling. With the main aim of developing upscaling methodologies, we use pore-scale modelling to investigate solute transport in (i) chemically evolving porous media due to mineral dissolution and precipitation and (ii) partially saturated porous media evaluating the impact of water films. Our investigations on chemically evolving porous media propose an alternative constitutive equation to classically applied Archie's law to quantify changes in transport properties of porous media as a result of mineral precipitation processes. Our achievements in investigating diffusion processes in partially saturated porous media involve the development of an advanced pore-scale model to capture the importance of water films on mineral surfaces and their effects on diffusive transport. Our model benchmarked against experimental datasets shows a better performance than the existing pore-scale models in the literature. In addition, we quantitatively analysed the influence of the electric double layer (EDL) on ion diffusion in variably saturated nano porous (compacted clay) media. It was found that the influence of the EDL on ion diffusion in pore-scale models depends on the ratio normalized volume charged density of the charge carried by the surface of the medium to the ion concentration within the pore electrolyte. The EDL in compacted clays has a stronger effect on ion transport under unsaturated conditions than under water-saturated conditions. We also developed a hybrid model bridging the pore-scale and the continuum scale.

Significance Statement

The construction of underground galleries, geotechnical barriers, and waste package emplacement induces perturbations at barrier interfaces due to chemical, thermal, and pressure gradients. These cause mineral dissolution and precipitation, impacting transport and mechanical properties. Reactive transport modelling (RTM) is a valuable tool to study these complex hydrogeochemical phenomena across various scales, from interfaces to the entire repository system. However, the application of RTM codes to real systems is impeded by the often-simplified description of coupled processes. To understand solute and radionuclide transport properties and enhance predictive capabilities, pore scale numerical investigations were conducted. This research improved conceptual approaches to describe diffusion of solute in chemically evolving and partially saturated porous media considering the effect of water film on mineral surfaces and the electric double layer.

Table of Content

List of figures

1. Chemical processes at perturbed interfaces in the near field

Deep geological repositories with a multi-barrier concept are foreseen by various countries for the disposal of high-level radioactive waste. The construction of underground galleries and geotechnical barriers in the host rock formation and the emplacement of nuclear waste packages will create perturbations induced by chemical, thermal and pressure gradients at the interfaces of the different barriers, leading to mineral dissolution and precipitation to achieve re-equilibration. Such coupled hydrogeochemical processes generate non-linear responses in transport and mechanical properties of barrier materials and host rocks, which must be considered for a more rigorous assessment of repository system evolution.

1.1 Upscaling diffusivity of evolving porous media

Reactive transport modeling is a valuable tool for evaluating the subsurface evolution of nuclear geological repositories, particularly in assessing hydrogeochemical processes at the disturbed interface within the near field. However, a major challenge lies in accurately representing the interplay between chemical processes and changes in transport parameters, such as porosity and diffusivity. In modeling studies, empirical relationships like Archie's law are commonly used but have already proven to be inadequate. There is a need to develop process-based relationships that integrate microstructural information (upscaling) into continuum-scale reactive transport models.

Pore-scale modeling has been employed to determine transport parameters and constitutive equations that describe the transport properties of evolving porous media. For instance, (Deng *et al.*, 2021) conducted numerical experiments to investigate the influence of celestine nucleation mechanisms, specifically surface precipitation (heterogeneous nucleation) and precipitation within pores (homogeneous nucleation), on the transport properties of an inert porous medium. Their study demonstrated that the classical Archie's law was inadequate for the system under examination, prompting the proposal of an extended law that introduces the concepts of critical porosity and critical effective diffusivity. Nevertheless, questions persisted regarding the physicochemical processes encompassed by the extended equation and whether it could be applied in cases involving coupled mineral dissolution and precipitation reactions. To answer these questions, we developed experimental micromodels and combined pore-scale modeling to investigate the impact of mineral dissolution and precipitation on the pore architecture. This enabled us to derive constitutive equations incorporating upscaled transport parameters.

1.1.1 Dynamic nature of porosity clogging and validation of extended equation

In this study, we provide new insights into mineral precipitation induced porosity clogging and its effect on the porosity-diffusivity relationship, combining innovative microfluidic experiments with pore-scale modelling. The experimental setup follows (Poonoosamy *et al.*, 2020). The design of the microfluidic reactor allowed a real-time monitoring of precipitation-dissolution reactions under purely diffusive transport conditions in a quasi-two-dimensional porous medium. The chemical system as well as the geometry of the microfluidic reactor were chosen in consideration of the work of (Chagneau *et al.*, 2015) and (Deng *et al.*, 2021). The microfluidic device consisted of a 2D pore network (*Figure 1*a) linked to two supply channels which enabled the diffusive mixing of Sr^{2+}aq and SO_4^{2-}aq ions, triggering the precipitation of celestine (*Figure 1*b). The clogging inhibited further mixing of reactants, leading to dissolution and recrystallization of celestine in a cyclic manner. Tracer experiments (not shown here) suggested the development of micro or nano porosity of the precipitates. These tracer experiments also enabled the determination of the critical effective diffussivity between 1×10^{-13} m^2s^{-1} and 4×10^{-13} m^2s^{-1}.

The effective diffusivity of the evolving porous medium was determined using pore scale modelling. The lattice Boltzmann method (LBM) which relies on the application of the Boltzmann transport equation to simulate fluid flow on discrete grids was used for this purpose. Numerical inert tracer experiments were conducted on the experimental 2D evolving porous medium collected by optical microscopy. For the

clogged state, solute diffusion through the precipitates is considered in our numerical investigations. The effective diffusivity with respect to porosity is given in *Figure 1*d.

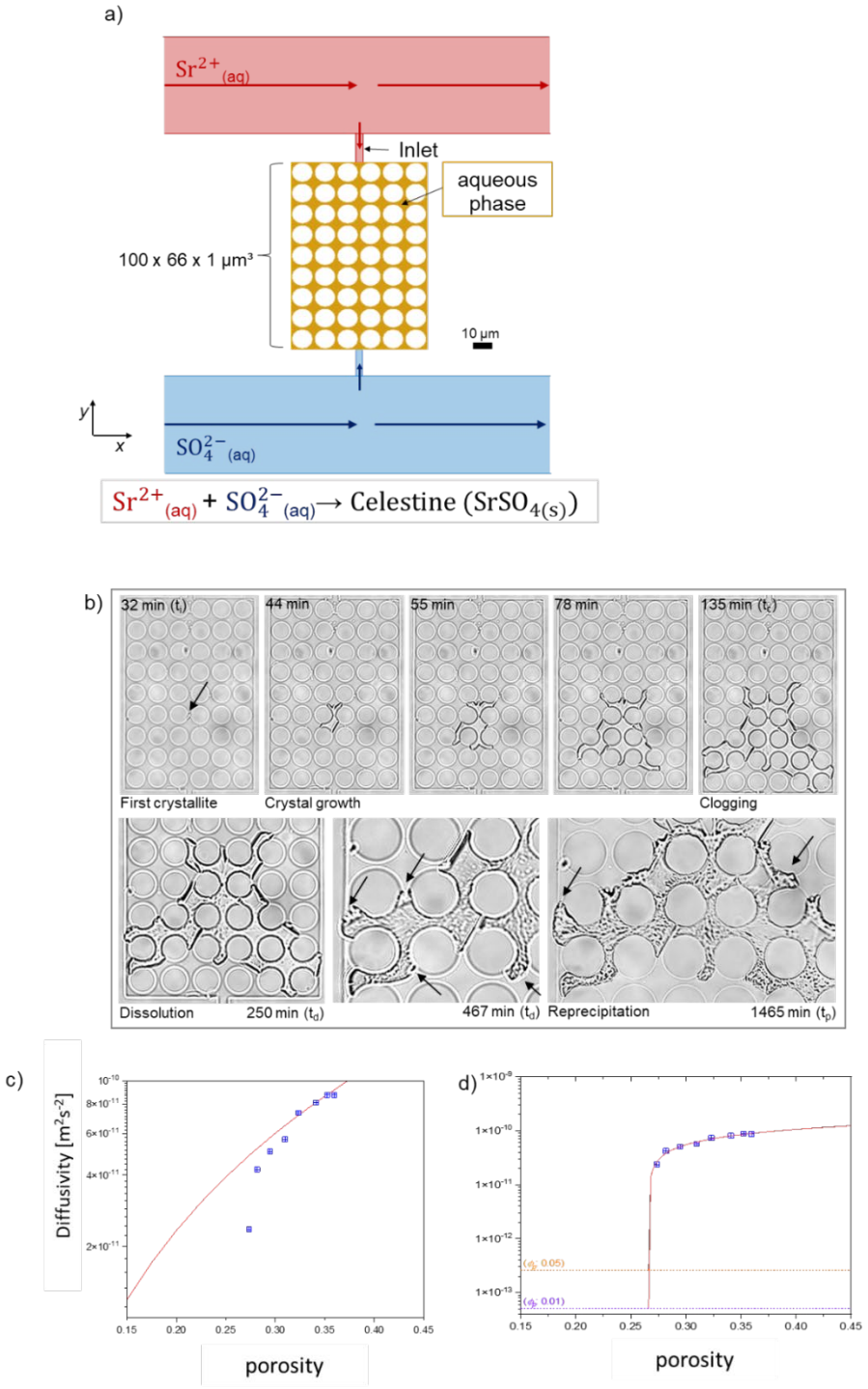

*Figure 1 – **a)** Micromodel design with reacting solution injected **(b)** time-lapse bright field images of mineral precipitation, clogging, dissolution and reprecipitation as post clogging reactions marked by black arrows to emphasize the non-final state of clogging. **(c)** The red curves represent Archie's law and **(d)** the extended law considering a minimum (5.1 x 10^{-14} m^2 s^{-1}, purple curve) and maximum (2.6 x 10^{-13} m^2 s^{-1}, orange curve) D_{ceff}.*

The extended equation as alternative to Archie's law, describing the effective diffusivity (D_e) as function of porosity (Φ) therefore write as follows:

$$D_e = D_{effc} + aD_0(\Phi - \Phi_{critical})^m \qquad \text{Equation 1}$$

whereby *a* and *m* represent empirical coefficients set to 0.24 and 2.4 to match experimental data. D_0 is set to 1 × 10^{-9} m^2 s^{-1} as molecular diffusion coefficient. The minimum porosity reached during clogging is defined as the critical porosity, $\phi_{critical}$. D_{ceff} represents the critical effective diffusivity of the clogged porous medium. The parameterized equation based on our experiments were in agreement with the pore scale modelling work conducted by (Deng *et al.*, 2021). The presented investigation showed that clogging at interfaces can be a dynamic process, precipitation, dissolution, recrystallization. This dynamic nature is coupled to the transport processes i.e., how fast or slow solutes are exchanged in the porous media. The nature of the mineral precipitating will also play a role e.g., for minerals like barite with very low solubility where this cyclic event of precipitation/dissolution might be significantly slower.

1.1.2 Coupled mineral dissolution and precipitation processes

Coupled mineral dissolution and precipitation processes are ubiquitous in nature and also at perturbed interfaces in deep geological repositories for nuclear waste e.g., dissolution of portlandite and precipitation of carbonates. In this study, we focus specifically on a reactive medium undergoing coupled mineral dissolution and precipitation evaluating wether the extended equation proposed earlier can be applied for this case scenario. The aim of this work is therefore to combine experiment and pore scale modelling to monitor transport coupled mineralogical reactions.

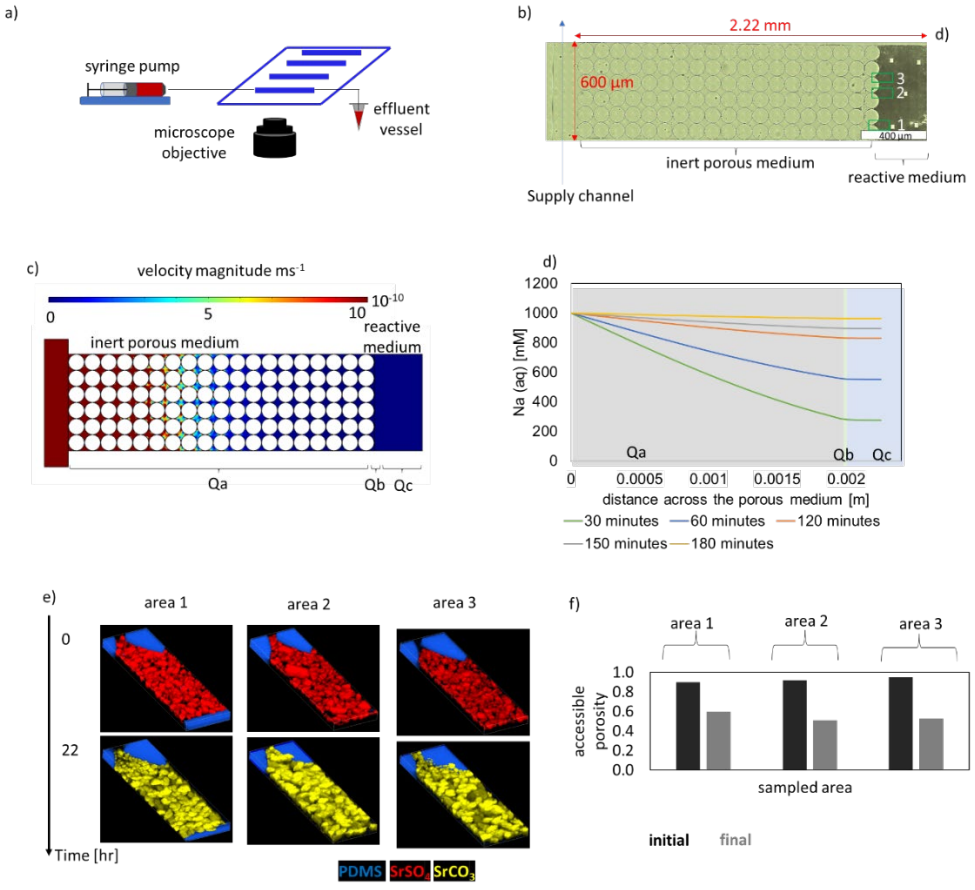

*Figure 2 – **a)** Experimental setup with **(b)** a zoom on the inert porous medium and reactive porous medium celestine ($SrSO_4$) crystals **(c)** modelling of velocity field in the microfluidic reactor using COMSOL Multiphysics indicating diffusive transport across the porous medium, **(d)** simulated concentration of total aqueous sodium across the reactor using OpenGeosys-6#Phreeqc as function of time, **(e)** initial and final Raman tomographs of the sampled areas, and **(f)** the associated porosity changes.*

A solution of sodium hydrogen carbonate ($NaHCO_3$) was injected in the supply channel (*Figure* 2a-b), i.e., a laminar flow in the supply channel and solutes diffusion in the porous medium (*Figure* 2c) leading to the following chemical reaction in the reactive porous medium:

$$CO_3{}^{2-}{}_{aq} + SrSO_{4(s)} \rightarrow SO_4{}^{2-}{}_{aq} + SrCO_{3(s)} \qquad \text{Equation 2}$$

The injection of the $NaHCO_3$ solution induces the dissolution of celestine in the reactive medium and the precipitation of strontianite ($SrCO_3$) (Equation 2), because of its much lower solubility product. This reaction is accompanied by a "net porosity" increase due to the smaller molar volume of strontianite (3.90×10^{-5} m^3 mol^{-1}) compared to that of celestine (4.63×10^{-5} m^3 mol^{-1}). The accessible porosities of the porous media before and after the reaction were quantified from 3D Raman tomographic images. Surprisingly, the volume occupied by newly formed precipitates exceeded that of pristine celestine crystals, leading to a decrease in the average accessible porosity of the reacted porous medium to approximately 0.54. In contrast, when considering the difference in molar volume between celestine and strontianite, the final net porosity was expected to increase from around 0.92 to about 0.93. Therefore, the replacement of celestine by strontianite resulted in an increase in net porosity but a decrease in accessible porosity for transport within the porous medium.

Tracer concentration in the reactive porous medium before and after reaction simulated using the lattice Boltzmann method is shown in *Figure 3*. For the evaluation of the effective diffusivity (De) of the reactive porous medium that had undergone mineral dissolution and precipitation, two numerical case studies were considered. Case 1 is a simplified case with diffusion of solutes only in the pore space. case 2 considers diffusion of solutes both in the pore space and through the newly formed strontianite precipitates. The diffusion coefficient of solutes in the newly formed precipitate is defined as D_s. The tracer concentration map across the domain before and after coupled dissolution and precipitation indicates a new pore architecture, whereby the final effective diffusivity is lower by a factor of ~0.5 (averaged for the 3 areas labelled area 1 -2 in Figure 2) as the initial effective diffusivity. When diffusion is allowed through the newly formed strontianite (*Figure 3*c), this factor increases slightly to 0.52 (averaged for the 3 areas). In addition, sensitivity analyses, with D_s/D_0 equal to 0.04 and 0.1 were conducted. All simulated results indicated a decrease in the effective diffusivity of the reacted porous medium with it being less pronounced as D_s/D_0 increases.

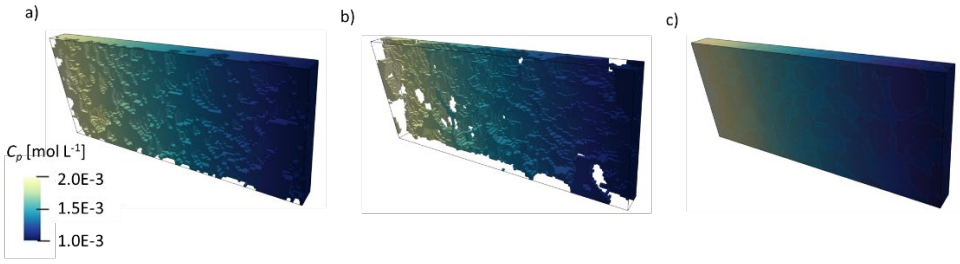

*Figure 3 – 3D view of the simulated tracer concentrations across the sampled porous media in (**a**) initial state (unreacted porous medium), (**b**) case 1 final state assuming no diffusion through the precipitates (D_s = 0), and (**c**) case 2 final state with diffusion through the precipitates with D_s/D_0 = 0.01.*

The relation between the simulated effective diffusivities and the calculated porosities from the 3D images is shown in *Figure 4*. For the unreacted porous media of porosities between 0.5 to 0.92, the associated diffusivities are indicated on the graph by the red data points. Our analysis shows that Archie's law parameterized for compacted sandy porous material reproduces well the simulated effective diffusion coefficient of the unreacted celestine medium at different porosities. In addition, we report the accessible porosities of the chemically altered media and the associated simulated effective diffusivities (grey data points in *Figure 4*). There is insignificant difference in calculated value for the effective diffusivities of the reacted porous media between case 1 and 2 (c.f data points reported in *Figure 4*).

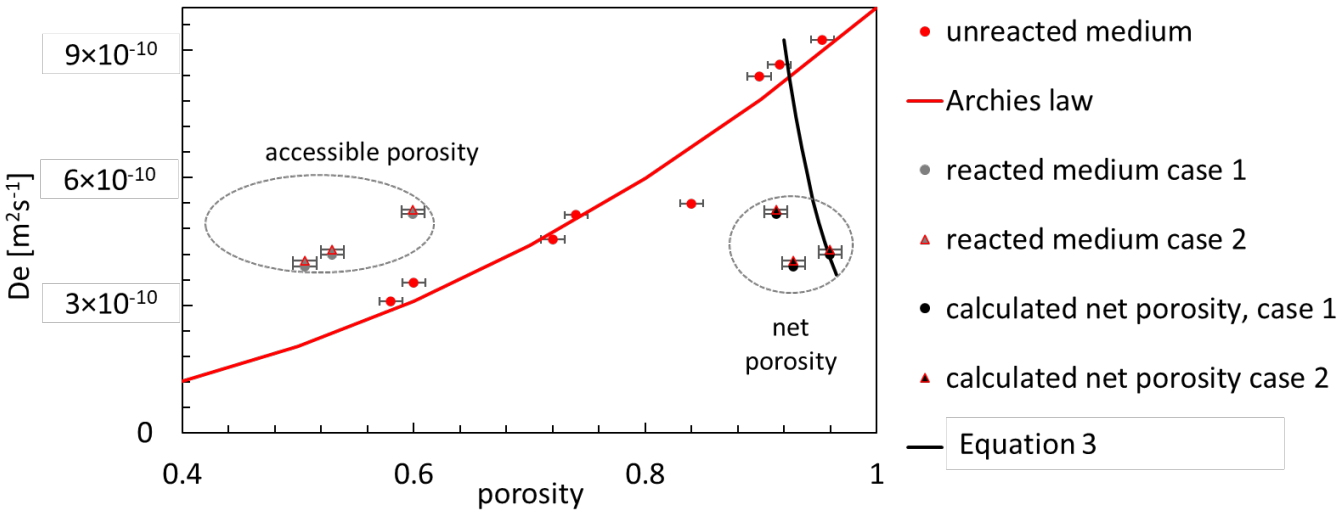

Figure 4 – Graph relating porosities of sampled areas with effective diffusivities.

In a continuum scale reactive transport model, the changes in diffusivities due to mineralogical reactions can only be accounted for the net porosity changes calculated from changes in molar volumes. Consequently, the net porosities (black data points in *Figure 4*) have to be considered instead of the accessible porosities in continuum scale reactive transport simulations. Here, Archie's law fails to reproduce the experimental observations. Therefore, we tested an alternative approach for describing the porosity-diffusivity relationship. As mentioned earlier, (Deng et al., 2021) conducted a series of numerical experiments on diffusion induced precipitation of celestine and proposed the porosity-diffusivity relationship given in Equation 1. In our experiment, where no porosity clogging is observed, we can assume that D_{effc} = 0, and therefore the ratio of the initial ($D_{e,initial}$) and final ($D_{e,t}$) effective diffusivity can be simplified to:

$$\frac{D_{e,t}}{D_{e,initial}} = \left(\frac{\Phi_t - \Phi_{critical}}{\Phi_0 - \Phi_{critical}}\right)^n \qquad \text{Equation 3}$$

where Φ_0 and Φ_t are the initial and final porosity, respectively. $\Phi_{critical}$ and n are the critical porosity and the exponent, and fitted to 0.65 and -6, respectively, resulting the black line in Figure 4.

Reactive transport modelling at the continuum scale was performed to evaluate the impact of coupled celestine dissolution and strontianite precipitation and consequences on the diffusivity evolution, using (i) the classical Archie's law and (ii) using the extended diffusivity relationship (Equation 3). The simulated mineralogical and associated porosity changes are the same for both studied cases and are presented in *Figure 5*a and b, respectively. The simulated mineralogical reactions (Chagneau, et al., 2015) with time are in good agreement with our experimental observations. *Figure 5*c and d show the simulated diffusive properties of the porous domain based on the two porosity-diffusivity models with a simulated diffusivity increase with Archie's law and a diffusivity decrease with the extended diffusivity relationship Equation 3. In the current study, the use of Archie's law and the extended law had little impact of the simulated net mineralogical reactions within the considered domain and time scale. However, if the domain was extended to cm or m scale, differences between the mineralogical profiles and consequently porosity across the domain will develop. The presented study highlights the complexity of predicting coupled dissolution and precipitation processes and associated changes in transport properties of porous media.

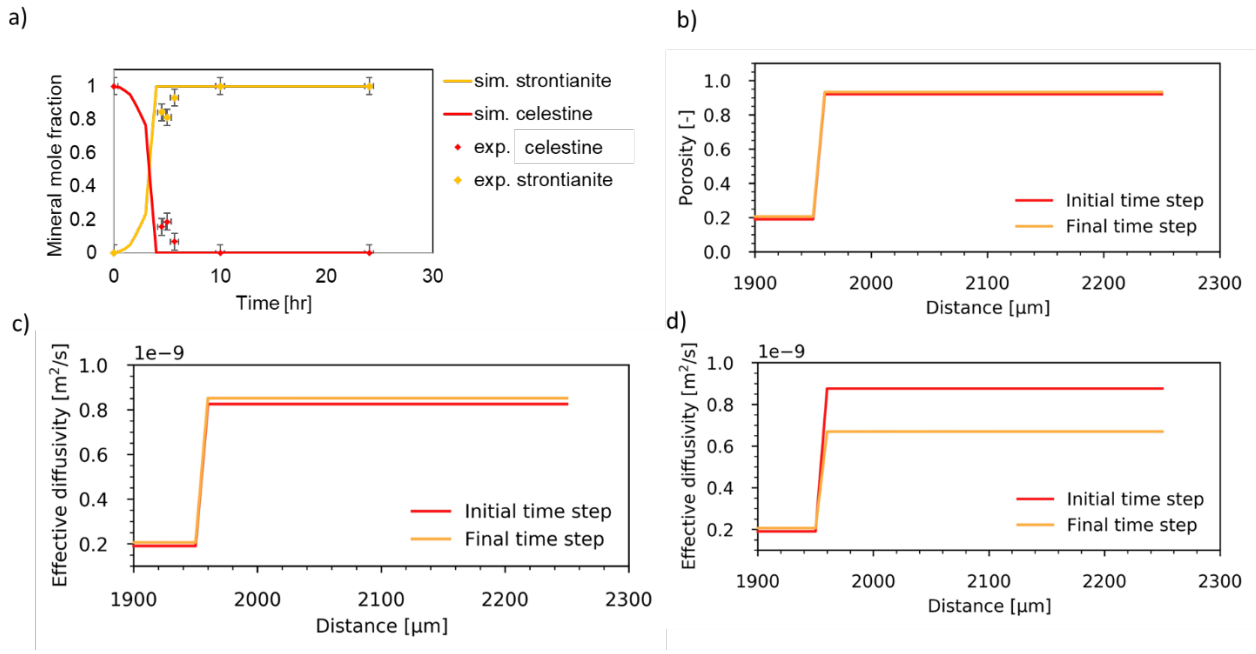

*Figure 5 (**a**) Comparison between experimental and simulated temporal mineral reactions, (**b**) simulated initial and final net porosity across the reactive medium (Q_b and Q_c region), (**c**) simulated diffusivity following Archie's law, and (**d**) following the extended law.*

2. Partial saturated conditions

Unsaturated conditions within the surrounding clay-based materials for long periods of time could be caused by the high temperature from decay heat and the hydrogen gas production from canister corrosion (Savoye *et al.*, 2010). Significant gas production and heat generation might cause fractures in clay-based materials and eventually affect the long-term integrity of the multibarrier system (Tamayo-Mas *et al.*, 2021). Therefore, understanding the mechanisms of solute transport through these clay-based materials under partially saturated conditions is critical for the evaluation of the long-term safety of geological repositories for radioactive wastes.

2.1 Pore-scale modelling of solute transport in partially and fully saturated porous media

The transport of solutes in partially and fully saturated porous media is an important fundamental process in many natural and technical settings such as contaminant transport in groundwater (Li *et al.*, 2023), radionuclide migration in the context of nuclear waste disposal (Miller and Wang, 2012), and concrete degradation (Friedmann *et al.*, 2008). Over the past few decades, a vast number of experiments (Savoye *et al.*, 2012) and simulations (Gimmi and Churakov, 2019; Yoon *et al.*, 2015) have resulted in an improved understanding and better predictions of solute transport in variably saturated porous media including soils, clay rocks, concretes, and crystalline rocks. In this task, we developed two numerical frameworks at the pore scale to simulate solute transport in variably saturated microporous media (i.e., sandy soils) and nano porous media (i.e., compacted clays), respectively.

2.1.1 Pore-scale modelling of accounting for solute transport in thin water films on the surface of soil particles

Within unsaturated microporous media, an improvement has been made to the classical pore-scale model to account for solute transport in thin water films on the surface of soil particles. This enhancement aims to yield a more realistic depiction of solute transport processes in variably saturated sandy soils. The presence of a water film on the surfaces of minerals is resolved by defining the numerical grids at

the water-gas interface with a reduced diffusion coefficient, D_0^*. Thus, the diffusion flux $\boldsymbol{J}_s$ across a water film of a thickness $\overline{d}$ is described as:

$$\boldsymbol{J}_s = \overline{d} D_0 \nabla C = dx D_0^* \nabla C. \quad (1)$$

where D_0 is the diffusivity in free water, dx the grid size, and ∇C the concentration gradient. *Figure 6a* shows an example of phase distribution in the microstructure with a volumetric water content of 0.4 using the Shan-Chen lattice Boltzmann model. *Figure 6b* compares the simulated diffusivity without a water film present and with a water film with a thickness of 1 μm, respectively. When the volumetric water content is larger than 0.25, the water film has little influence on ion transport. However, at low volumetric water content (0.1 - 0.15), transport pathways in the absence of water films depercolate. The water film on the clay surface controls solute diffusion at low water contents. Thus, our novel pore-scale model considering water films shows a better performance than the existing pore-scale models in the literature.

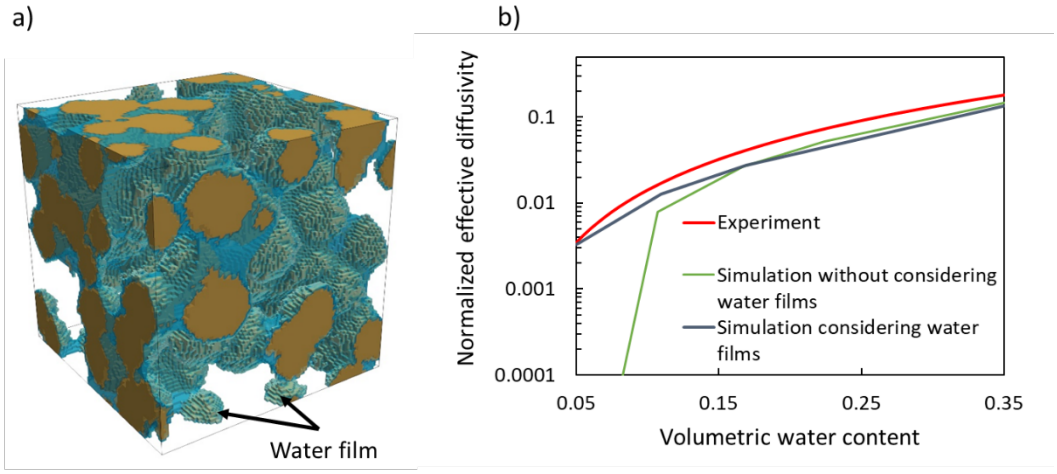

*Figure 6. (**a**) Gas-liquid-solid distribution (yellow: solid phase; blue: liquid phase), (**b**) comparison of simulated relative effective diffusivities in sandy clays for different water film thicknesses; the red line is the fitting line of the experimental datasets (Hu and Wang, 2003).*

2.1.2 Novel pore-scale modelling of solute diffusion in the partially and fully saturated clays

In unsaturated nano porous media, electrical double layer (EDL) effects caused by the charged surface of clays can significantly enhance cation diffusion but reduce anion diffusion (Wu *et al.*, 2020; Yang and Wang, 2019). On the other hand, since the polarizability of anions is normally larger than that of cations, anions are closer to the air/water interface than cations in partially saturated porous media (Jungwirth and Tobias, 2002; Olivieri *et al.*, 2018). As the thickness of the water layer reaches the nanoscale, the air-water and water-solid interfaces may both have a significant influence on ion distribution and further affect ion transport in partially saturated porous media. A novel pore-scale model to solve coupled Poisson-Nernst-Planck equations has been established to simulate solute diffusion in unsaturated compacted clays. Our modelling results of phase distribution, the diffusion of cation (Na^+) and anion (Cl^-) in unsaturated nanoscale porous media are shown in *Figure 7*. Both results indicate the critical influence of the electrical double layer effect on ionic radionuclide transport in nanopores of clay-based materials. *Figure 8* compares the simulation results with experimental data measured in compacted sedimentary rocks (García-Gutiérrez *et al.*, 2023), Callovo-Oxfordian (COx) claystones (Savoye *et al.*, 2012; Savoye *et al.*, 2010), compacted kaolinite (Wang *et al.*, 2022), and illite/sand mixtures (Savoye *et al.*, 2014).

While unsaturated conditions in the compacted sedimentary rocks were obtained by the equilibrium method, in other cases the osmotic method was used to control the suction. The simulated relative effective diffusion coefficients D_e^* for HTO and the anionic tracer iodide agree well with the experimental data from García-Gutiérrez et al. (García-Gutiérrez *et al.*, 2023). However, the experimental data obtained using the osmotic method shows a sharper drop than the simulations. This discrepancy could be attributed to two primary reasons: i) a non-equilibrium state of water and pressure distributions in samples using osmotic methods for controlling water saturation; and ii) an inconsistency of the pore geometries between our regenerated clay and the real samples. This discrepancy should be addressed in future studies.

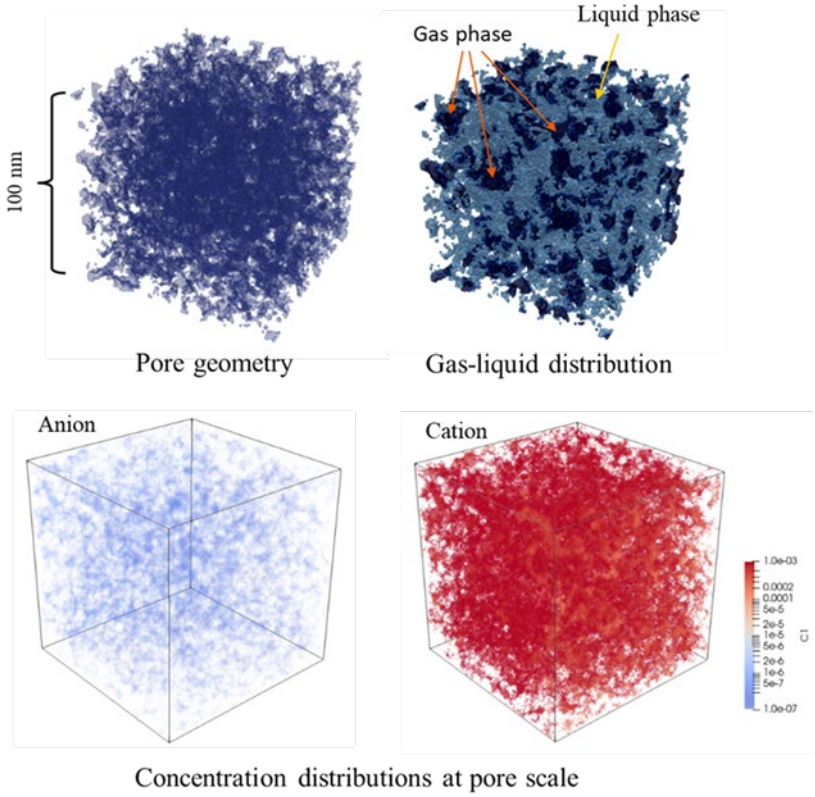

Figure 7. Schematic overview of pore geometry, gas-liquid distribution and simulated concentration distributions of anions/cations at the nanoscale. The solid phase is not shown.

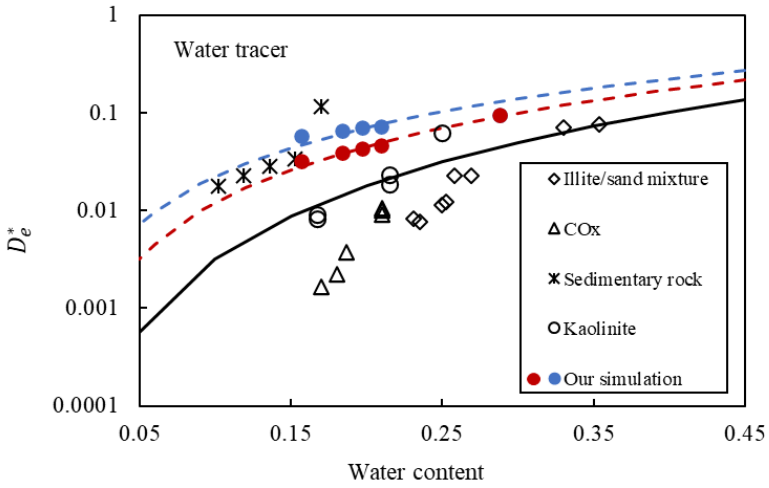

Figure 8. Comparisons of relative effective diffusion coefficients determined by the simulations with reported experimental data and simulations for water tracers (i.e., deuterated and tritiated water) as a function of water content. The experimental data are indicated by different black markers. The coloured circles refer to the simulations performed in this work: blue and red are from our model. The black solid line refers to previous 2D simulations (Gimmi and Churakov, 2019). Dashed lines are the best-fitting curves of the simulation results.

3. Multi-scale/ bridging the scales

3.1 Hybrid coupled multi-physical reactive transport codes by combining continuum-scale with pore-scale models

For scenarios with the presence of reaction fronts confined in the pore domains (e.g. clogged interfaces), spatial domain decomposition can be employed. Within subdomains where the validity of macroscale equations is questionable, pore-scale equations are used as a suitable substitute (Tartakovsky *et al.*, 2008). The preservation of mass and mass flux continuity at the interface of the two distinct subdomains is a primary challenge of this hybrid methodology. When the subdomain, defined in the pore-scale model, is much less than the entire computational domain, the hybrid model can significantly accelerate computations as compared to direct pore-scale simulations (Tang *et al.*, 2015). Therefore, in this task, a hybrid coupled multi-physical reactive transport codes by combining OpenGeoSys (continuum scale) with TransLBM codes (pore-scale) has been developed. As illustrated in *Figure 9*, the mesh of our hybrid model has three regions: the black grids are used by the finite element method (FEM) at the continuum scale, the red grids for the lattice Boltzmann method (LBM) at the pore scale, and the overlapping regions. The key challenge for the hybrid model is the continuities of species' concentrations and fluxes at the interfacial regions or the overlapping regions. Therefore, to transfer the information and ensure the continuities of values between the continuum scale and the pore scale, we solve both LBM and FEM in the overlapping regions, whereas the grid size for FEM there is half of that for LBM. For LBM, the macroscopic concentration is calculated at the center of the grid while the boundary conditions are applied at the boundary of one grid. Therefore, the concentration values at the boundary in LBM are given by FEM at the same position. Finally, this hybrid mode was validated with the analytic solutions.

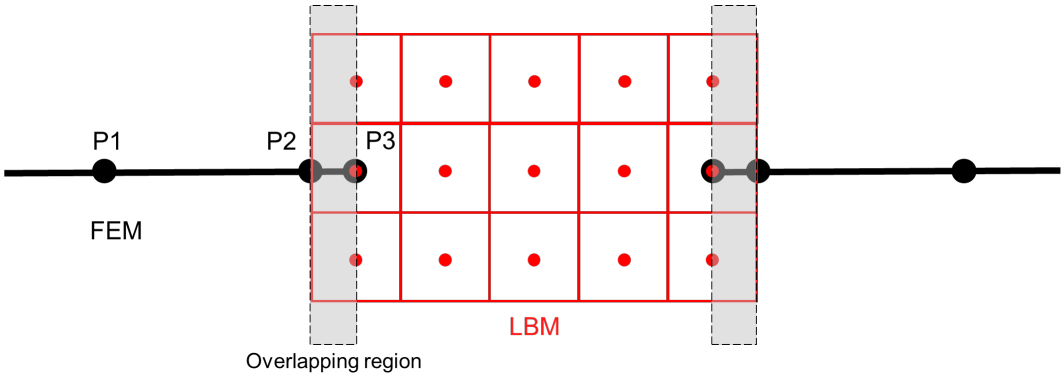

Figure 9. Sketch of the computational discretization in the hybrid model, where the red region is the grids for LBM at the pore scale and the black region is that for FEM at the continuum scale. These two regions have an overlapping part (grey region) designed for the data transformation.

References

Chagneau, A., Claret, F., Enzmann, F., Kersten, M., Heck, S., Madé, B., Schäfer, T., 2015. Mineral precipitation-induced porosity reduction and its effect on transport parameters in diffusion-controlled porous media. Geochemical Transactions 16, 13.
Deng, H., Tournassat, C., Molins, S., Claret, F., Steefel, C.I., 2021. A Pore-Scale Investigation of Mineral Precipitation Driven Diffusivity Change at the Column-Scale. Water Resources Research 57, e2020WR028483.
Friedmann, H., Amiri, O., Aït-Mokhtar, A., 2008. Physical modeling of the electrical double layer effects on multispecies ions transport in cement-based materials. Cement and Concrete Research 38, 1394-1400.
García-Gutiérrez, M., Mingarro, M., Morejón, J., Alonso, U., Missana, T., 2023. Analysis of the role of water saturation degree in HTO, 36Cl, and 75Se diffusion in sedimentary rock. Minerals 13, 593.
Gimmi, T., Churakov, S.V., 2019. Water retention and diffusion in unsaturated clays: Connecting atomistic and pore scale simulations. Applied Clay Science 175, 169-183.
Hu, Q., Wang, J.S.Y., 2003. Aqueous-phase diffusion in unsaturated geologic media: a review. Critical Reviews in Environmental Science and Technology 33, 275-297.
Jungwirth, P., Tobias, D.J., 2002. Ions at the air/water interface. The Journal of Physical Chemistry B 106, 6361-6373.
Li, W., Wang, W., Yang, Y., Hou, X., Ha, H., 2023. Energy and vapour transfer in evaporation processes over saturated bare soil and water surface - lysimeter studies. Hydrological Processes 37, e14894.
Miller, A.W., Wang, Y., 2012. Radionuclide interaction with clays in dilute and heavily compacted systems: a critical review. Environmental Science & Technology 46, 1981-1994.
Olivieri, G., Parry, K.M., D'Auria, R., Tobias, D.J., Brown, M.A., 2018. Specific anion effects on Na+ adsorption at the aqueous solution-air interface: MD simulations, SESSA calculations, and photoelectron spectroscopy experiments. The Journal of Physical Chemistry B 122, 910-918.
Poonoosamy, J., Soulaine, C., Burmeister, A., Deissmann, G., Bosbach, D., Roman, S., 2020. Microfluidic flow-through reactor and 3D Raman imaging for in situ assessment of mineral reactivity in porous and fractured porous media. Lab on a Chip 20, 2562-2571.
Savoye, S., Beaucaire, C., Fayette, A., Herbette, M., Coelho, D., 2012. Mobility of cesium through the Callovo-Oxfordian claystones under partially saturated conditions. Environmental Science & Technology 46, 2633-2641.
Savoye, S., Imbert, C., Fayette, A., Coelho, D., 2014. Experimental study on diffusion of tritiated water and anions under variable water-saturation and clay mineral content: comparison with the Callovo-Oxfordian claystones. Geological Society, London, Special Publications 400, 579-588.
Savoye, S., Page, J., Puente, C., Imbert, C., Coelho, D., 2010. New experimental approach for studying diffusion through an intact and unsaturated medium: a case study with Callovo-Oxfordian argillite. Environmental science & technology 44, 3698-3704.
Tamayo-Mas, E., Harrington, J.F., Brüning, T., Shao, H., Dagher, E.E., Lee, J., Kim, K., Rutqvist, J., Kolditz, O., Lai, S.H., Chittenden, N., Wang, Y., Damians, I.P., Olivella, S., 2021. Modelling advective gas flow in compact bentonite: Lessons learnt from different numerical approaches. International Journal of Rock Mechanics and Mining Sciences 139.
Tang, Y., Valocchi, A.J., Werth, C.J., 2015. A hybrid pore-scale and continuum-scale model for solute diffusion, reaction, and biofilm development in porous media. Water Resources Research 51, 1846-1859.
Tartakovsky, A.M., Redden, G., Lichtner, P.C., Scheibe, T.D., Meakin, P., 2008. Mixing-induced precipitation: Experimental study and multiscale numerical analysis. Water Resources Research 44, W06S04.
Wang, J., Savoye, S., Ferrage, E., Hubert, F., Lefevre, S., Radwan, J., Robinet, J.C., Tertre, E., Gouze, P., 2022. Water and ion diffusion in partially-water saturated compacted kaolinite: role played by vapor-phase diffusion in water mobility. Journal of Contaminant Hydrology 248, 103989.
Wu, T., Yang, Y., Wang, Z., Shen, Q., Tong, Y., Wang, M., 2020. Anion diffusion in compacted clays by pore-scale simulation and experiments. Water Resources Research 56, e2019WR027037.
Yang, Y., Wang, M., 2019. Cation diffusion in compacted clay: a pore-scale view. Environmental Science & Technology 53, 1976-1984.
Yoon, H., Kang, Q., Valocchi, A.J., 2015. Lattice Boltzmann-based approaches for pore-scale reactive transport. Reviews in Mineralogy and Geochemistry 80, 393-431.

Part B: porousMedia4Foam: Multi-scale open-source platform for hydro-geochemical simulations with OpenFOAM®.

[1,]Soulaine, C., [1,2]Pavuluri S., [2]Claret, F. [1,3]Tournassat, C.

[1]Insitut des sciences de la Terre d'Orléans, Université d'Orléans-CNRS-BRGM, France

[2]BRGM, 3 avenue Claude Guillemin, 45060 Orléans, France

[3]Lawrence Berkeley National Laboratory, Berkeley, CA, USA

This work was published in:

- Soulaine, C., Pavuluri S., Claret, F and Tournassat, C. porousMedia4Foam: Multi-scale open-source platform for hydro-geochemical simulations with OpenFOAM®, Environmental Modelling & Software, Volume 145, 2021, https//doi.org/10.1016/j.envsoft.2021.105199.
- Pavuluri, S., Tournassat, C., Claret, F. *et al.* Reactive Transport Modeling with a Coupled OpenFOAM®-PHREEQC Platform. *Transp Porous Med* **145**, 475–504 (2022). https://doi.org/10.1007/s11242-022-01860-x.

The present report is an extended summary of the conducted work. For a complete description of the work, please refer to the two above (**gold open access for the first one**) publications.

The project leading to this application has received funding from the European Union's Horizon 2020 research and innovation programme under grant agreement No 847593.

Abstract

porousMedia4Foam is an open-source package with included benefits to account for reactive transport processes occurring at various scales—pore, hybrid, and Darcy scales. While the flow and transport part is solved using OpenFOAM® one of the most popular open-source numerical toolbox, chemistry is solved using one of the state of the art geochemical solver as to said Phreeqc-RM. The coupling across the scale has been benchmark considering complex and well-established cases available in the reactive transport modeling community. A unique formulation can handle pore-scale, hybrid-scale and continuum-scale simulations for hydro-geochemical processes. This hybrid-scale approach relies on the Darcy-Brinkman-Stokes (DBS) equation that allows for the modelling of flow and transport in regions free of solid and porous regions in a single framework. In a logic of cascade of scales nested within each other, fractured porous media can be modelled by: i) pore-scale approaches, ii) discrete fracture networks, iii) dual porosity models. The hybrid-scale approach that was proposed here is intermediate between a full pore-scale description in which the fracture and the pores in the matrix are fully resolved and a discrete fracture network in which the matrix is modelled as a porous medium and the fractures as discrete elements that exchange matter with the matrix. The hybrid-scale approach is therefore crucial to characterize and improve the effective parameters (e.g. transfer functions between the porous matrix and the fracture) used in discrete fracture networks and larger-scale models

Significance Statement

Reactive transport modeling has established itself as a powerful, versatile and essential tool for tackling the complexity of the multi-space and temporal-scale issues engineers and scientists face. Active topics of research dealing with reactive transport modelling include the development of pore scale and hybrid, or multiple continua, models to capture the scale dependence of coupled reactive transport processes. At the continuum scale, the reactive transport constitutive equations rely on the description of the porous medium with respect to its macroscopically measurable properties (e.g. permeability, diffusability). At the pore scale each point of the space is occupied by either a fluid or a solid phase and macroscopically measurable properties do not apply. Coupling the pore scale and the continnum scale is a challenge and the porousMedia4Foam developed plateform allow to do it in a smart manner using only one equation.

Table of content

1. Context and main highlights

Reactive transport modeling is probably one of the most efficient techniques used to account for and quantify the complexity of coupling processes over a long period of time (Bildstein *et al.*, 2019). While simulation at continuum scale (the scale where the porous media can be represent by macroscopically measurable properties (e.g. permeability, porosity) is well established (see Bildsein et al. (2019) for a review), the upscaling from the pore scale to the continuum scale to capture the scale dependence of coupled reactive transport is an active topics of research (see Bildsein et al. (2019) for a review). Here, porousMedia4Foam an open-source multi-scale solver for flow and transport in porous media has been elaborated (Soulaine *et al.*, 2021). It is is an OpenFOAM-based package that uses PHREEQC for handling geochemical reactions. It relies on micro-continuum approach to bridge the scale. According to Steefel et al. (2015) it is a scale with resolution intermediate between true pore scale models and macro-continuum models, and in which parameters and properties such as permeability or reactive surface area need to be averaged or upscaled in some fashion. In this study, this hybrid-scale approach relies on the Darcy-Brinkman-Stokes (DBS) equation that allows for the modelling of flow and transport in regions free of solid and porous regions in a single framework. When flow is described in true pore scale domains the momentum equation tends to the Navier–Stokes equation, whereas for flow in continuum scale the momentum equation tends asymptotically to Darcy's Law. The developed platform was validated against existing benchmark. At the continuum scale the reference benchmark have been published in Xie (2015) and (Poonoosamy *et al.*, 2021). The obtained results have been published in (Pavuluri *et al.*, 2022). At the pore scale, the reference benchmark was the one published by (Molins *et al.*, 2021) and the result discussed in Soulaine (2021). At the hybrid-scale the ability of porousMedia4Foam modelling framework was demonstrated simulating dissolution and precipitation processes in fractured porous media. Here, the reactive medium consisted of celestite grains that reacted with a barium chloride solution injected into the system, leading to the dissolution of celestite and the growth of barite. Differences in mineral precipitation has been observed in dissolution patterns by varying the injection rates.

To sum up this new package allow the assessment of confinement performance for geological barriers. Future development such as introduction of two phases flow will allow tackling gas migration in a deep geological storage.

Code source

porousMedia4Foam is built using open-source libraries including OpenFOAM and PHREEQC. The source code and the cases presented in the paper are available on GitHub (https://github.com/csoulain/porousMedia4Foam).

References

Bildstein, O., Claret, F., Frugier, P., 2019. RTM for Waste Repositories. Reviews in Mineralogy and Geochemistry 85, 419-457.
Molins, S., Soulaine, C., Prasianakis, N.I., Abbasi, A., Poncet, P., Ladd, A.J.C., Starchenko, V., Roman, S., Trebotich, D., Tchelepi, H.A., Steefel, C.I., 2021. Simulation of mineral dissolution at the pore scale with evolving fluid-solid interfaces: review of approaches and benchmark problem set. Computational Geosciences 25, 1285-1318.
Pavuluri, S., Tournassat, C., Claret, F., Soulaine, C., 2022. Reactive Transport Modeling with a Coupled OpenFOAM®-PHREEQC Platform. Transport in Porous Media 145, 475-504.
Poonoosamy, J., Wanner, C., Alt Epping, P., Águila, J.F., Samper, J., Montenegro, L., Xie, M., Su, D., Mayer, K.U., Mäder, U., Van Loon, L.R., Kosakowski, G., 2021. Benchmarking of reactive transport codes for 2D simulations with mineral dissolution–precipitation reactions and feedback on transport parameters. Computational Geosciences 25, 1337-1358.
Soulaine, C., Pavuluri, S., Claret, F., Tournassat, C., 2021. porousMedia4Foam: Multi-scale open-source platform for hydro-geochemical simulations with OpenFOAM®. Environmental Modelling & Software 145, 105199.
Steefel, C.I., Beckingham, L.E., Landrot, G., 2015. Micro-Continuum Approaches for Modeling Pore-Scale Geochemical Processes. Reviews in Mineralogy and Geochemistry 80, 217-246.
Xie, M., Mayer, K.U., Claret, F., Alt-Epping, P., Jacques, D., Steefel, C., Chiaberge, C., Simunek, J., 2015. Implementation and evaluation of permeability-porosity and tortuosity-porosity relationships linked to mineral dissolution-precipitation. Computational Geosciences 19, 655-671.

Environmental Modelling and Software 145 (2021) 105199

Contents lists available at ScienceDirect

Environmental Modelling and Software

journal homepage: www.elsevier.com/locate/envsoft

porousMedia4Foam: Multi-scale open-source platform for hydro-geochemical simulations with OpenFOAM®

Cyprien Soulaine [a,*], Saideep Pavuluri [a,b], Francis Claret [b], Christophe Tournassat [a,c]

[a] Institut des Sciences de la Terre d'Orléans, CNRS, Université d'Orléans, BRGM, Orléans, France
[b] BRGM, French Geological Survey, Orléans, France
[c] Energy Geosciences Division, Lawrence Berkeley National Laboratory, Berkeley, CA, USA

ARTICLE INFO

Keywords:
Reactive transport modelling
Multi-scale simulations
Micro-continuum
OpenFOAM
PHREEQC

ABSTRACT

porousMedia4Foam is a package for solving flow and transport in porous media using OpenFOAM® - a popular open-source numerical toolbox. We introduce and highlight the features of a new generation open-source hydro-geochemical module implemented within *porousMedia4Foam*, which relies on micro-continuum concept and which makes it possible to investigate hydro-geochemical processes occurring at multiple scales i.e. at the pore-scale, reservoir-scale and at the hybrid-scale. Geochemistry is handled by a third party package (e.g. PHREEQC) that is coupled to the flow and transport solver of OpenFOAM®. We conducted benchmarks across different scales to validate the accuracy of our simulator. We further looked at the evolution of mineral dissolution/precipitation in a fractured porous system. Application fields of this new package include the investigation of hydro-bio-geochemical processes in the critical zone, the modelling of contaminant transport in aquifers, as well as and the assessment of confinement performance for geological barriers.

1. Introduction

Over the last decades, reactive transport modelling (RTM) has become an essential tool for the study of subsurface processes involving flow, transport and geochemical reactions (Steefel et al., 2015a). This discipline is at the junction of two scientific communities, namely geochemistry and transport in porous media. RTM consists of computational models that describe the coupled physical, chemical, and biological processes that interact with each other over a broad range of spatial and temporal scales. RTM modelling tools enable the prediction of contaminant migration in polluted aquifers, and are used to design enhanced remediation techniques. Integration of physical and biogeochemical processes makes RTM also an ideal research instrument for elucidating the complex and non-linear interactions between roots, micro-organisms, water composition and minerals in the Critical Zone (Li et al., 2017). Other applications include the assessment of the long-term integrity of reservoirs for storing carbon dioxide, hydrogen or nuclear wastes in deep geological formations (DePaolo and Cole, 2013; Claret et al., 2018). In practice, three different kinds of models are used to describe reactive transport in porous media as illustrated in Fig. 1: *(i)* continuum models, *(ii)* pore-scale models, and *(iii)* hybrid models that combine both former approaches.

Continuum models (see Fig. 1c) are representative of the historical and standard approach for solving reactive transport in large-scale natural porous systems (Lichtner, 1985). Continuum-scale RTM codes include, among others, MIN3P (Mayer et al., 2002), CrunchFlow (Steefel et al., 2015a), TOUGHREACT (Xu et al., 2006), PFlotran (Lichtner et al., 2015) or HP1 (Jacques et al., 2008). In such codes, flow and transport equations are formulated in terms of volume-averaged equations with respect to a Representative Elementary Volume (REV) of the porous structure (Bear, 1972) and are coupled with geochemical reactions (see Steefel et al., 2015a for an comprehensive description of the coupling). The topology of the rock micro-structures is described using effective properties including porosity, tortuosity, permeability – or hydraulic conductivity – and specific surface area. Flow is usually modelled using Darcy's law and multi-component species transport relies on a set of advection-dispersion-reaction equations. In addition to the classic challenges related to transport in porous media, including the medium heterogeneity awareness and the description of hydrodynamic dispersion, RTM has to consider the variation of rock properties in response to chemical reactions. Indeed, by enlarging or clogging pore throats and fractures, geochemical processes such as minerals dissolution and precipitation can alter the local flowfield and subsequently modify the rock properties, e.g permeability, tortuosity, accessible reactive surface area

* Corresponding author.
E-mail addresses: cyprien.soulaine@cnrs-orleans.fr, cyprien.soulaine@gmail.com (C. Soulaine).

https://doi.org/10.1016/j.envsoft.2021.105199
Accepted 7 September 2021
Available online 15 September 2021

(Poonoosamy et al., 2020; Seigneur et al., 2019).

Changes in rock properties with chemical reaction is usually described in continuum-scale RTM as heuristic functions of the porosity. For example, in most of reactive transport codes, tortuosity is described using Archies's law, permeability change is modelled using Kozeny-Carman relationship, and mineral surface areas evolve as a two-third power law of the porosity (Xie et al., 2015). However, the complex interplay between reactions, advection, and diffusion can lead to highly nonlinear porosity feedback that is poorly captured using this kind of relationships that were not built on a strong theoretical background (Daccord and Lenormand, 1987; Garing et al., 2015). The limiting factor of the continuum-scale models is therefore the determination of empirical parameters and their evolution as a function of the progress of geochemical processes. To circumvent these challenges, recent efforts have focused on the numerical modelling of coupled hydro-geochemical processes at the pore-scale (Békri et al., 1997; Chen et al., 2013; Tartakovsky et al., 2007; Molins et al., 2014; Molins et al., 2017).

In pore-scale models (see Fig. 1a), the pore network is fully resolved, i.e. each point of space is occupied by either a fluid or solid phase. As the exact knowledge of the phase distribution is known, continuum-scale concepts such as porosity, permeability, and reactive surface area do not apply at the pore-scale. They can be obtained, however, by averaging pore-scale simulation results if the computational domain is large enough to reach the size of a REV (Whitaker, 1999; Soulaine et al., 2013). The strategy that consists in simulating flow and transport in a three-dimensional image of a porous sample to characterize its continuum-scale properties has become an independent scientific discipline sometimes referred to as Digital Rock Physics (Blunt et al., 2013; Andrä et al., 2013a; Andrä et al., 2013b; Soulaine et al., 2021). Most of the efforts so far have been devoted to solve the Navier-Stokes equations under single (Spanne et al., 1994; Bijeljic et al., 2013; Guibert et al., 2015; Soulaine et al., 2016) and two-phase flow conditions (Horgue et al., 2013; Raeini et al., 2014; Graveleau et al., 2017; Maes and Soulaine, 2018; Pavuluri et al., 2020) to compute absolute and relative permeabilities. Despite the growing investment in the development of RTM at the pore-scale – pioneer simulators date back to the late 90s (Békri et al., 1997) – the pore-scale RTM field is still emerging. One of the main challenge of this approach consists in moving the fluid/solid boundary with respect to chemical reactions at the mineral boundaries (Noiriel and Soulaine, 2021). A comprehensive review of the different approaches used to solve this problem can be found in Molins et al. (Molins et al., 2020). It is only very recently that pore-scale simulators have been proved mature for reproducing accurately and without any adjusting parameters the dissolution of a calcite crystal (Soulaine et al., 2017; Molins et al., 2020), or of a gypsum grain (Dutka et al., 2020). Actually, the benchmark presented in Molins et al. (Molins et al., 2020) is a first effort based on a relatively simple geochemical reaction (a single component that reacts with a single mineral using a first-order kinetics) to demonstrate the ability of current codes to accurately simulate mineral dissolution at the pore scale in a reproducible manner with several codes. Further developments and verifications still need to be done for simulating multi-component aqueous solutions interacting with heterogeneous multi-mineral media using comprehensive reaction networks.

Naturally occurring porous media involve a wide range of spatial scales. For example, the important contrast in pore-size distributions in fractured porous rocks comes from much larger characteristic lengths for the fractures than for the surrounding porous matrix. Therefore, the domain size required to reach a REV limits the use of pure pore-scale modelling. Hybrid-scale models have been proposed to describe systems that include multiple characteristic length-scales, for which some regions are described using pore-scale modelling while others are modelled with continuum approaches (see Fig. 1b) (Liu and Ortoleva, 1996; Liu et al., 1997). Two different approaches have been developed to solve hybrid-scale problems. On the one hand, the domain decomposition technique solves different physics on separate domains – one for Darcy flow, another for Stokes flow – linked together through appropriate boundary conditions (Molins et al., 2019) including Beaver-Joseph and Ochoa-Tapia-Whitaker conditions (Beavers and Joseph, 1967; Ochoa-Tapia and Whitaker, 1995). On the other hand, micro-continuum models use a single set of partial differential equations throughout the computational domain regardless of the content of a grid block (Steefel et al., 2015b; Soulaine and Tchelepi, 2016). The latter approach is particularly well-suited to capture the dynamic displacement of the interface between the porous and solid-free regions without involving complex re-meshing strategies. For example, micro-continuum models have been used successfully to simulate the formation and growth of wormholes in acidic environments (Ormond and Ortoleva, 2000; Golfier et al., 2002; Soulaine and Tchelepi, 2016). Hybrid-scale modelling is also a powerful tool in image-based

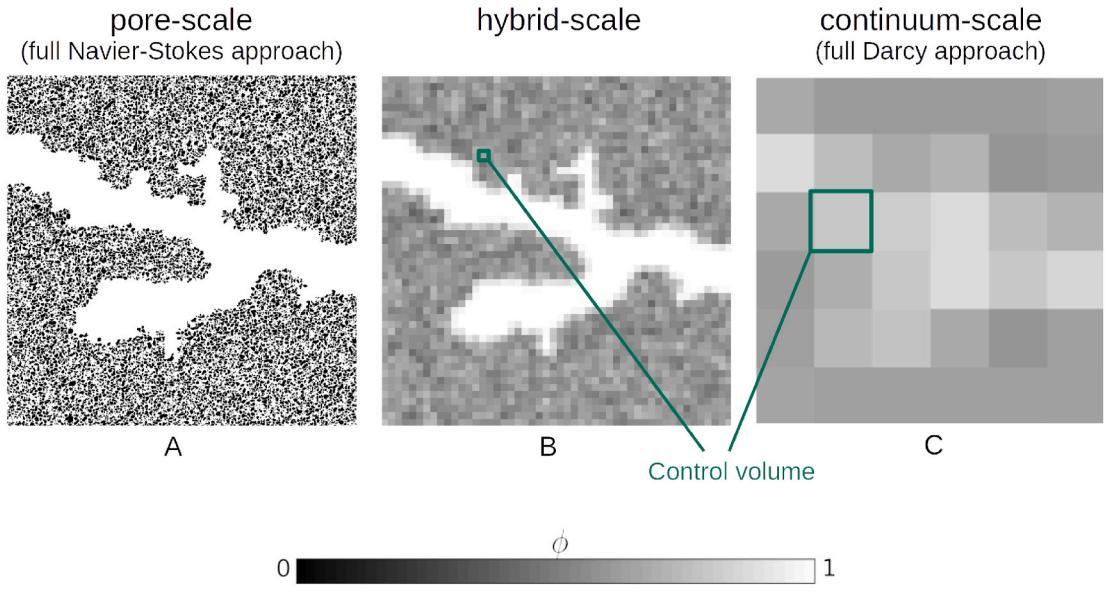

Fig. 1. Porosity distribution considered in: *a)* a pure pore-scale approach (Navier-Stokes) for which the porosity is fully resolved, *b)* a micro-continuum approach (DBS) that handles region free of solid and porous region in the same framework, *c)* a pure continuum-scale approach (Darcy) for which all the control volumes contain an aggregate of fluid and solid.

simulations to account for microscale features that are not visible in the images because they are smaller than the imaging instrument resolution (Arns et al., 2005; Apourvari and Arns, 2004; Scheibe et al., 2015; Soulaine et al., 2016; Soulaine et al., 2019).

In this study, we developed a comprehensive open-source simulator to model coupled hydro-geochemical processes at continuum-, pore- and hybrid-scales. This unique multi-scale framework relies on the micro-continuum model and its ability to tend asymptotically toward continuum-scale models if grid block contains solid content ($0 < \varphi < 1$) or towards pore-scale models otherwise ($\varphi = 1$) (Soulaine and Tchelepi, 2016). The resulting advanced RTM allows the treatment of complex reactions network as a function of flow conditions, water composition and minerals distribution within the rock including the complex porosity feedback between flow and chemistry. It is part of *porousMedia4Foam*, an open-source package developed by the authors to solve flow and transport in porous media within the popular simulation platform OpenFOAM®. Because of its versatility and advanced features such as three-dimensional unstructured grids, dynamic meshes, and high-performance computing, there is a growing interest in the community to develop mathematical models for solving flow and transport in porous media within OpenFOAM® (Horgue et al., 2015; Maes and Geiger, 2018; Orgogozo et al., 2014; Soulaine et al., 2017). We developed a generic interface to combine flow and transport models with existing geochemical packages. We illustrate the versatility of our coupling interface by combining flow models with geochemical models using PHREEQC (Parkhurst and Wissmeier, 2015), an open-source and popular geochemistry package that is used in many continuum-scale RTM (Rolle et al., 2018; Healy et al., 2018; Muniruzzaman and Rolle, 2019; Muniruzzaman et al., 2020; Moortgat et al., 2020).

In Section 2, we present the mathematical models implemented in *porousMedia4Foam* including a multi-scale and a continuum-scale flow solver, a wide range of porous properties models and the packages used to perform geochemical calculations. In Section 3, we verify the robustness of the coupled hydro-geochemical platform by simulating cases for which reference solutions exist both at the continuum-scale and at the pore-scale. Simulation results are compared with the results obtained with state-of-the-art reactive transport codes. Then in Section 4, we use the simulation framework to illustrate the potential of *porousMedia4Foam* to model hybrid-scale cases.

2. The *porousMedia4Foam* package

The multi-scale solver for simulating hydro-geochemical problems is part of *porousMedia4Foam* (https://github.com/csoulain/porousMedia4Foam), a generic platform for solving flow and transport in porous media at various scales of interest. *porousMedia4Foam* is an open-source platform developed by the authors using the C++ library OpenFOAM (http://www.openfoam.org). Hence, the package benefits from all the features of OpenFOAM including the solution of partial differential equations using the finite-volume method on three-dimensional unstructured grids as well as High Performance Computing. Although *porousMedia4Foam* has capabilities for solving two-phase flow (liquid-liquid and liquid-gas) in porous systems, the geochemistry coupling that is introduced in this paper only considers single-phase flow.

The code is organized in three interacting parts: a class that describes porous media properties (Section 2.4), the flow solvers (Section 2.2) and the geochemical packages (Section 2.3). As *porousMedia4Foam* intends to be a versatile platform, it is designed in a such way that other porous media models, other flow solvers or other geochemical packages can be easily implemented using the C++ code architecture. In this section, we introduce the models and their numerical implementation in the code. It is organized as a multiple-entry document in which each model is presented in a self-contained manner so that users can directly refer to the subsection associated with the said model.

2.1. Mineral distribution and porosity

A geological medium is made of an assembly of N_s minerals whose porous properties are defined in Section 2.4. The distribution of each mineral i on the computational grid is determined by the volume fraction,

$$Y_{s,i}(x,y,z,t) \quad \text{with} \quad i \in [1, N_s], \tag{1}$$

in each grid block. The N_s solid volume fraction fields are dimensionless. They can be initialized with uniform or distributed values. The evolution of $Y_{s,i}$ due to geochemical reactions is dictated by the geochemical packages that are described in Section 2.3. In some simulations, it is relevant to define an inert mineral, $Y_{s,\text{inert}}$, that is not part of the geochemical calculation.

The porosity field is computed by,

$$\varphi = 1 - \sum_{i}^{N_s - 1} Y_{s,i} - Y_{s,\text{inert}}, \tag{2}$$

and can be updated at any moment following dissolution or precipitation processes. The porosity update at every time-step is optional.

2.2. Flow solvers

porousMedia4Foam for hydro-geochemical simulations includes three flow models: a multi-scale flow solver based on the micro-continuum approach, a continuum-scale Darcy solver and a constant velocity solver (see Table 1).

2.2.1. dbsFoam: *Multi-scale micro-continuum flow model*

dbsFoam is a multi-scale flow solver based on the micro-continuum modelling approach developed in Soulaine and Tchelepi (Soulaine and Tchelepi, 2016). Micro-continuum approaches are intermediate between a pure Navier-Stokes description of the transport for which all the porosity is fully resolved (see Fig. 1a), and a pure continuum-scale modelling for which the flow is governed by Darcy's law (see Fig. 1c). This hybrid-scale approach relies on the Darcy-Brinkman-Stokes (DBS) equation (Brinkman, 1947) that allows for the modelling of flow and transport in regions free of solid and porous regions in a single framework (Neale and Nader, 1974; Soulaine and Tchelepi, 2016). DBS equation arises from the integration of Navier-Stokes equations over a control volume (Vafai and Tien, 1981; Hsu and Cheng, 1990; Bousquet-Melou et al., 2002; Goyeau et al., 2003). The momentum equation reads,

$$\frac{1}{\varphi}\left(\frac{\partial \rho_f \boldsymbol{v}_f}{\partial t} + \nabla.\left(\frac{\rho_f}{\varphi}\boldsymbol{v}_f\boldsymbol{v}_f\right)\right) = -\nabla p_f + \rho_f \boldsymbol{g} + \nabla.\left(\frac{\mu_f}{\varphi}\left(\nabla \boldsymbol{v}_f + {}^t\nabla \boldsymbol{v}_f\right)\right) - \mu_f k^{-1}\boldsymbol{v}_f, \tag{3}$$

where φ is the porosity, $\boldsymbol{v}_f$ is the seepage velocity, p_f is the fluid pressure, $\boldsymbol{g}$ is the gravity, ρ_f is the fluid density, μ_f is the fluid viscosity and k is the cell permeability. The porous media properties including porosity and

Table 1
Summary of the flow solvers implemented in *porousMedia4Foam* for simulating hydro-geochemical processes.

Name	Model	Setion	Comments
dbsFoam	Micro-continuum (Darcy-Brinkman-Stokes)	Sec. 2.2.1	pore-scale, hybrid-scale, continuum-scale, (Soulaine and Tchelepi, 2016).
darcyFoam	Darcy's law	Sec. 2.2.1	continuum-scale only.
constantVelocityFoam	constant velocity profile	Sec. 2.2.3	uniform or non-uniform velocity profiles.

permeability change dynamically with geochemical processes and are updated at every time steps.

Eq. (3) is valid throughout the computational domain regardless the content of a cell. In regions that contain fluid only, $\varphi = 1$, and the drag force $\mu_f \boldsymbol{k}^{-1}\boldsymbol{v}_f$ vanishes so that the momentum equation tends to the Navier-Stokes equation. In regions that contain an aggregate of fluid and solid, $0 < \varphi < 1$, and the drag force is dominant over the inertial and viscous forces so that Eq. (3) tends asymptotically to Darcy's law.

The momentum equation, Eq. (3), can be used to model pore-scale flows. Indeed, if a solid region is approximated by a low-permeability low-porosity matrix, the velocity in this region goes to near zero which forces a no-slip boundary condition at the fluid/solid interface. This feature of the DBS equation is particularly relevant to solve Navier-Stokes problems using Cartesian grids only (also called penalized approach) (Angot et al., 1999; Soulaine and Tchelepi, 2016) and to move the fluid/solid interface with respect to geochemical processes such as precipitation/dissolution (Soulaine et al., 2017; Molins et al., 2020) or swelling by using the local porosity field, φ, as a phase indicator function (Carrillo and Bourg, 2019).

The pressure-velocity coupling is achieved by solving the momentum equation along with the micro-continuum continuity equation for multiple minerals. For an incompressible Newtonian aqueous fluid, the latter reads,

$$\nabla . \boldsymbol{v}_f = \sum_{i=1}^{N_s} \dot{m}_{s,i} \left(\frac{1}{\rho_f} - \frac{1}{\rho_{s,i}} \right), \tag{4}$$

where $\rho_{s,i}$ is the solid density of mineral i and $\dot{m}_{s,i}$ represents the rate of phase change of solid into fluid, or of a fluid into solid. For example, it can represent the rate of solid minerals that is dissolved into aqueous solution. Inversely, it can describe an amount of fluid that is removed of a control volume because it has precipitated. The right-hand side of Eq. (4) is provided by the geochemistry calculation (Section 2.3). Although this term if often neglected in continuum-scale models, it ensures the mass balance at the fluid/solid interface in pore-scale simulations (Soulaine et al., 2017), as well as in continuum-scale simulations (Seigneur et al., 2018).

The flow model formed by Eqs (3) and (4) is discretized using the finite volume method and solved sequentially. The pressure-velocity coupling is handled by a predictor-corrector strategy based on the PIMPLE algorithm implemented in OpenFOAM. It consists in a combination of PISO (Pressure Implicit with Splitting of Operator, Issa, 1985) and SIMPLE (Semi-Implicit Method for Pressure Linked Equations, Patankar, 1980). PIMPLE algorithm allows both transient and steady-state simulations. Moreover, PIMPLE enables larger time steps than PISO. Further information regarding the numerics is found in Soulaine and Tchelepi (2016).

2.2.2. darcyFoam: *Darcy's law*

darcyFoam is a standard continuum-scale solver that is based on Darcy's law,

$$\boldsymbol{v}_f = -\frac{k}{\mu_f} \left(\nabla p_f - \rho_f \boldsymbol{g} \right), \tag{5}$$

for describing flow in porous media. Numerically, Eq. (5) is combined along with Eq. (4) to form a Laplace equation solving implicitly for the pressure field, p_f. Then, the velocity field is calculated point-wise using Eq. (5) and p_f. If activatePorosityFeedback is switched on, Darcy's law is recalculated at every time steps to update the velocity and pressure fields according to the new permeability value.

Boundary conditions can be described by imposing fixed pressure or fixed velocity values on the domain edges. However, as darcyFoam solves implicitly for the pressure field, the boundary conditions on the velocity are transformed into pressure gradient conditions using Darcy's law:

$$\boldsymbol{n} \cdot \nabla p_f = -\boldsymbol{n} \cdot \left(\mu_f k^{-1} \boldsymbol{v}_f - \rho_f \boldsymbol{g} \right), \tag{6}$$

where $\boldsymbol{n}$ is the vector normal to the domain boundary. In the code, Eq. (6) is achieved using the boundary condition darcyGradPressure (Horgue et al., 2015).

2.2.3. constantVelocityFoam: *Constant flow rate*

The flow solver constantVelocityFoam is used to model cases in which the chemical species are transported using a steady-state velocity field, $\boldsymbol{v}_f$ –uniform or non-uniform– provided as an input data that can come from a separate flow simulation. constantVelocityFoam is particularly useful if the feedback between geochemical reactions and the flow is negligible. Indeed, in such a case, the characteristic timescale of flow changes is much longer than the characteristic time of species transport and the calculation of the velocity profile can be decoupled from the species transport.

2.3. *Geochemical packages*

In *porousMedia4Foam*, complex reaction networks are handled by geochemical packages. The aqueous components are transported using the velocity profile, $\boldsymbol{v}_f$, computed by the flow solver (see section 2.2) and surface reactions rely on the reactive surface area, A_e, calculated with the porous media models (see section 2.4.2). The code architecture of *porousMedia4Foam* is generic so that a wide variety of third-party geochemical packages can be coupled with our platform for solving hydro-geochemical processes at the pore-scale and at the continuum-scale. In this paper, we illustrate the potential of the coupled simulation framework using the popular geochemistry package PHREEQC (Parkhurst and Appelo, 2013; Parkhurst and Wissmeier, 2015). Models currently implemented in *porousMedia4Foam* to account for geochemistry are summarized in Table 2.

The geochemical packages update the water composition, C_j, and the distribution of the solid minerals, $Y_{s,i}$, and return the rate of solid changes,

$$\dot{m}_{s,i} = -\frac{\partial \rho_{s,i} Y_{s,i}}{\partial t}, \tag{7}$$

where $\rho_{s,i}$ is the density of solid mineral i.

2.3.1. *phreeqcRM*

The phreeqcRM class calls the general-purpose geochemical reaction model PHREEQC through the PhreeqcRM module. It carries out the transport of the aqueous solution composition, C_j (in mol/kg$_{water}$), along with equilibrium and kinetic reactions with the solid minerals described by $Y_{s,i}$. phreeqcRM is set with components, i.e. SOLUTION_MASTER_SPECIES total concentration.

The geochemistry setup is carried out using an input file that follows PHREEQC format. Hence, the aqueous composition is defined in the

Table 2
Summary of the geochemical packages implemented in *porousMedia4Foam* for simulating hydro-geochemical processes.

Name	Model	Section	Comments
phreeqcRM	PHREEQC	Sec. 2.3.1	Parkhurst and Wissmeier (2015)
simpleFirstOrderKineticMole	first order kinetic, C_i in mol/m^3	Sec. 2.3.2	Molins et al. (2020); Soulaine et al. (2017)
transportOnly	no geochemistry	Sec. 2.3.3	–
fiowOnly	no transport, no geochemistry	Sec. 2.3.4	–

block SOLUTION (0 for the composition of the injected fluid at the inlet boundary, 1 for the initial aqueous composition in the bulk). The EQUILIBRIUM_PHASES and KINETICS blocks are generated automatically within the code and the user only has to assign before the calculation which mode of reactions is used for each mineral. Moreover, *porousMedia4Foam* can load any customized database using PHREEQC format.

The coupling between transport and reactions relies on an operator-splitting approach based on the Strang's algorithm (Strang, 1968). First, all species concentration fields, C_j, are transported sequentially using the advection-dispersion equations,

$$\frac{\partial \varphi C_j}{\partial t} + \nabla\cdot\left(\boldsymbol{v}_f C_j\right) - \nabla\cdot\left(\varphi \mathrm{D}_j^* .\nabla C_j\right) = 0, \tag{8}$$

where $\boldsymbol{v}_f$ is the fluid velocity computed with the flow solver (see Section 2.2) and D_j^* is an effective diffusion tensor that accounts for tortuosity and hydrodynamic dispersion effects (see Section 2.4.3). The transport equation is discretized on the computational domain using the finite-volume method and solved implicitly using OpenFOAM's engines.

Then, the volume fractions of solid minerals, $Y_{s,i}$, are updated according to phase equilibrium and/or kinetic reaction calculations provided by PHREEQC. Reaction kinetics use the surface area computed at every time steps using the surface area models in section 2.4.2. It corresponds to the surface area per volume and its units are $\mathrm{m}^2/\mathrm{m}^3$ (or m^{-1}). Hence, the RATE block provided in PHREEQC database to describe reaction rates has to be defined accordingly.

2.3.2. simpleFirstOrderKineticMole

simpleFirstOrderKineticMole is a simple geochemical engine for solving the transport of a single species labelled *A* that reacts with solid minerals using first order kinetic reactions. It is an extension to multiple minerals of the model used in the benchmark presented in Molins et al. (2020) in which pore-scale simulators were used to model the dissolution of a calcite crystal by hydrochloric acid.

The chemical reaction reads,

$$\mathrm{Mineral}_{i(s)} + \mathrm{A} = \mathrm{B}_i. \tag{9}$$

The mass balance equation for species *A* reads,

$$\frac{\partial \varphi C_A}{\partial t} + \nabla\cdot\left(\boldsymbol{v}_f C_A\right) - \nabla\cdot\left(\varphi \mathrm{D}_j^* .\nabla C_A\right) = -\left(\sum_{j=1}^{N_s} A_{s,j}\left(k_{j,A}\gamma_A\right)\right) C_A, \tag{10}$$

where $\boldsymbol{v}_f$ is the fluid velocity, D_j^* is an effective diffusion tensor, $A_{s,j}$ is the reactive surface area of mineral j (in m^{-1}), and $\left(k_{j,A}\gamma_A\right)$ is the constant of reaction of the species *A* with the mineral j (in m/s) following the notations adopted in Molins et al. (2020). In simpleFirstOrderKineticMole, the concentration field, C_j, is defined in $\mathrm{mol}/\mathrm{m}^3$. The equation is discretized on the computational grid using the finite-volume method and solved implicitly.

The distribution of solid minerals evolves according to,

$$\frac{\partial Y_{s,i}}{\partial t} = -A_{s,A}\left(k_{i,A}\gamma_A\right) V_{m_{s,i}} C_A, \tag{11}$$

where $V_{m_{s,i}}$ (in $\mathrm{m}^3/\mathrm{mol}$) is the molar volume of the reacting mineral.

2.3.3. transportOnly

transportOnly solves the advection-dispersion equation,

$$\frac{\partial \varphi C_j}{\partial t} + \nabla\cdot\left(\boldsymbol{v}_f C_j\right) - \nabla\cdot\left(\varphi \mathrm{D}_j^* .\nabla C_j\right) = 0, \tag{12}$$

without considering geochemistry. It allows the transport of species using the dispersion models implemented in *porousMedia4Foam* (see Table 5).

2.3.4. flowOnly

flowOnly is an empty class for computing velocity profiles without species transport nor geochemistry. For example, Poonoosamy et al. (2020) used the multi-scale flow solver of *porousMedia4Foam* to compute the steady-state velocity profile in absence of geochemical reactions within a two-scale domain, i.e. a domain that contains both solid-free regions and porous regions (see Fig. 1b). This option is particularly interesting in cases for which geochemistry and flow can be treated independently from each other.

2.4. Porous media models

The flow solvers and geochemistry modules rely on porous media properties including absolute permeability, specific surface area and dispersion tensor. These properties describe pore-scale effects related to the micro-structure geometry of the porous medium. Hence, they may change if the micro-structure evolves with geochemical reactions.

2.4.1. Absolute permeability models

The absolute permeability describes the ability of a porous medium to conduct the flow. This property is intrinsic to the medium micro-structure and therefore evolves with geochemical processes including precipitation and dissolution. *porousMedia4Foam* includes several porosity-permeability relationships summarized in Table 3.

2.4.2. Surface area models

The estimation of the reactive surface area is crucial to model geochemical processes described by kinetic reactions. Actually, reactive surface area is a difficult quantity to assess as only a portion of the geometric surface area is accessible to the reactants. For example, in an advection-dominated transport, only the surfaces at the vicinity of the faster flowlines react (Soulaine et al., 2017) leading to a reactive surface area smaller than the geometric surface area. Moreover, the evolution of the specific surface area as the mineral volume fractions change due to dissolution or precipitation is not necessarily monotonic (Noiriel et al., 2009). Table 4 summarizes the models implemented in *porousMedia4Foam* to describe the surface area as a function of the mineral volume fraction.

Unlike continuum-scale simulations, the surface area in pore-scale modelling is not an input parameter but is a direct output of the simulation. Indeed at the pore-scale, the micro-structure of the porous medium is fully resolved in the computational grid and there is a sharp interface between the fluid and the solid mineral. The Volume-of-Solid

Table 3
Summary of the permeability-porosity models implemented in *porousMedia4Foam*. In the table, subscripts 0 refers to variable data at initial time. Optionally, φ_0 and k_0 are updated at every time-steps.

Name	Expression	Comments
none	$k = 0$	–
constant	$k = k_0$	k_0 is uniform or non-uniform.
Power-law	$k = k_0\left(\frac{\varphi}{\varphi_0}\right)^n$	n is a user defined variable.
Kozeny-Carman	$k = k_0\left(\frac{\varphi}{\varphi_0}\right)^n\left(\frac{1-\varphi_0}{1-\varphi}\right)^m$	by default, $n = 2$ and $m = 3$ (Kozeny, 1927; Carman, 1937).
Verma-Pruess	$k = k_0\left(\frac{\varphi-\varphi_c}{\varphi_0-\varphi_c}\right)^n$	n is a model parameter. φ_c refers to the critical porositywhere permeability reduces to 0 (Verma and Pruess, 1988).
Hele-Shaw	$k = \frac{h^2}{12}$	for simulating 2D depth-averaged flow in micromodels (e.g. Poonoosamy et al., 2020; Roman et al., 2016).

Table 4
Summary of the specific surface area models implemented in *porousMedia4-Foam*. Units of specific surface area are m^{-1}.

Name	Expression	Comments
None	$A_s = 0$	If specific surface area is not necessary, e.g. for phase equilibrium calculation.
Constant	$A_s = A_0$	–
Volume of solid	$A_s = \lvert\nabla Y_s\rvert\psi$	for pore-scale simulations only. Compute thelocal surface area based on the mineral mapping. ψ is a diffuse interface function (Soulaine et al., 2017).
Power-law	$A_s = A_0(Y_s)^n$	n is a user defined variable
Sugar-lump	$A_s = \left(A_0 + A_m\left(1 - \left(\frac{Y_s}{Y_0}\right)^{n_1}\right)^{n_2}\right)\left(\frac{Y_s}{Y_0}\right)^{n_3}$	Evolution of the surface area of an aggregateduring dissolution (Noiriel et al., 2009). $A_m$is the maximum surface area given by the sum of the surface areas of all individual particles, n_1, n_2 and n_3 are user-defined parameters.
Hydro-geochemical coupling	$A_s = A_0\left(\frac{Y_s}{Y_0}\right)^n(1 - \exp(Pe^{-p}Da^{-q}))$	including surface reduction due to hydro-geochemical coupling (Soulaine et al., 2017). n, p, q are user defined parameters.

model computes the surface area of an explicit fluid/solid interface using the gradient of the volume fraction of mineral (see Soulaine et al., 2017 for additional details on the technique).

2.4.3. Dispersion models

In porous media, the spreading of a solute is not governed only by molecular diffusion (D_i) but also by the micro-structure and the local velocity field. On the one hand, the tortuosity of the porous structure tends to slow down the spreading. On the other hand, hydrodynamic dispersion stretches a solute band in the flow direction during its transport. In *porousMedia4Foam*, a single effective diffusion tensor, D_i^*, is used to represent both mechanisms. The models implemented in the code are summarized in Table 5.

Table 5
Summary of the dispersion models implemented in *porousMedia4Foam*. I is the unit tensor.

Name	Expression	Comments
none	$\mathsf{D}_i^* = 0$	for modelling transport by advection only.
diffusionOnly	$\mathsf{D}_i^* = D_i\mathsf{I}$	no tortuosity effects, no hydrodynamic dispersion.
archiesLaw	$\mathsf{D}_i^* = \varphi^n D_i\mathsf{I}$	tortuosity is represented by φ^n. By default, $n = 0$.
linearDispersion	$\mathsf{D}_i^* = \varphi^n\left((D_i + \alpha_T\lvert\boldsymbol{v}\rvert)\mathsf{I} + \frac{(\alpha_L - \alpha_T)}{\lvert\boldsymbol{v}\rvert}\boldsymbol{vv}\right)$	tortuosity is represented by φ^n. α_L and $\alpha_L$are model parameters describing lateraland longitudinal dispersion respectively.

3. Verification of the hydro-geochemical simulation platform

In this section, the multi-scale hydro-geochemical simulation package *porousMedia4Foam* introduced in Section 2 is used along with PHREEQC to investigate several scenarios for which reference solutions exist. The verification of the results is achieved by comparison against benchmarks published in literature both at the continuum-scale and at the pore-scale. Essential files required to run all the test cases presented in this section are available as examples within the package. All simulations were run on Intel Xeon with 2.60 GHz.

3.1. Verification at the continuum-scale

We verify the ability of *porousMedia4Foam* to simulate coupled hydro-geochemical processes that include porosity feedback on the transport properties at the continuum-scale. We also verify that the multi-scale solver dbsFoam tends asymptotically towards Darcy's law in porous domains. The case is based on the Benchmark 1 described in Xie et al. (2015). It consists of a 2 meters long 1D column initially filled with 35% of inert mineral and 30% of calcite. An acid (pH = 3) is continuously injected at the inlet to initiate the dissolution of calcite according to,

$$\begin{aligned} &CaCO_3 + H^+ \leftrightarrow Ca^{2+} + HCO_3^-, \\ &HCO_3^- \leftrightarrow H^+ + CO_3^{2-}. \end{aligned} \tag{13}$$

Table 6 provides the initial and boundary conditions data specific to the primary components. A difference of 0.007 m in hydraulic head is applied between the inlet and outlet (Xie et al., 2015) by fixing the pressure at 70 Pa and 0 Pa respectively at the inlet and outlet boundaries throughout the simulation.

The calcite dissolution with porosity feedback is simulated using both the multi-scale solver dbsFoam and the continuum-scale solver darcyFoam. The aqueous species are transported by advection only. The calcite dissolution is modelled using a kinetic rate of reaction with $k_{\text{calcite}} = 5 \times 10^{-5}$ mol/m^2/s and the initial specific area $A_0 = 1$ m^2/m^3. As the calcite dissolves, the surface area decreases according to a power-law function with $n = 2/3$ (see Table 4). The porosity-permeability relationship is described by the Kozeny-Carman equation (Table 3). The initial permeability of the column is set to $k_0 = 1.186 \times 10^{-11}$ m^2. The column is spatially discretized with $\Delta x = 25$ mm (80 cells). 150 years are simulated with $\Delta t = 21600$ s.

There is a perfect match between dbsFoam and darcyFoam confirming that the multi-scale solver converges well to the continuum-scale solution predicted by Darcy's law (Fig. 2). The analysis of results includes the evolution of porosity (Fig. 2a), calcite volume fraction (Fig. 2b), hydraulic head (Fig. 2c) along the column length and the outflux over time (Fig. 2d). To be consistent with the benchmark of Xie et al. (2015), we consider the cross-sectional area of the column to be 1 m^2. As the dissolution of calcite occurs, the calcite volume fraction decreases and the porosity increases over time. In Fig. 2c, we notice different slopes of hydraulic head at different times. The slope is minimal where porosity is large and vice-versa. The velocity – and therefore the outflux – increases over time as the permeability (and porosity) of the system increases. The evolution of porosity, calcite volume fraction, hydraulic head and outflux predicted by *porousMedia4Foam* solvers are in close agreement with

Table 6
Initial and boundary conditions of the primary components for calcite dissolution under kinetic conditions considering porosity feedback.

Primary components	Units	Initial conditions	Boundary condition
pH	–	9.38	3
–	–	9.38	3
Ca	mol/kg$_{\text{water}}$	1.56×10^{-4}	9.97×10^{-5}
C(4)	mol/kg$_{\text{water}}$	2.56×10^{-4}	9.97×10^{-3}
S(6)	mol/kg$_{\text{water}}$	9.97×10^{-11}	6.44×10^{-4}

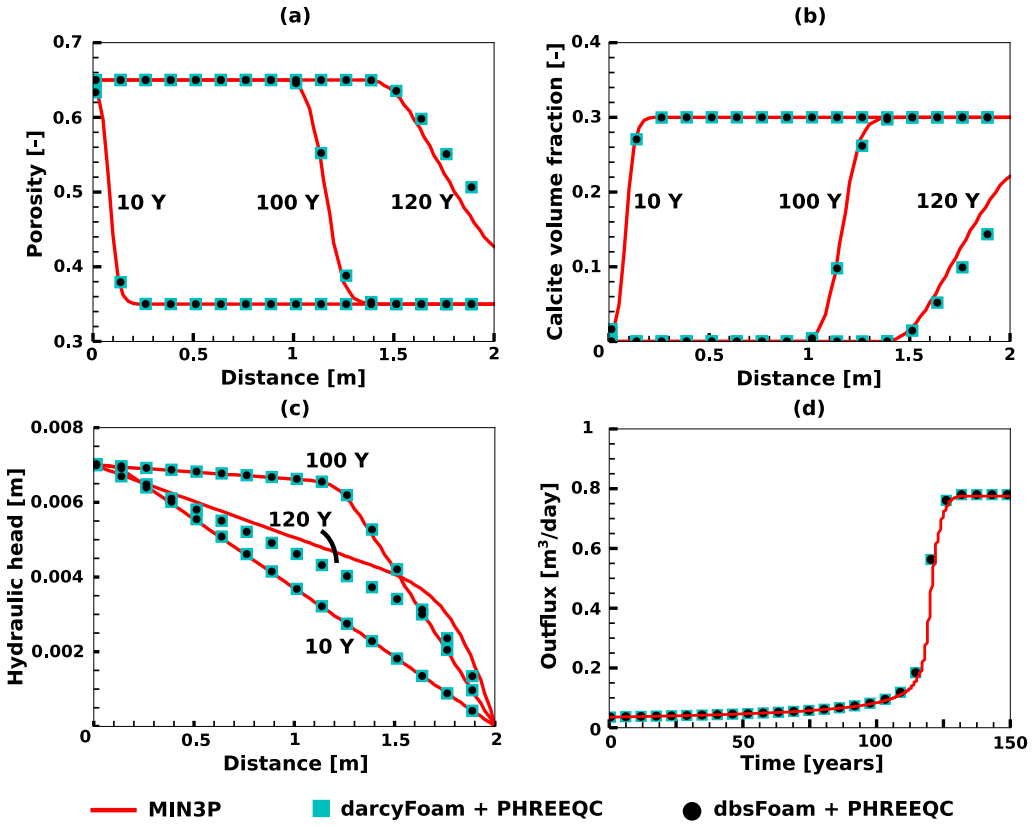

Fig. 2. Calcite dissolution under kinetic conditions considering feedback of porous media properties. Evolution of (a) porosity, (b) calcite volume fraction, (c) hydraulic head along the channel and (d) evolution of outflux. MIN3P data is from Xie et al. (2015) for comparison.

those of MIN3P which demonstrates the ability of our platform to simulate hydro-geochemical processes with porosity feedback.

3.2. Verification at the pore-scale

In this section, we highlight the capabilities of our OpenFOAM package to model hydro-geochemical interactions occurring at the pore-scale using PHREEQC.

In *porousMedia4Foam*, pore-scale simulations are run using the micro-continuum approach through the flow solver dbsFoam. At the pore-scale, the reaction rates are directly applied at the fluid-mineral interface that is described explicitly in the computational grid using the mineral volume fraction. The micro-continuum approach has been used to simulate the dissolution of a calcite crystal at the pore-scale and compared successfully with microfluidic experiments (Soulaine et al., 2017). In Molins et al. (2020), the approach is compared with state-of-the-art RTM at the pore-scale using various numerical techniques including Chombo-Cruch with Level-Set (Molins et al., 2017), Lattice Boltzmann Method (Prasianakis et al., 2018), dissolFoam moving grids with conformal mapping (Starchenko et al., 2016), and Vortex methods (Sanchez et al., 2019). The benchmark consists of a 0.2 mm diameter calcite crystal posted in a 1 mm long 0.5 width channel (see Fig. 3). An acidic solution of pH = 2 is continuously injected from the inlet at a rate of $U_{\text{inj}} = 1.2 \times 10^{-3}$ m/s. The calcite crystal dissolution is described considering a kinetic rate,

$$r = A_{\text{calcite}}(k_{\text{calcite}}\gamma)c_{H^+}, \tag{14}$$

where r is the reaction rate in mol/m^3/s, A_{calcite} is the reactive surface area in m^2/m^3 computed using the volume-of-solid approach (see Table 4), $(k_{\text{calcite}}\gamma) = 0.89 \times 10^{-3}$ m/s is the reaction rate constant of calcite and, c_{H^+} is the concentration of H^+ in mol/m^3. This reaction rate may not be fully representative of the underlying geochemical processes. It has been chosen in Molins et al. (2020) to demonstraste the ability of various approaches to move the fluid-mineral interface according to geochemical processes. All the numerical methods were able to capture accurately the shape evolution of the calcite crystal, giving confidence in pore-scale simulators for moving fluid-mineral interfaces along with geochemical processes.

Actually, in Soulaine et al. (2017) and Molins et al. (2020), the micro-continuum approach, dbsFoam, was combined with the

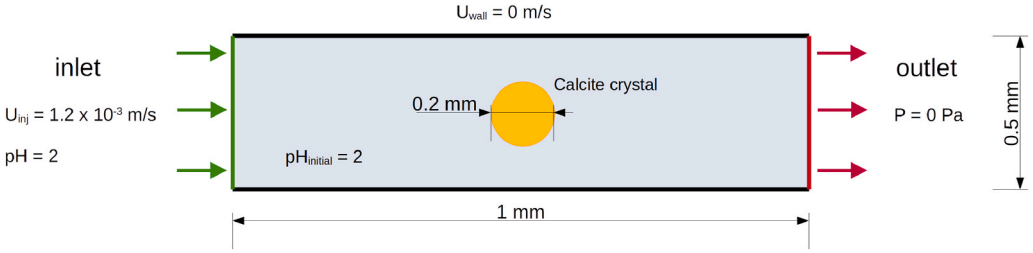

Fig. 3. The considered model set-up along with initial and boundary conditions to investigate calcite grain dissolution in a microchannel.

geochemical package simpleFirstOrderKineticsMole (see Table 2) that solves Eq. (14) using OpenFOAM's internal engines. This limits drastically the applicability of the approach to comprehensive reaction networks. In this section, we reproduce the two-dimensional case presented in Molins et al. (2020) using dbsFoam and phreeqcRM to demonstrate the robustness of our coupling between OpenFOAM and PHREEQC at the pore-scale. The kinetic rate in PHREEQC input file has been modified to match Eq. (14). The system is spatially discretized using a Cartesian mesh of 128×64 cells. The simulation is run for 45 minutes using a time step size $\Delta t = 5$ ms.

The shape evolution of the calcite grain determined by the two approaches matches perfectly (Fig. 4) which verifies, therefore, that in our modelling plateform, PHREEQC can be used to model hydro-geochemical interactions occurring at the pore-scale. This gives us confidence for further investigations that rely on more complex reactive transport phenomena occurring at the pore-scale.

4. Hybrid-scale simulation in fractured porous media

In most subsurface environments, fractures intercept porous media domains. These fractures act as free-flow zones transporting substantial quantities of fluids alongside chemical species compared to the flow and transport that occur within the porous medium (Noiriel et al., 2007; Ajo-Franklin et al., 2018). The complex interplay between advection, diffusion, and reaction can lead to very different dissolution and precipitation patterns. For example, Poonoosamy et al. (2020) uses micro-Raman spectroscopy to visualise the replacement of celestite with barite in a fractured porous media flooded with a solution that contains barium ions. They observe that the mineral replacement occurs either uniformly or at the vicinity of the fracture-matrix interface. This difference in the mineral distribution was attributed to the injection flow rates leading to advection or diffusion-dominated transport.

We investigate such a multiscale system, where a fracture is sandwiched in between a reactive porous matrix made of 50% celestite ($SrSO_4$) having specific reactive surface area of $A_0 = 20000$ m^2/m^3 as shown in Fig. 5. The fracture has a length of $\ell = 0.03$ m and height $h = 0.002$ m. Transport phenomena in the fracture is fully resolved, i.e. the flow is governed by Navier-Stokes equations whereas the flow in the matrix is described by Darcy's law. This hybrid-scale case is modelled using the dbsFoam solver. The initial porosity and permeability of the porous medium are $\varphi_0 = 0.5$ and $k_0 = 10^{-12}$ m^2, respectively. A solution containing 300 mol/m^3 of barium (Ba^{2+}) is continuously injected through the inlet at a constant velocity U_{inj} for 200 hours. The dispersivity of species within the porous matrix are taken into account considering linear dispersion law (Table 5) with molecular diffusion set to $D_j = 10^{-9}$ m^2/s, hydrodynamic dispersion coefficient set to $\alpha_L = 10^{-5}$ m and tortuosity exponent set to $n = 2$. Once the barium ions reach the porous matrix, celestite dissociates into strontium (Sr^{2+}) and sulphate (SO_4^{2-}) ions. The barium ions react with sulphate ions resulting in the precipitation of barite ($BaSO_4$) according to the following reaction (Poonoosamy et al., 2018),

$$Ba^{2+} + SrSO_4 \rightarrow BaSO_4 + Sr^{2+}. \quad (15)$$

Celestite dissolution is taken into account considering kinetics with $k_{\text{celestite}} = 10^{-5.66}$ mol/m^2/s whereas, barite precipitation is accounted considering phase equilibrium. Celestite reactive surface area evolves linearly with its volume fraction. The matrix permeability is updated according to Kozeny-Carman.

We investigate the ongoing hydrogeochemistry within this system considering two different injection velocities, $U_{\text{inj}} = 10^{-2}$ m/s and $U_{\text{inj}} = 10^{-6}$ m/s. The Péclet number, $Pe = U_{\text{inj}}\ell/D_j$ (where the reference length-scale is the fracture aperture), characterizes the importance of advection with respect to diffusion within the fracture. The highest velocity corresponds to advection-dominated transport ($Pe \approx 10^4$) while the lowest corresponds to diffusion-dominated regime ($Pe \approx 1$). For both cases, the second Damkhöler number that determines the timescale of reaction with respect to the timescale of species diffusion at the mineral surface is $Da_{II} = k_{\text{celestite}}\ell/(c_{Ba^{2+}} D_j) \approx 3.6 \times 10^{-4}$ (where the reference length-scale is the inverse of the specific surface area, $\ell = A_0^{-1}$, according to Soulaine et al. (2017)).We notice differences in the pattern of celestite dissolution and barite precipitation whether the transport in the fracture is dominated by advection or by diffusion in agreement with Poonoosamy et al. (2020) observations (Fig. 6). For advection dominated regime ($Pe > 1$), there are two characteristic timescales for the solute transport: first, the barium ions flow through the fracture by advection, then they diffuse laterally into the matrix. Because of the timescale contrast between the two processes, the concentration profile of barium ions is uniform along the porous matrix which leads to a uniform pattern of celestite dissolution and barite precipitation as seen in Figs. 6 and 7. For diffusion-dominated regimes ($Pe \leq 1$), the characteristic transport timescales both in the fracture and in the matrix are of the same order of magnitude. Therefore, the front of barium ions in the matrix follows the

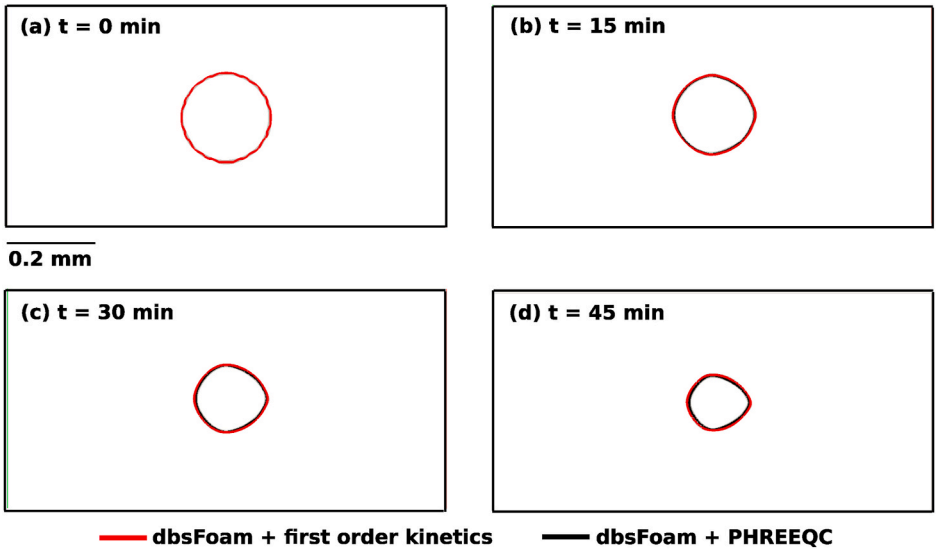

Fig. 4. Evolution of the shape of the calcite grain as a function of time ((a) t = 0 min, (b) t = 15 min, (c) t = 30 min and (d) t = 45 min) predicted by dbsFoam + first order kinetics geochemical module (simpleFirstOrderKineticsMole, red line) and dbsFoam + PHREEQC (phreeqcRM geochemical module of *porousMedia4Foam*, black line). The red and black lines represent cells having calcite volume fraction of 0.5.

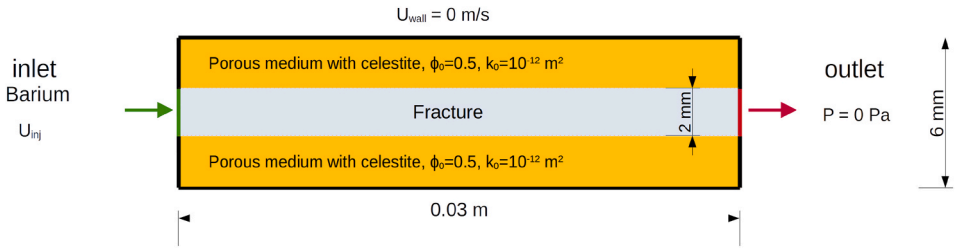

Fig. 5. Numerical set-up for the hybrid-scale case study. A fracture is sandwiched in between two layers of reactive porous medium. The reactive porous medium comprises of celestite. Barium is injected at the inlet. We investigate this scenario considering two different injection velocities, $U_{\text{inj}} = 10^{-2}$ m/s and $U_{\text{inj}} = 10^{-6}$ m/s.

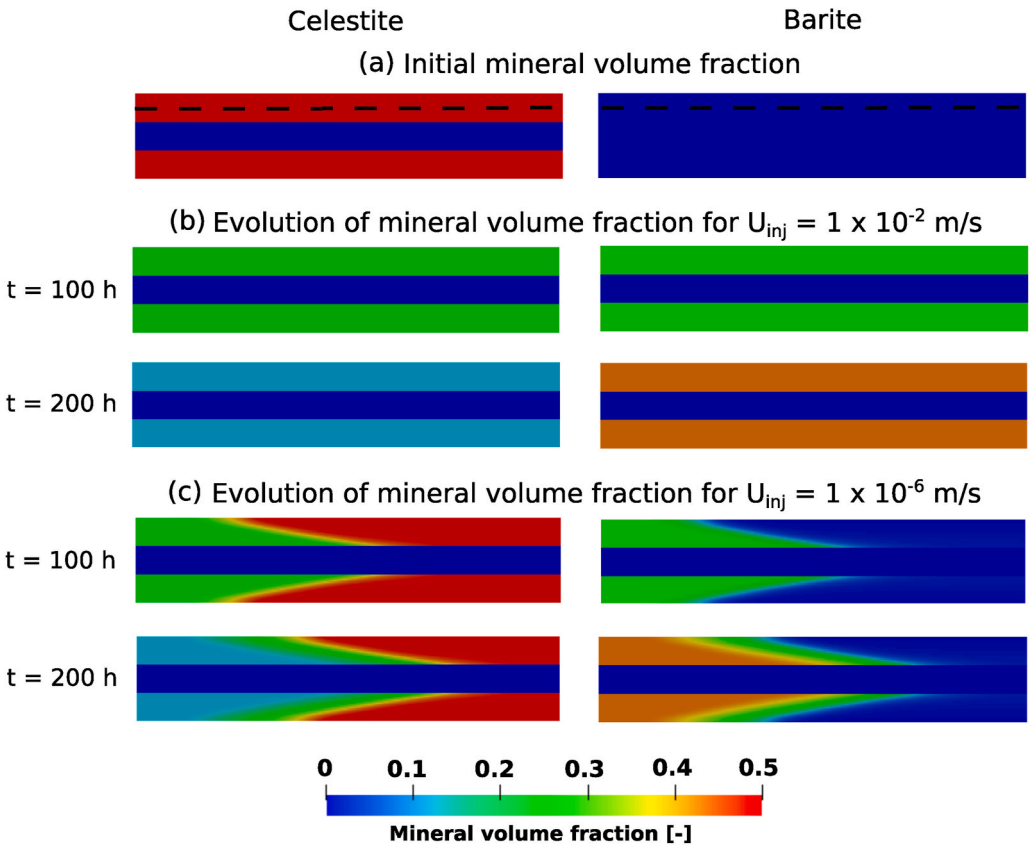

Fig. 6. Evolution of mineral volume fractions - celestite on the left and barite on the right - at different injection velocities. (a) Initial (t = 0 s) mineral volume fractions. (b) Mineral volume fractions at 100 h and 200 h for $U_{\text{inj}} = 1 \times 10^{-2}$ m/s, and (c) mineral volume fractions at 100 h and 200 h for $U_{\text{inj}} = 1 \times 10^{-6}$ m/s.

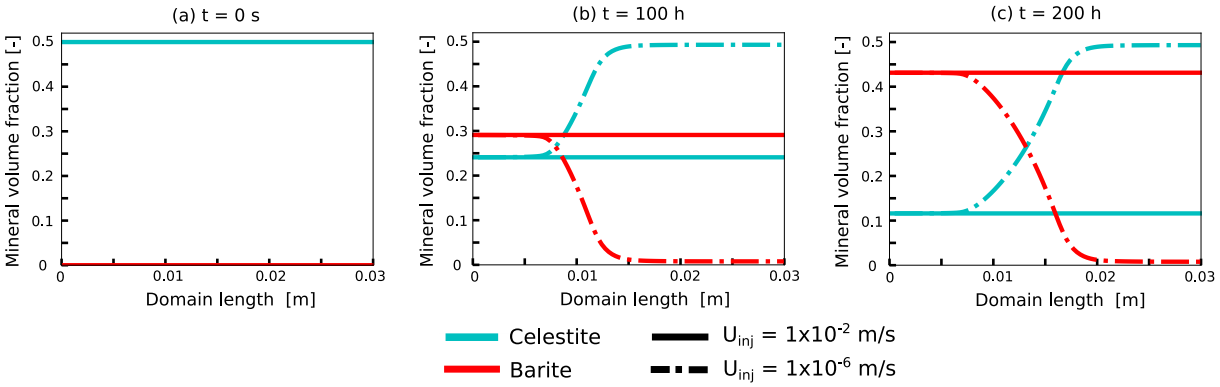

Fig. 7. Plots comparing the mineral volume fractions of celestite and barite at three different time intervals (a) t = 0 s, (b) t = 100 h and (c) t = 200 h for different injection velocities. The mineral volume fraction data is collected along the length of the domain at a distance of 0.001 m from the top wall boundary as highlighted by dashed black line in Fig. 6 (see initial mineral volume fraction).

diffusive front within the fracture. Subsequently, we observe mineral dissolution (celestite) and precipitation (barite) fronts within the porous matrix (Figs. 6 and 7).

This illustration emphasizes the capabilities of *porousMedia4Foam* to model dual-porosity systems in reactive environments using hybrid-scale approach. Our platform is therefore a powerful tool to complement and augment reactive transport experiments including high-resolution imaging of the evolution the fracture aperture including the effect of the weathered zone (Noiriel et al., 2007; Noiriel et al., 2009; Ajo-Franklin et al., 2018; Deng et al., 2020) and two-scale reactive microfluidic experiments (Poonoosamy et al., 2020; Nissan et al., 2021; Osselin et al., 2016).

In a logic of cascade of scales nested within each other, fractured porous media can be modelled by: *i)* pore-scale approaches, *ii)* discrete fracture networks, *iii)* dual porosity models. The hybrid-scale approach that we propose in this paper is intermediate between a full pore-scale description in which the fracture and the pores in the matrix are fully resolved and a discrete fracture network in which the matrix is modelled as a porous medium and the fractures as discrete elements that exchange matter with the matrix. The hybrid-scale approach is therefore crucial to characterize and improve the effective parameters (e.g. transfer functions between the porous matrix and the fracture) used in discrete fracture networks and larger-scale models.

5. Conclusion

We developed an integrated open-source simulator to model hydro-geochemical processes at various scales of interest including pore-scale and reservoir-scale. The simulation platform is part of *porousMedia4-Foam*, a package that solves flow and transport in porous media using the open-source library OpenFOAM. The modelling framework handles complex reactions network as a function of flow conditions, water composition and minerals distribution within the rock including the complex porosity feedback between flow and chemistry. Moreover, *porousMedia4Foam* benefits from all features of OpenFOAM libraries. Hence, the code is fully parallel and handles structured as well as unstructured grids in one, two and three dimensions. The interface between the flow simulator and the geochemistry is generic and can be used to couple a large variety of geochemical packages. In this paper, we illustrated the hydro-geochemical capabilities of the coupled solver using PHREEQC.

Unlike other reactive transport simulators, *porousMedia4Foam* is multi-scale, i.e. a unique flow solver describes transport processes both at the continuum-scale and the pore-scale. Importantly, the two scales can be solved simultaneously in geological formations that feature large contrast of permeability and porosity. For example, in fractured rocks, *porousMedia4Foam* solves Stokes flow in the fracture network and Darcy's law in the porous matrix. This multi-scale model is achieved using the micro-continuum approach, hybrid-scale approach based on the Darcy-Brinkman-Stokes equation. Indeed, this approach is intermediate between a pure Navier-Stokes description of the transport for which all the porosity is fully resolved and pure continuum-scale modeling based on Darcy's law. Besides this hybrid-scale approach, *porousMedia4Foam* also includes a standard Darcy solver for continuum-scale simulations. Therefore, the same simulator can be used to simulate flow, transport, and geochemical reactions in an reservoir and in 3D micro-tomography images.

The coupled hydro-geochemical simulator was verified by running cases for which reference solutions exist. These solutions are well-established and used in the reactive transport community to benchmark state-of-the-art codes available both at the continuum-scale (Xie et al., 2015) and at the pore-scale (Molins et al., 2020). Finally, we demonstrated the ability of our advanced modelling framework to simulate dissolution and precipitation processes in fractured porous media at the pore-scale using the hybrid-scale approach. Here, the reactive medium consisted of celestite grains that reacted with a barium chloride solution injected into the system, leading to the dissolution of celestite and the growth of barite. We observed differences in mineral precipitation - dissolution patterns by varying the injection rates.

Because *porousMedia4Foam* has already capabilities for modelling two-phase flow in porous media both at the pore- and Darcy's scales using two-phase micro-continuum technique (Soulaine et al., 2019; Soulaine et al., 2018; Carrillo et al., 2020), true multiscale and multi-phase RTM is envisioned to be implemented in *porousMedia4Foam* framework.

Software and data availability

porousMedia4Foam, the software introduced in this paper is built using open-source libraries including OpenFOAM and PHREEQC. The source code and the cases presented in the paper are available on GitHub (https://github.com/csoulain/porousMedia4Foam).

Contributions of the authors

CS is the *porousMedia4Foam* architect. CS and SP implemented new models in *porousMedia4Foam* and corrected bugs. SP and CT designed and setup the benchmark problems. SP run the simulations. CS, SP, CT and FC discussed, interpreted the results and wrote the paper. CS, CT and FC applied for funding.

Declaration of competing interest

The authors declare that they have no known competing financial interests or personal relationships that could have appeared to influence the work reported in this paper.

Acknowledgments

The research leading to these results has received funding from the French Agency for Research (Agence Nationale de la Recherche, ANR) through the labex Voltaire ANR-10-LABX-100-01, the grant CATCH ANR-18-CE05-0035, and through the FraMatI project under contract ANR-19-CE05-0002. It has also received financial support from the CNRS through the MITI interdisciplinary programs. This project has received funding from the European Union's Horizon 2020 research and innovation programme under grant agreements No 847593 (WP DONUT) and No 850626 (REFLECT Project). SP postdoctoral fellowship was funded by BRGM through the PORE-REACTIF project from the Alliance Nationale de Coordination de la Recherche pour l'Energie (ANCRE). The authors benefitted from the use of the cluster at the Centre de Calcul Scientifique en région Centre-Val de Loire.

References

Ajo-Franklin, J., Voltolini, M., Molins, S., Yang, L., 2018. Coupled processes in a fractured reactive system: a dolomite dissolution study with relevance to GCS caprock integrity. Caprock Integrity in Geological Storage: Hydrogeochemical and Hydrogeomechanical Processes and Their Impact on Storage Security. Wiley Publishing, New York.

Andrä, H., Combaret, N., Dvorkin, J., Glatt, E., Han, J., Kabel, M., Keehm, Y., Krzikalla, F., Lee, M., Madonna, C., Marsh, M., Mukerji, T., Saenger, E.H., Sain, R., Saxena, N., Ricker, S., Wiegmann, A., Zhan, X., 2013a. Digital rock physics benchmarks Part I: imaging and segmentation. Comput. Geosci. 50, 25–32. ISSN 0098-3004. https://doi.org/10.1016/j.cageo.2012.09.005. http://www.sciencedirect.com/science/article/pii/S0098300412003147, (benchmark problems, datasets and methodologies for the computational geosciences).

Andrä, H., Combaret, N., Dvorkin, J., Glatt, E., Han, J., Kabel, M., Keehm, Y., Krzikalla, F., Lee, M., Madonna, C., Marsh, M., Mukerji, T., Saenger, E.H., Sain, R., Saxena, N., Ricker, S., Wiegmann, A., Zhan, X., 2013b. Digital rock physics benchmarks Part II: computing effective properties. Comput. Geosci. 50, 33–43. ISSN 0098-3004. https://doi.org/10.1016/j.cageo.2012.09.008. http://www.sciencedirect.com/science/article/pii/S0098300412003172, (benchmark problems, datasets and methodologies for the computational geosciences).

Angot, P., Bruneau, C.-H., Fabrie, P., 1999. A penalization method to take into account obstacles in incompressible viscous flows. Numer. Math. 81 (4), 497–520.

Arns, C., Bauget, F., Limaye, A., Sakellariou, A., Senden, T., Sheppard, A., Sok, R., Pinczewski, W., Bakke, S., Berge, L., Oeren, P.-E., Knackstedt, M., 2005. Pore-scale characterization of carbonates using X-ray microtomography. SPE J. 10 (4), 475–484.
Bear, J., 1972. Dynamics of Fluids in Porous Media. Elsevier, New York. URL Dynamicsoffluidsinporousmedia.
Beavers, G.S., Joseph, D.D., 1967. Boundary conditions at a naturally permeable wall. J. Fluid Mech. 30, 197–207. https://doi.org/10.1017/S0022112067001375.
Békri, S., Thovert, J.-F., Adler, P., 1997. Dissolution and deposition in fractures. Eng. Geol. 48 (3–4), 283–308. https://doi.org/10.1016/S0013-7952(97)00044-6.
Bijeljic, B., Raeini, A., Mostaghimi, P., Blunt, M.J., 2013. Predictions of non-Fickian solute transport in different classes of porous media using direct simulation on pore-scale images. Phys. Rev. E 87, 013011. https://doi.org/10.1103/PhysRevE.87.013011. URL.
Blunt, M.J., Bijeljic, B., Dong, H., Gharbi, O., Iglauer, S., Mostaghimi, P., Paluszny, A., Pentland, C., 2013. Pore-scale imaging and modelling. Adv. Water Resour. 51, 197–216.
Bousquet-Melou, P., Goyeau, B., Quintard, M., Fichot, F., Gobin, D., 2002. Average momentum equation for interdendritic flow in a solidifying columnar mushy zone. ISSN 0017-9310 Int. J. Heat Mass Tran. 45 (17), 3651–3665. https://doi.org/10.1016/S0017-9310(02)00077-7. URL. http://www.sciencedirect.com/science/article/pii/S0017931002000777.
Brinkman, H.C., 1947. A calculation of the viscous force exerted by a flowing fluid on a dense swarm of particles. Appl. Sci. Res. A1, 27–34.
Carman, P.C., 1937. Fluid flow through granular beds. Trans. Inst. Chem. Eng. 15, 150–166.
Carrillo, F.J., Bourg, I.C., 2019. A Darcy-Brinkman-Biot approach to modeling the hydrology and mechanics of porous media containing macropores and deformable microporous regions. Water Resour. Res. 55 (10), 8096–8121. https://doi.org/10.1029/2019WR024712. URL.
Carrillo, F.J., Bourg, I.C., Soulaine, C., 2020. Multiphase flow modeling in multiscale porous media: an open-source micro-continuum approach. J. Comput. Phys. X 8, 100073. https://doi.org/10.1016/j.jcpx.2020.100073. ISSN 2590-0552.
Chen, L., Kang, Q., Robinson, B.A., He, Y.-L., Tao, W.-Q., 2013. Pore-scale modeling of multiphase reactive transport with phase transitions and dissolution-precipitation processes in closed systems. Phys. Rev. E 87, 043306. https://doi.org/10.1103/PhysRevE.87.043306.
Claret, F., Marty, N., Tournassat, C., 2018. Modeling the Long-Term Stability of Multi-Barrier Systems for Nuclear Waste Disposal in Geological Clay Formations. chap. 8. John Wiley & Sons, Ltd. ISBN 9781119060031, 395–451. https://doi.org/10.1002/9781119060031.ch8.
Daccord, G., Lenormand, R., 1987. Fractal patterns from chemical dissolution. Nature 325 (6099), 41–43.
Deng, H., Fitts, J.P., Tappero, R.V., Kim, J.J., Peters, C.A., 2020. Acid erosion of carbonate fractures and accessibility of arsenic-bearing minerals: in operando synchrotron-based microfluidic experiment. Environ. Sci. Technol. 54 (19), 12502–12510. https://doi.org/10.1021/acs.est.0c03736 pMID: 32845141.
DePaolo, D.J., Cole, D.R., 2013. Geochemistry of geologic carbon sequestration: an overview. Rev. Mineral. Geochem. 77 (1), 1–14. https://doi.org/10.2138/rmg.2013.77.1}.
Dutka, F., Starchenko, V., Osselin, F., Magni, S., Szymczak, P., Ladd, A.J., 2020. Time-dependent shapes of a dissolving mineral grain: comparisons of simulations with microfluidic experiments. Chem. Geol. 540, 119459.
Garing, C., Gouze, P., Kassab, M., Riva, M., Guadagnini, A., 2015. Anti-correlated porosity–permeability changes during the dissolution of carbonate rocks: experimental evidences and modeling. Transport Porous Media 107 (2), 595–621.
Golfier, F., Zarcone, C., Bazin, B., Lenormand, R., Lasseux, D., Quintard, M., 2002. On the ability of a Darcy-scale model to capture wormhole formation during the dissolution of a porous medium. J. Fluid Mech. 457, 213–254.
Goyeau, B., Lhuillier, D., Gobin, D., Velarde, M., 2003. Momentum transport at a fluid–porous interface. Int. J. Heat Mass Tran. 46 (21), 4071–4081.
Graveleau, M., Soulaine, C., Tchelepi, H.A., 2017. Pore-scale simulation of interphase multicomponent mass transfer for subsurface flow. Transport Porous Media 120 (2), 287–308.
Guibert, R., Nazarova, M., Horgue, P., Hamon, G., Creux, P., Debenest, G., 2015. Computational permeability determination from pore-scale imaging: sample size, mesh and method sensitivities. Transport Porous Media 107 (3), 641–656. https://doi.org/10.1007/s11242-015-0458-0. ISSN 0169-3913.
Healy, R.W., Haile, S.S., Parkhurst, D.L., Charlton, S.R., 2018. VS2DRTI: simulating heat and reactive solute transport in variably saturated porous media. Ground Water 56 (5), 810–815. https://doi.org/10.1111/gwat.12640.
Horgue, P., Augier, F., Duru, P., Prat, M., Quintard, M., 2013. Experimental and numerical study of two-phase flows in arrays of cylinders. Chem. Eng. Sci. 102, 335–345. https://doi.org/10.1016/j.ces.2013.08.031. ISSN 0009-2509. http://www.sciencedirect.com/science/article/pii/S0009250913005745.
Horgue, P., Soulaine, C., Franc, J., Guibert, R., Debenest, G., 2015. An open-source toolbox for multiphase flow in porous media. ISSN 0010-4655 Comput. Phys. Commun. 187, 217–226. https://doi.org/10.1016/j.cpc.2014.10.005. URL. http://www.sciencedirect.com/science/article/pii/S0010465514003403.
Hsu, C., Cheng, P., 1990. Thermal dispersion in a porous medium. Int. J. Heat Mass Tran. 33 (8), 1587–1597.
Issa, R.I., 1985. Solution of the implicitly discretised fluid flow equations by operator-splitting. J. Comput. Phys. 62, 40–65.
Jacques, D., Simunek, J., Mallants, D., Van Genuchten, M.T., 2008. Modeling coupled hydrologic and chemical processes: long-term uranium transport following phosphorus fertilization. Vadose Zone J. 7 (2), 698–711.
Kozeny, J., 1927. Uber kapillare leitung der wasser in boden, Royal Academy of Science, Vienna, Proc. Class. Irel. 136, 271–306.
Li, L., Maher, K., Navarre-Sitchler, A., Druhan, J., Meile, C., Lawrence, C., Moore, J., Perdrial, J., Sullivan, P., Thompson, A., et al., 2017. Expanding the role of reactive transport models in critical zone processes. Earth Sci. Rev. 165, 280–301.
Lichtner, P.C., 1985. Continuum model for simultaneous chemical reactions and mass transport in hydrothermal systems. Geochem. Cosmochim. Acta 49 (3), 779–800.
Lichtner, P.C., Hammond, G.E., Lu, C., Karra, S., Bisht, G., Andre, B., Mills, R., Kumar, J., 2015. PFLOTRAN user manual: a massively parallel reactive flow and transport model for describing surface and subsurface processes. Tech. Rep., United States. URL. https://www.osti.gov/servlets/purl/1168703.
Liu, X., Ortoleva, P., 1996. A general-purpose, geochemical reservoir simulator. SPE Annual Technical Conference and Exhibition. Society of Petroleum Engineers.
Liu, X., Ormond, A., Bartko, K., Ying, L., Ortoleva, P., 1997. A geochemical reaction-transport simulator for matrix acidizing analysis and design. J. Petrol. Sci. Eng. 17 (1), 181–196.
Maes, J., Geiger, S., 2018. Direct pore-scale reactive transport modelling of dynamic wettability changes induced by surface complexation. Adv. Water Resour. 111, 6–19.
Maes, J., Soulaine, C., 2018. A new compressive scheme to simulate species transfer across fluid interfaces using the Volume-Of-Fluid method. Chem. Eng. Sci. 190, 405–418.
Mayer, K.U., Frind, E.O., Blowes, D.W., 2002. Multicomponent reactive transport modeling in variably saturated porous media using a generalized formulation for kinetically controlled reactions. Water Resour. Res. 38 (9), 13–1.
Molins, S., Trebotich, D., Yang, L., Ajo-Franklin, J.B., Ligocki, T.J., Shen, C., Steefel, C.I., 2014. Pore-scale controls on calcite dissolution rates from flow-through laboratory and numerical experiments. Environ. Sci. Technol. 48 (13), 7453–7460.
Molins, S., Trebotich, D., Miller, G.H., Steefel, C.I., 2017. Mineralogical and transport controls on the evolution of porous media texture using direct numerical simulation. Water Resour. Res. 53 (5), 3645–3661.
Molins, S., Trebotich, D., Arora, B., Steefel, C.I., Deng, H., 2019. Multi-scale model of reactive transport in fractured media: diffusion limitations on rates. Transport Porous Media 128 (2), 701–721.
Molins, S., Soulaine, C., Prasianakis, N., Abbasi, A., Poncet, P., Ladd, A., Starchenko, V., Roman, S., Trebotich, D., Tchelepi, H., Steefel, C., 2020. Simulation of mineral dissolution at the pore scale with evolving fluid-solid interfaces: review of approaches and benchmark problem set. Comput. Geosci. 1–34ISSN 1573–1499.
Moortgat, J., Li, M., Amooie, M., Zhu, D., 2020. A higher-order finite element reactive transport model for unstructured and fractured grids. Sci. Rep. 10, 15572. https://doi.org/10.1038/s41598-020-72354-3.
Muniruzzaman, M., Rolle, M., 2019. Multicomponent ionic transport modeling in physically and electrostatically heterogeneous porous media with PhreeqcRM coupling for geochemical reactions. Water Resour. Res. 55 (12), 11121–11143. https://doi.org/10.1029/2019WR026373. URL.
Muniruzzaman, M., Karlsson, T., Ahmadi, N., Rolle, M., 2020. Multiphase and multicomponent simulation of acid mine drainage in unsaturated mine waste: modeling approach, benchmarks and application examples. ISSN 0883-2927 Appl. Geochem. 120, 104677. https://doi.org/10.1016/j.apgeochem.2020.104677. URL. https://www.sciencedirect.com/science/article/pii/S0883292720301682.
Neale, G., Nader, W., 1974. Practical significance of Brinkman's extension of Darcy's law: coupled parallel flows within a channel and a bounding porous medium. Can. J. Chem. Eng. 52 (4), 475–478.
Apourvari, S.N., Arns, C.H., 2004. An Assessment of the Influence of Micro-porosity for Effective Permeability Using Local Flux Analysis on Tomographic Images. In: International Petroleum Technology Conference, 19-22 January, Doha, Qatar.
Noiriel, C., Madé, B., Gouze, P., 2007. Impact of coating development on the hydraulic and transport properties in argillaceous limestone fracture. Water Resour. Res. 43 (9), 1–16.
Nissan, A., Alcolombri, U., de Schaetzen, F., Berkowitz, B., Jimenez-Martinez, J., 2021. Reactive transport with fluid–solid interactions in dual-porosity media. ACS EST Waterhttps://doi.org/10.1021/acsestwater.0c00043. ISSN 2690-0637.
Noiriel, C., Luquot, L., Madé, B., Raimbault, L., Gouze, P., van der Lee, J., 2009. Changes in reactive surface area during limestone dissolution: an experimental and modelling study. Chem. Geol. 265 (1–2), 160–170. ISSN 0009-2541. https://doi.org/10.1016/j.chemgeo.2009.01.032. http://www.sciencedirect.com/science/article/pii/S0009254109000643. cO2 geological storage: Integrating geochemical, hydrodynamical, mechanical and biological processes from the pore to the reservoir scale.
Noiriel, C., Soulaine, C., 2021. Pore-scale imaging and modelling of reactive flow in evolving porous media: tracking the dynamics of the fluid-rock interface. Transport Porous Mediahttps://doi.org/10.1007/s11242-021-01613-2.
Ochoa-Tapia, J.A., Whitaker, S., 1995. Momentum transfer at the boundary between a porous medium and a homogeneous fluid: I. Theoretical development. Int. J. Heat Mass Tran. 38 (14), 2635–2646.
Orgogozo, L., Renon, N., Soulaine, C., Hénon, F., Tomer, S., Labat, D., Pokrovsky, O., Sekhar, M., Ababou, R., Quintard, M., 2014. An open source massively parallel solver for Richards equation: mechanistic modelling of water fluxes at the watershed scale. ISSN 0010-4655 Comput. Phys. Commun. 185 (12), 3358–3371. https://doi.org/10.1016/j.cpc.2014.08.004. URL. http://www.sciencedirect.com/science/article/pii/S0010465514002719.
Ormond, A., Ortoleva, P., 2000. Numerical modeling of reaction-induced cavities in a porous rock. J. Geophys. Res.: Solid Earth 105 (B7), 16737–16747.
Osselin, F., Kondratiuk, P., Budek, A., Cybulski, O., Garstecki, P., Szymczak, P., 2016. Microfluidic observation of the onset of reactive-infiltration instability in an analog fracture. Geophys. Res. Lett. 43, 6907–6915. https://doi.org/10.1002/2016gl069261. ISSN 0094-8276.

Parkhurst, D., Appelo, C., 2013. Description of input and examples for PHREEQC Version 3—a computer program for speciation, batch-reaction, one-dimensional transport, and inverse geochemical calculations, 6-A43. U.S. Department of the Interior, U.S. Geological Survey Techniques and Methods.

Parkhurst, D.L., Wissmeier, L., 2015. PhreeqcRM: a reaction module for transport simulators based on the geochemical model PHREEQC. Adv. Water Resour. 83, 176–189.

Patankar, S.V., 1980. Numerical Heat Transfer and Fluid Flow. Taylor & Francis, Washington, DC.

Pavuluri, S., Maes, J., Yang, J., Regaieg, M., Moncorgé, A., Doster, F., 2020. Towards pore network modelling of spontaneous imbibition: contact angle dependent invasion patterns and the occurrence of dynamic capillary barriers. Comput. Geosci. 24, 951–969. https://doi.org/10.1007/s10596-019-09842-7.

Poonoosamy, J., Wanner, C., Alt Epping, P., Águila, J.F., Samper, J., Montenegro, L., Xie, M., Su, D., Mayer, K.U., Mäder, U., Van Loon, L.R., Kosakowski, G., 2018. Benchmarking of reactive transport codes for 2D simulations with mineral dissolution–precipitation reactions and feedback on transport parameters. Comput. Geosci. 1–22. https://doi.org/10.1007/s10596-018-9793-x.

Poonoosamy, J., Soulaine, C., Burmeister, A., Deissmann, G., Bosbach, D., Roman, S., 2020. Microfluidic flow-through reactor and 3D Raman imaging for in situ assessment of mineral reactivity in porous and fractured porous media. Lab-on-a-Chip 20 (14), 2562–2571. https://doi.org/10.1039/d0lc00360c.

Prasianakis, N.I., Gatschet, M., Abbasi, A., Churakov, S.V., 2018. Upscaling strategies of porosity-permeability correlations in reacting environments from pore-scale simulations, 2018 Geofluids 1–8. https://doi.org/10.1155/2018/9260603. ISSN 1468-8115.

Raeini, A.Q., Blunt, M.J., Bijeljic, B., 2014. Direct simulations of two-phase flow on micro-CT images of porous media and upscaling of pore-scale forces. Adv. Water Resour. 74, 116–126. ISSN 0309-1708, URL. http://www.sciencedirect.com/science/article/pii/S0309170814001730.

Rolle, M., Sprocati, R., Masi, M., Jin, B., Muniruzzaman, M., 2018. Nernst-Planck-based description of transport, coulombic interactions, and geochemical reactions in porous media: modeling approach and benchmark experiments. Water Resour. Res. 54 (4), 3176–3195. https://doi.org/10.1002/2017WR022344. URL.

Roman, S., Soulaine, C., AlSaud, M.A., Kovscek, A., Tchelepi, H., 2016. Particle velocimetry analysis of immiscible two-phase flow in micromodels. ISSN 0309-1708 Adv. Water Resour. 95, 199–211. https://doi.org/10.1016/j.advwatres.2015.08.015. URL. http://www.sciencedirect.com/science/article/pii/S0309170815002018.

Sanchez, D., Hume, L., Chatelin, R., Poncet, P., 2019. Analysis of the 3D non-linear Stokes problem coupled to transport-diffusion for shear-thinning heterogeneous microscale flows, applications to digital rock physics and mucociliary clearance. Math. Model.Numer. Anal. 53 (1124), 1083. https://doi.org/10.1051/m2an/2019013. ISSN 0764-583X.

Scheibe, T.D., Perkins, W.A., Richmond, M.C., McKinley, M.I., Romero-Gomez, P.D.J., Oostrom, M., Wietsma, T.W., Serkowski, J.A., Zachara, J.M., 2015. Pore-scale and multiscale numerical simulation of flow and transport in a laboratory-scale column. ISSN 1944-7973, doi:10.1002/2014WR015959 Water Resour. Res. 51 (2), 1023–1035. https://doi.org/10.1002/2014WR015959. URL.

Seigneur, N., Lagneau, V., Corvisier, J., Dauzères, A., 2018. Recoupling flow and chemistry in variably saturated reactive transport modelling - an algorithm to accurately couple the feedback of chemistry on water consumption, variable porosity and flow. ISSN 0309-1708 Adv. Water Resour. 122, 355–366. https://doi.org/10.1016/j.advwatres.2018.10.025. URL. https://www.sciencedirect.com/science/article/pii/S0309170818306304.

Seigneur, N., Mayer, K.U., Steefel, C.I., 2019. Reactive transport in evolving porous media. Rev. Mineral. Geochem. 85 (1), 197–238. https://doi.org/10.2138/rmg.2019.85.7.

Soulaine, C., Tchelepi, H.A., 2016. Micro-continuum approach for pore-scale simulation of subsurface processes. Transport Porous Media 113, 431–456. https://doi.org/10.1007/s11242-016-0701-3.

Soulaine, C., Davit, Y., Quintard, M., 2013. A two-pressure model for slightly compressible single phase flow in bi-structured porous media. ISSN 0009-2509 Chem. Eng. Sci. 96, 55–70. https://doi.org/10.1016/j.ces.2013.03.060. URL. http://www.sciencedirect.com/science/article/pii/S0009250913002492.

Soulaine, C., Gjetvaj, F., Garing, C., Roman, S., Russian, A., Gouze, P., Tchelepi, H., 2016. The impact of sub-resolution porosity of X-ray microtomography images on the permeability. Transport Porous Media 113 (1), 227–243. https://doi.org/10.1007/s11242-016-0690-2.

Soulaine, C., Roman, S., Kovscek, A., Tchelepi, H.A., 2017. Mineral dissolution and wormholing from a pore-scale perspective. J. Fluid Mech. 827, 457–483. https://doi.org/10.1017/jfm.2017.499.

Soulaine, C., Roman, S., Kovscek, A., Tchelepi, H.A., 2018. Pore-scale modelling of multiphase reactive flow. Application to mineral dissolution with production of CO2. J. Fluid Mech. 855, 616–645. https://doi.org/10.1017/jfm.2018.655.

Soulaine, C., Creux, P., Tchelepi, H.A., 2019. Micro-continuum framework for pore-scale multiphase fluid transport in shale formations. Transport Porous Media 127, 85–112.

Soulaine, C., Maes, J., Roman, S., 2021. Computational microfluidics for geosciences. Frontiers in Water 3, 1–11. https://doi.org/10.3389/frwa.2021.643714.

Spanne, P., Thovert, J., Jacquin, C., Lindquist, W., Jones, K., Adler, P., 1994. Synchrotron computed microtomography of porous media: topology and transports. Phys. Rev. Lett. 73 (14), 2001.

Starchenko, V., Marra, C.J., Ladd, A.J., 2016. Three-dimensional simulations of fracture dissolution. J. Geophys. Res.: Solid Earth 121, 6421–6444. https://doi.org/10.1002/2016JB013321.

Steefel, C., Appelo, C., Arora, B., Jacques, D., Kalbacher, T., Kolditz, O., Lagneau, V., Lichtner, P., Mayer, K.U., Meeussen, J., et al., 2015a. Reactive transport codes for subsurface environmental simulation. Comput. Geosci. 19 (3), 445–478.

Steefel, C.I., Beckingham, L.E., Landrot, G., 2015b. Micro-continuum approaches for modeling pore-scale geochemical processes. Rev. Mineral. Geochem. 80, 217–246. https://doi.org/10.2138/rmg.2015.80.07.

Strang, G., 1968. On the construction and comparison of difference schemes. SIAM J. Numer. Anal. 5 (3), 506–517. ISSN 00361429, URL. http://www.jstor.org/stable/2949700.

Tartakovsky, A.M., Meakin, P., Scheibe, T.D., West, R.M.E., 2007. Simulations of reactive transport and precipitation with smoothed particle hydrodynamics. J. Comput. Phys. 222 (2), 654–672.

Vafai, K., Tien, C., 1981. Boundary and inertia effects on flow and heat transfer in porous media. Int. J. Heat Mass Tran. 24 (2), 195–203.

Verma, A., Pruess, K., 1988. Thermohydrological conditions and silica redistribution near high-level nuclear wastes emplaced in saturated geological formations. J. Geophys. Res.: Solid Earth 93 (B2), 1159–1173. https://doi.org/10.1029/JB093iB02p01159. URL.

Whitaker, S., 1999. The Method of Volume Averaging, vol. 13. Kluwer Academic, Dorderecht of Theory and Applications of Transport in Porous Media.

Xie, M., Mayer, K.U., Claret, F., Alt-Epping, P., Jacques, D., Steefel, C., Chiaberge, C., Simunek, J., 2015. Implementation and evaluation of permeability-porosity and tortuosity-porosity relationships linked to mineral dissolution-precipitation. Comput. Geosci. 19 (3), 655–671.

Xu, T., Sonnenthal, E., Spycher, N., Pruess, K., 2006. TOUGHREACT—a simulation program for non-isothermal multiphase reactive geochemical transport in variably saturated geologic media: applications to geothermal injectivity and CO2 geological sequestration. ISSN 0098-3004 Comput. Geosci. 32 (2), 145–165. https://doi.org/10.1016/j.cageo.2005.06.014. URL. http://www.sciencedirect.com/science/article/pii/S0098300405001500.

Part C: Fracture mechanics and scale transition schemes for coupled THM processes

[2,1]Yoshioka, K., [1]Mollaali, M., J., [1]Ziaei-Rad, V., [1,3]You, T.,

[1]Wang, W., [1,4]Kolditz, O.

With contributions to Task 2 and 4 by

[1]Buchwald, J., [1]Grunwald, N., [3,1]Naumov, D., [3,1]Nagel, Th.

[1]UFZ, Helmholtz Centre for Environmental Research, Germany

[2]MUL, Montanuniversität Leoben, Austria

[3]TUBAF, Technische Universität Bergakademie Freiberg, Germany

[4]TUDD, Dresden University of Technology, Germany

The project leading to this application has received funding from the European Union's Horizon 2020 research and innovation programme under grant agreement No 847593.

Abstract

The UFZ team, in close collaboration with Technische Universität Bergakademie Freiberg, Montanuniversität Leoben, and Dresden University of Technology, has been involved in several tasks of DONUT. High performance computing methods were developed by MPI and OpenMP parallelizations especially for the phase field method and successfully applied for the interpretation of laboratory and field experiments (Task 2). The HPC simulations were performed on different HPC platforms for example on Tier 1 (JUWELS at FZJ) and Tier 3 (EVE at UFZ). This also improved the robustness of HPC methods on different computer architectures. In Task 2, methods of scaling numerical methods for fracture mechanics processes from the laboratory to the field scale were developed. This was based on the variational phase field method, which can be used to represent fracture mechanics processes at different scales. The scaling method was successfully applied to experimental data from the underground research laboratory Mont Terri (Switzerland) (CD-A experiment). In Task 4, methods for the quantification of uncertainties for coupled THM processes were developed and also successfully applied to an experiment in Mont Terri (FE experiment). Originally, the UFZ had only planned contributions in Task 3. Due to the dynamic development of the OpenGeoSys platform, the field of activity could also be extended into Tasks 2 and 4. As a result, numerous publications were published in high-ranking international journals.

Significance Statement

The UFZ team contributions to EURAD DONUT, in close Technische Universität Bergakademie Freiberg, Montanuniversität Leoben, and Dresden University of Technology are important in multiple ways. First, new methods for fracture mechanical THM processes were developed and verified with laboratory and field data. Thus, the mechanical integrity of the multi-barrier system (geotechnical and geological barrier) can be better evaluated in the future and is an important contribution for future safety and performance analyses. Furthermore, the numerical methods could be scaled from laboratory to field scale using HPC. Thus, the numerical methodology gains significantly in practical relevance. Verification was performed using laboratory and field experiments (underground research laboratory Mont Terri, Switzerland). Last but not least, the developments have been incorporated into the open source platform OpenGeoSys and will be available to the community in the future. A number of test examples have been made available for the OGS benchmark collection as Jupyter notebooks.

Table of Content

List of figures

List of Tables

Glossary

DECOVALEX	DEvelopment of COupled models and their VALidation against Experiments
OGS	OpenGeoSys
MPI	multiple passing language
VPF	variational phase field method

1. Variational Phase Field Method for Fracture Mechanics

We briefly introduce the basics of variational phase field (VPF) method here (section 1) which provides the basis for multi-scale analysis of fracture processes in barrier materials. In section 2 we conduct a fracture process studies based on experimental data which have been produced in the DECOVALEX 2023 project before applying the VPF method to laboratory experiments (section 3) and field experiments in the Underground Research Laboratory in Mont Terri (section 4). High-Performance-Computing (section 5) and uncertainty analysis (section 6) have been supporting the multi-scale analysis of fracture processes in Task 3 of WP DONUT.

1.1 Introduction

Fracture opening (aperture) is typically happening in the order of the micro meters scale while the fracture length is several orders of magnitude higher (i.e. meters). This disproportional aspect ratio poses a great challenge for numerical discretization in finite element methods as most existing numerical formulations are not very forgiving to high aspect ratio elements. In the numerical simulation of fractures, phase-field models have become exceptionally popular in the last couple of decades because of their capabilities to accurately handle sharp interfaces (fractures or faults) in a diffused manner. This diffused or smeared representation of fracture enabled the model to have expanded its computational applications into areas well beyond originally devised quasi-static fracture propagation in brittle materials (i.e. glass, ceramic,) to ductile materials, dynamic propagation, or hydraulic fracturing.

Despite the significant theoretical advancements in these more complex physical settings, the quantification of crack opening displacement has received little attention. It is understandable as most fracturing applications do not explicitly require the crack opening displacement to determine the morphological evolution of different cracks. However, one of the exceptions is hydraulic fracturing where the crack propagation is driven by the fluid pressure which strongly depends on the crack opening displacement. In the Reynolds equation, generally adopted in fracture flow models, the fracture mass flow rate is proportional to the cube of the aperture, also called cubic law. Thus, quantitative resolution of the crack opening is crucial in the numerical simulation of hydraulic fracturing.

Thus far, largely two approaches for computing the crack opening displacement have been proposed. One approach is to use a line integral for an estimate of the jump quantity across the discontinuity [Bourdin et al. 2012] and the other is to regard the displacement quantity at a certain distance away from the crack as that of the crack lip following a level-set approach [Lee et al. 2017]. The first presents some numerical issues in the actual implementation as to how the integral line is drawn especially near the crack tip. On the other hand, the "certain distance" required in the latter approach has not yet clearly defined or studied before.

Here we studied the two known approaches - a line integral and a level-set method - for crack opening computation mainly from an implementation point of view. Firstly, we derive an approximation of a discontinuous function field in the variational phase-field (VPF) setting which is then applied to obtain the crack opening (displacement jump) and verify the approximation against a closed solution. We then propose a “certain distance from the crack" required for the level-set function using a one-dimensional analysis. Finally, we compare these approaches under several different conditions such as crack alignment to the mesh or under loading (asymmetric displacement field) and investigate the convergence with respect to the mesh size.

1.2 Methodology

Following Bourdin et al. (2012), a normal displacement jump over the crack can be approximated from a line integral as:

$$\|\boldsymbol{u}\| = \int_{-\infty}^{+\infty} \boldsymbol{u} \cdot \nabla v \, dy$$

The actual implementation of this line integral can follow Algorithm 1 below:

Algorithm 1 Crack opening computation at the element e_i

Let v_i be the element average of v and $\vec{x}_i$ be the centroid coordinate of element e_i
Set $j = i$, $\vec{n}_{\Gamma,i} = \nabla v_i / |\nabla v_i|$, and $s = \text{sign}(\vec{n}_{\Gamma,i} \cdot \vec{n}_{\Gamma,j})$
while $v_{j+1} < 1$ or $\vec{n}_{\Gamma,j+1} \cdot \vec{n}_{\Gamma,i} \geq 0$ **do**
    Let $\vec{x}_{j+1} = \vec{x}_j + s \triangle l_\varepsilon \vec{n}_{\Gamma,j}$
    Identify the neighbor element, e_{j+1}, which contains $\mathbf{x}_{i+1}$
    if $\vec{n}_{\Gamma,j+1} = 0$ **then**
        $\vec{n}_{\Gamma,j+1} = \vec{n}_{\Gamma,j}$ // Continue in the same search direction
    else if $\vec{n}_{\Gamma,j+1} \cdot \vec{n}_{\Gamma,j} < 0$ **then**
        $\vec{n}_{\Gamma,i} = -\vec{n}_{\Gamma,i}$ // Flip the search direction
        $s = \text{sign}(\vec{n}_{\Gamma,i} \cdot \vec{n}_{\Gamma,j})$
    $w = w + \triangle l_\varepsilon (\vec{u}_j \cdot \nabla v_j + \vec{u}_{j+1} \cdot \nabla v_{j+1})/2$ // Line integral
Set $j = i$, $\vec{n}_{\Gamma,i} = -\nabla v_i / |\nabla v_i|$ and $s = \text{sign}(\vec{n}_{\Gamma,i} \cdot \vec{n}_{\Gamma,j})$
while $v_{j+1} < 1$ or $\vec{n}_{\Gamma,j+1} \cdot \vec{n}_{\Gamma,i} \geq 0$ **do**
    4–11

The level-set method proposed in [Lee et al. 2017] computes the normal displacement jump from:

$$\|\boldsymbol{u}\| = (\boldsymbol{u} \cdot \boldsymbol{n}_{LS})^+ + (\boldsymbol{u} \cdot \boldsymbol{n}_{LS})^-$$

where $\boldsymbol{n}_{LS}$ is the vector normal to the level-set at the threshold value of c_s. The value is arbitrarily proposed as 0.8 in [Lee et al. 2017] and is suggest to use 0.618 based on a one-dimensional analysis in [Yoshioka et al. 2020]. The computation can be achieved via vtk-library as in Algrorithm 2.

Algorithm 2 Level-set width finding algorithm

Compute piecewise linear contour of the phase-field for a given level-set value using the vtkContourFilter.
for all straight line segments c_i with endpoints $\mathbf{x}_i$ and $\mathbf{x}_{i+1}$: **do**
    $\vec{n}_i = \mathcal{R}(\mathbf{x}_{i+1} - \mathbf{x}_i)/|\mathbf{x}_{i+1} - \mathbf{x}_i|$ // Normal vector of c_i
    // where $\mathcal{R} := \begin{bmatrix} 0 & -1 \\ 1 & 0 \end{bmatrix}$
    $\vec{u}_i = \vec{u}(\mathbf{x}_i) + \vec{u}(\mathbf{x}_{i+1})$ // Sum of the displacements on c_i
    $w_i = \vec{u}_i \cdot \vec{n}_i$ // Width on c_i

Further reading concerning the basics of the VPF method can be found in following EURAD publications:

- Yoshioka, K., Mollaali, M., Kolditz, O. (2021): Variational phase-field fracture modeling with interfaces. Comput. Meth. Appl. Mech. Eng. 384 , art. 113951
- Kolditz, O., Görke, U.-J., Konietzky, H., Maßmann, J., Nest, M., Steeb, H., Wuttke, F., Nagel, T. (eds., 2021): GeomInt–Mechanical integrity of host rocks. Terrestrial Environmental Sciences. Springer Nature, Cham, 277 pp.
- Yoshioka, K., Sattari, A., Nest, M., Günther, R.-M., Wuttke, F., Fischer, T., Nagel, T. (2022): Numerical models of pressure-driven fluid percolation in rock salt: nucleation and propagation of flow pathways under variable stress conditions. Environ. Earth Sci. 81 (5), art. 139
- You, T., Yoshioka, K. (2023): On poroelastic strain energy degradation in the variational phase-field models for hydraulic fracture. Comput. Meth. Appl. Mech. Eng. 416 , art. 116305
- Mollaali, M., Kolditz, O., Hu, M., Park, C.-H., Park, J.-W., McDermott, C.I., Chittenden, N., Bond, A., Yoon, J.S., Zhou, J., Pan, P.-Z., Liu, H., Hou, W., Lei, H., Zhang, L., Nagel, T., Barsch, M., Wang, W., Nguyen, S., Kwon, S., Lee, C., Yoshioka, K. (2023): Comparative verification of hydro-mechanical fracture behavior: Task G of international research project DECOVALEX–2023. Int. J. Rock Mech. Min. Sci. 170 , art. 105530

2. Fracture process studies

In the frame of the DECOVALEX project extensive benchmarking studies based on analytical solutions have been conducted for fracture processes in different rock types (Mollaali et al. 2023). In EURAD DONUT we present new benchmarking studies for dynamic fracture processes based on experimental studies with the GREAT cell at University of Edinburgh (McDermott et al. 2018).

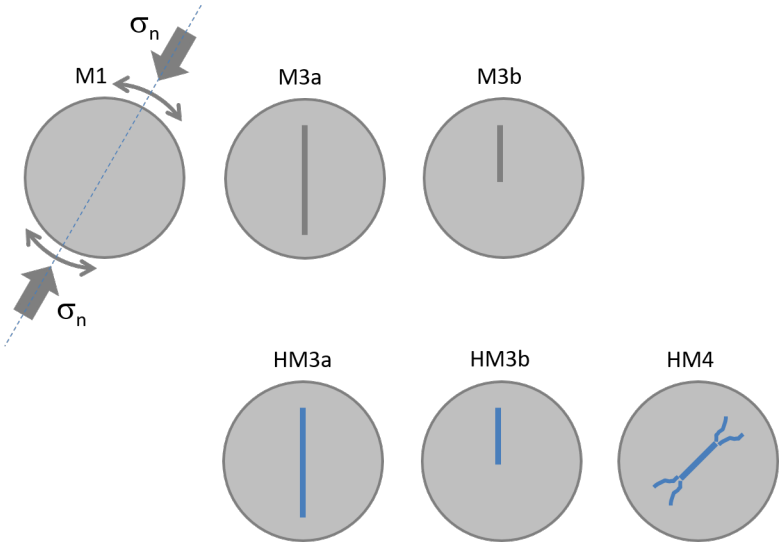

Figure 10 - Benchmarking idea for 2D plane-strain conditions; upper figures represent M processes, lower figures represent HM processes

As a prerequisite to the model analyses of the GREAT cell experiments, we conduct a thorough benchmarking exercise to provide a sound basis of model capabilities and accuracies (e.g. required discretization for comparable accuracy). The benchmark exercises represent simplified variants of the GREAT cell experiments covering general features (e.g. fracture pattern and coupled processes).

The benchmark exercises will be conducted in 2D (plane strain). For this purpose, we consider a horizontal section through the rock samples tested in the GREAT cell (see below). The main characteristics of the HM fracture mechanics can be studied in a 2D plane-strain fashion. The 2D option is easier to model and is intended to encourage more modelers to participate in the benchmark exercises. The benchmarking concept is based on a stepwise increase in complexity, including mechanical (M) and hydromechanical (HM) exercises (Figure 10). The base case (M1) represents the mechanical response of the rock sample due to rotating boundary conditions. M3 considers two different fractured samples. HM2 and HM3 are hydromechanical extensions due to point and line fluid injections respectively. The HM4 case allows for fracture propagation.

The benchmark exercises are briefly summarized below:

M-Process

- M1: Mechanical response of an intact sample to polyaxial stress boundary conditions
- M3a: Mechanical response of a fractured sample to polyaxial stress boundary conditions (two-wing fracture)
- M3b: Mechanical response of a half-fractured sample to polyaxial stress boundary conditions (one-wing fracture)

HM-Process

- HM3a: M1 plus fluid injection in a static fracture (HM process with line injection)
- HM3b: M1 plus fluid injection in a static half-fracture (HM process with line injection)

- HM4: M3a plus fluid injection in a dynamic fracture (HM process with line injection and fracture propagation)

2.1 Mechanical (M) processes

The primary objective of the first benchmark exercise is to validate the mechanical deformation of the GREAT cell under different boundary conditions in a 2D plane strain (*Figure 11*). Two loading scenarios are considered: true-triaxial and axisymmetric loading.

2.1.1 Intact samples (M1)

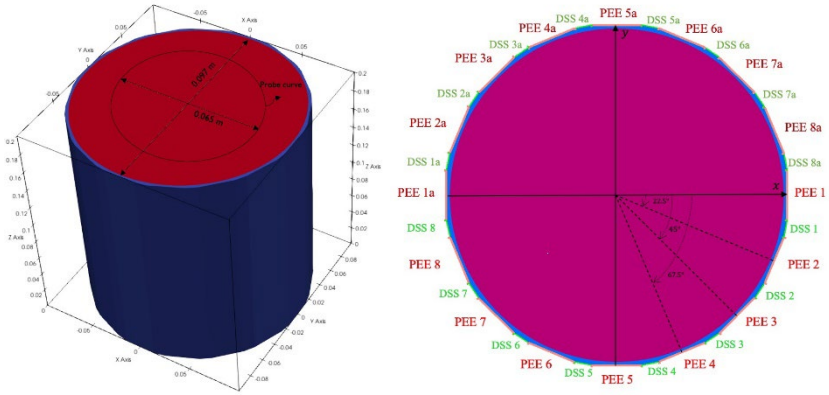

Figure 11 - Geometry and location of Pressure-Exerting Elements (PEEs) and Dynamic-Sealing-Strips (DSSs).

The specimen consists of an opaque, non-crystalline thermoplastic polymer. In laboratory tests involving fluid flow, a 2mm-thick Viton sheath is introduced between the specimen and the Pressure- Exerting Elements (PEEs) / Dynamic-Sealing-Strips (DSSs). This sheath serves to safeguard the attached fiber optic cable and to establish a complete hydraulic seal during fluid flow tests. Consequently, our computational model incorporates two distinct elastic materials within its domain: a central circle thermoplastic polymer Polymethylmethacrylate (PMMA) sample surrounded by a rubber sheath (in 2D). The material properties of the samples are provided in Table . To conduct the simulation, a 2D mesh is generated using GMSH software (https://gmsh.info/), consisting of triangle elements. The mesh includes 2416 nodes and 4735 elements.

Figure 11 illustrates the 2D representation of the benchmark exercise, highlighting the locations of the PEEs and DSSs. The loading specifications for the PEEs are available in *Table 1*. Meanwhile, the load acting on the DSSs is determined as the average of the loads applied to adjacent PEEs. In the true triaxial scenario, the stress field follows σ1 > σ2 > σ3, whereas, in the axisymmetric scenario: σ1 > σ2 = σ3. For the purpose of enforcing boundary conditions, the zero circumferential displacement boundary condition is defined at the intersection of the sample with the x and y axes:

$$u_x(x, y) = 0, \text{ for } \quad x = 0.0 \quad \text{and} \quad (y = 0.9894 \text{ or } y = -0.09894),$$

$$u_y(x, y) = 0, \quad \text{for} \quad y = 0.0 \quad \text{and} \quad (x = 0.9894 \text{ or } x = -0.09894),$$

These constraints ensure that the displacement components u_x and u_y are zero at the specified boundaries of the 2D domain.

True Triaxial	Axisymmetric
PEEs 1 & 1a: 7.73 MPa	PEEs 1 & 1a: 7.71 MPa
PEEs 2 & 2a: 5.70 MPa	PEEs 2 & 2a: 7.70 MPa
PEEs 3 & 3a: 4.39 MPa	PEEs 3 & 3a: 8.30 MPa
PEEs 4 & 4a: 2.40 MPa	PEEs 4 & 4a: 7.80 MPa
PEEs 5 & 5a: 2.30 MPa	PEEs 5 & 5a: 7.74 MPa
PEEs 6 & 6a: 4.00 MPa	PEEs 6 & 6a: 7.70 MPa
PEEs 7 & 5a: 6.40 MPa	PEEs 7 & 7a: 8.30 MPa
PEEs 8 & 8a: 7.70 MPa	PEEs 8 & 8a: 7.72 MPa
DSSs: average of loads of adjacent PEEs	DSSs: average of loads of adjacent PEEs

Table 1 – Loading scenarios for mechanical deformation benchmarks

Material Property	**Symbol**	**Value**	**Unit**
Sample Young's modulus	E	3.85	GPa
Sample Poisson's ratio	ν	0.4	-
Rubber sheath Young's modulus	E	0.1	GPa
Rubber sheath Poisson's ratio	ν	0.4	-

Table 2 - Material properties

In the post-processing step, we plot either the volumetric strain

$$\varepsilon_{vol} = \varepsilon_{xx} + \varepsilon_{yy}$$

or surface strain (a ratio of the change in length of the material to its initial length) as a function of the angle. The angle is measured clockwise from the positive x-axis and is evaluated at $(x,y) \in R^2 \mid |x^2 + y^2 - 0.065^2| < 10^{-6}$. The length unit is the meter.

The result of the strain profile in $M1$ benchmark for both loading scenarios in 2D is shown in Figure 12. Furthermore, the volumetric strain at various angles is graphically represented for both loading scenarios on the probe curve in Figure 13.

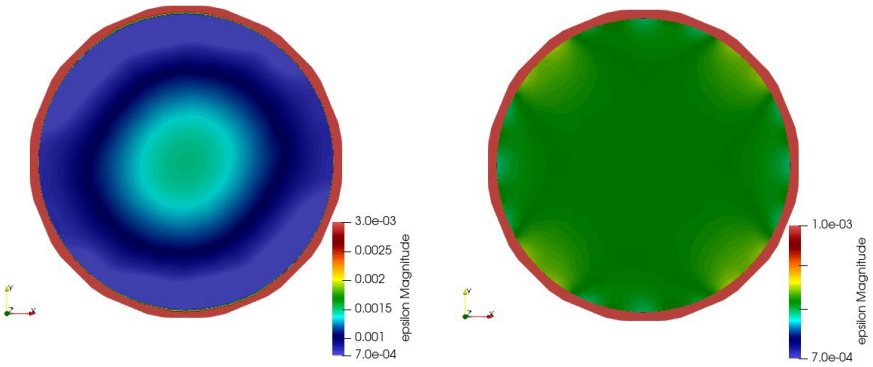

Figure 12 - The results of the strain field for the 2D benchmark exercise M1 are shown, with loading scenarios defined in Table above. It's important to note the distinct strain ranges; the strain value at the sheath is much higher than the visualization range. Left: true triaxial, Right: Axisymmetric

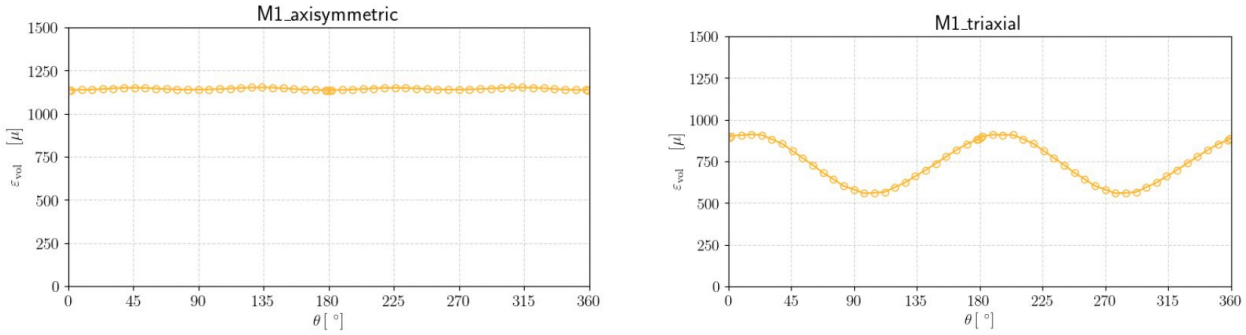

M1 Axisymmetric M1 True Triaxial

Figure 13 - Volumetric strain versus angle for an intact sample (M1).

2.1.2 Fractured samples (M3a & M3b)

The objective of the second set of benchmarks is to explore the mechanical deformation in fractured samples. In the initial set of benchmarks, our focus was on a symmetric central line fracture denoted as $\Gamma = [-0.065, 0.065] \times \{0\}$. However, in the second set, we have only considered half of the fracture, specifically $\Gamma = [0, 0.065] \times \{0\}$. For the numerical simulations, we assume the fracture to be static by defining a high critical energy release rate (G_c) for the fracture. The material properties utilized in the simulations are presented in *Table 2*. Essentially, we maintain a constant fracture angle and vary the loading by rotating it. This can be considered as rotating the fracture within the sample while keeping the load constant. The specific loading conditions for the benchmarks are outlined in Table 3. Additionally, we impose Dirichlet boundary conditions as given in the equation above. The result of the strain profile in $M3a$ (two-wing fractures, Figure 14) and $M3b$ (one-wing fracture) benchmarks for different loading scenarios in 2D are shown in the following section. (2.2) Furthermore, the volumetric strain at various angles is graphically represented for both loading scenarios on the probe curve in Figure 15 and Figure 16.

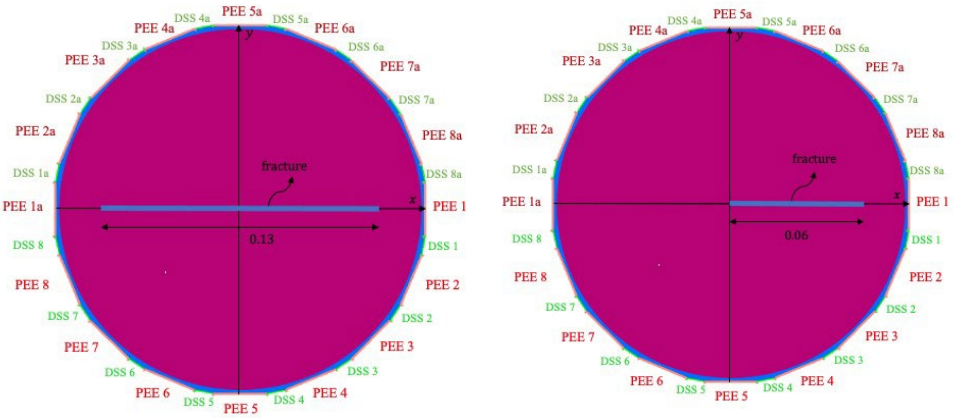

2D, two-wings fracture, M3a 2D, one-wing fracture, M3b

Figure 14 - Geometry and location of PEEs and DSSs

Angle (°)	**Loading Conditions**
0	PEEs 1 & 1a: 8 MPa PEEs 5 & 5a: 8 MPa PEEs 8 & 8a: 8 MPa
22.5	PEEs 4 & 4a: 8 MPa PEEs 7 & 7a: 8 MPa
45	PEEs 3 & 3a: 8 MPa PEEs 6 & 6a: 8 MPa
67.5	PEEs 2 & 2a: 8 MPa
	DSSs: zero

Table 3 - Loading Conditions for Different Angles

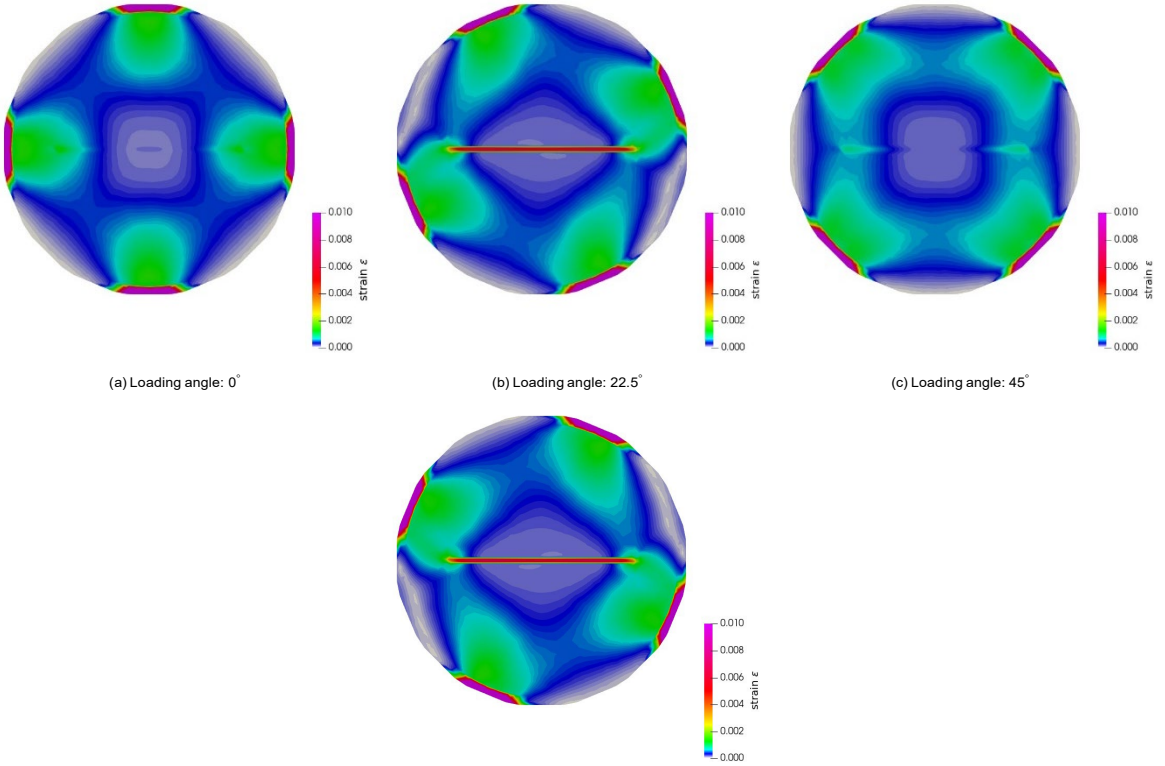

(a) Loading angle: 0°

(b) Loading angle: 22.5°

(c) Loading angle: 45°

(d) Loading angle: 67.5°

Figure 15 - Strain profile for 2D specimens include two-wings fracture (M 3a)

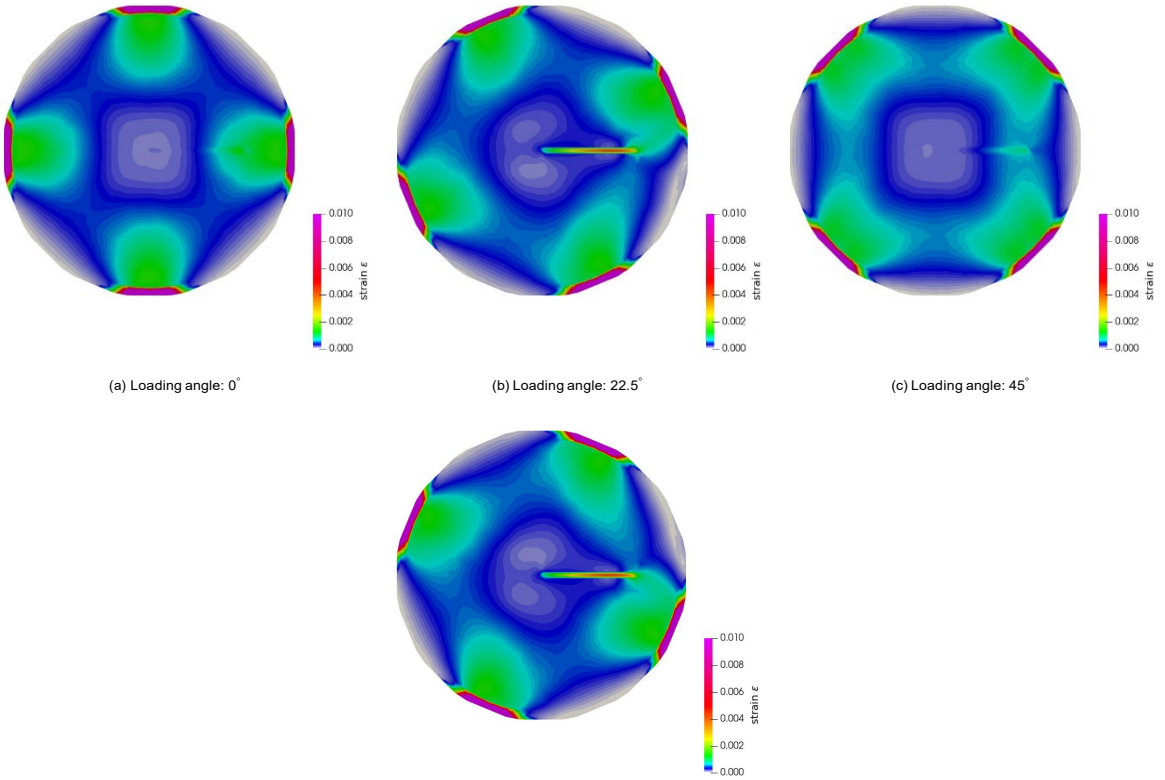

(a) Loading angle: 0°

(b) Loading angle: 22.5°

(c) Loading angle: 45°

(d) Loading angle: 67.5°

Figure 16 - Strain profile for 2D specimens include one-wing fracture (M3b)

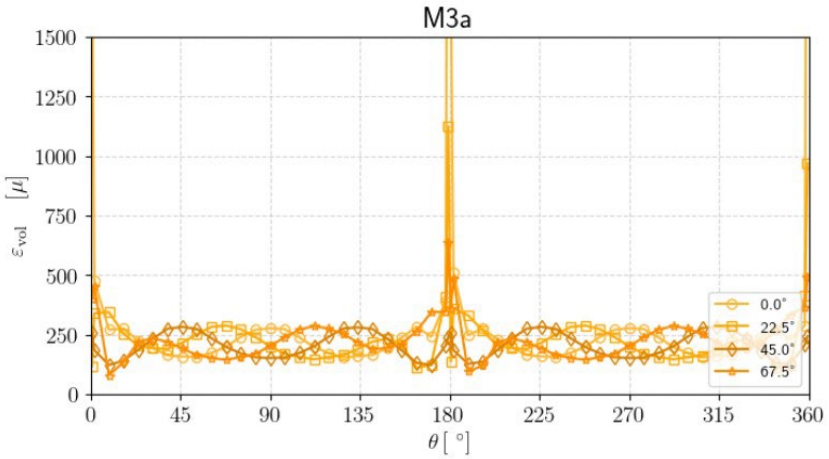

(a) $M3a$: one-wing fracture

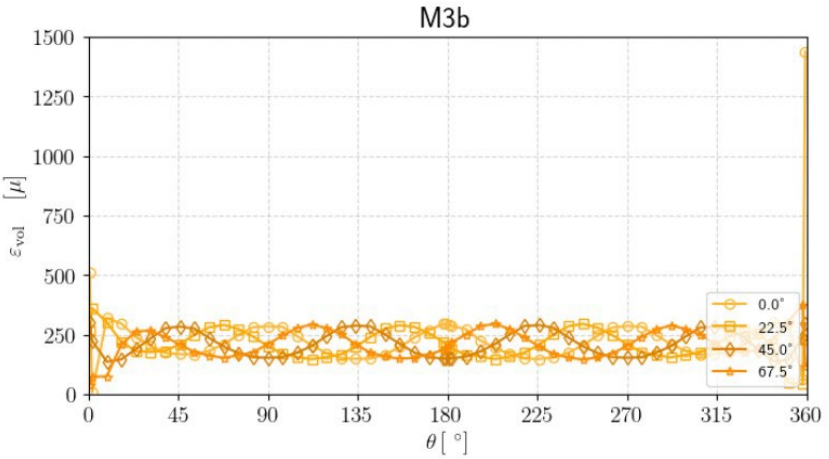

(b) $M3b$: two-wings fracture

Figure 17 - Volumetric strain versus angle for fractured samples (M 3a and M 3b)

2.2 Hydro-Mechanical (HM) processes

2.2.1 Pressurized samples (HM3a & HM3b)

The main aim of the fourth benchmark is to examine the hydro-mechanical behavior exhibited by a fractured sample. To achieve this, we employ the identical samples and boundary conditions detailed in the previous section. In this particular benchmark, a pressure of 5 MPa is uniformly applied to the surfaces of the fracture (Figure 18). Moreover, we assume the fracture to be impermeable. These numerical experiment conditions provide insights into the coupled response of the fractured sample under the influence of both hydraulic and mechanical factors.

The result of the strain profile of $HM3a$ and $HM3b$ benchmarks for different loading scenarios in 2D are shown in Figure 19 and Figure 20, respectively. Furthermore, the volumetric strain at various angles is graphically represented for both loading scenarios on the probe curve in Figure 21.

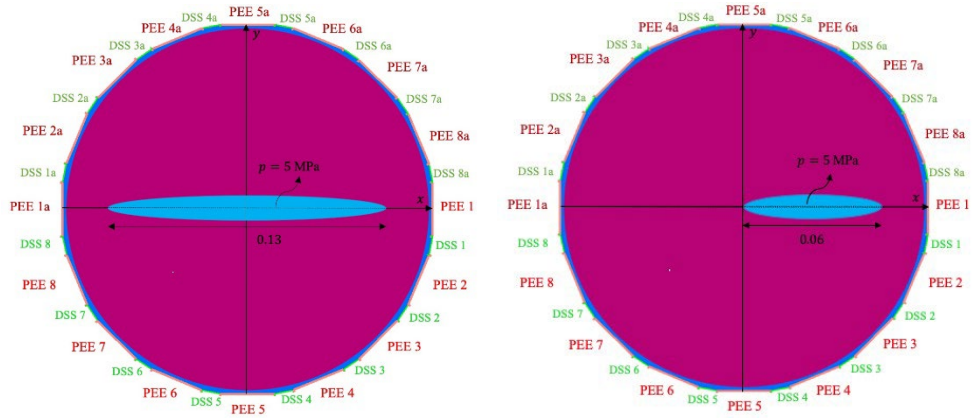

2D, two-wings fracture, HM3a 2D, one-wing fracture, HM3b

Figure 18 - Geometry and location of PEEs and DSSs

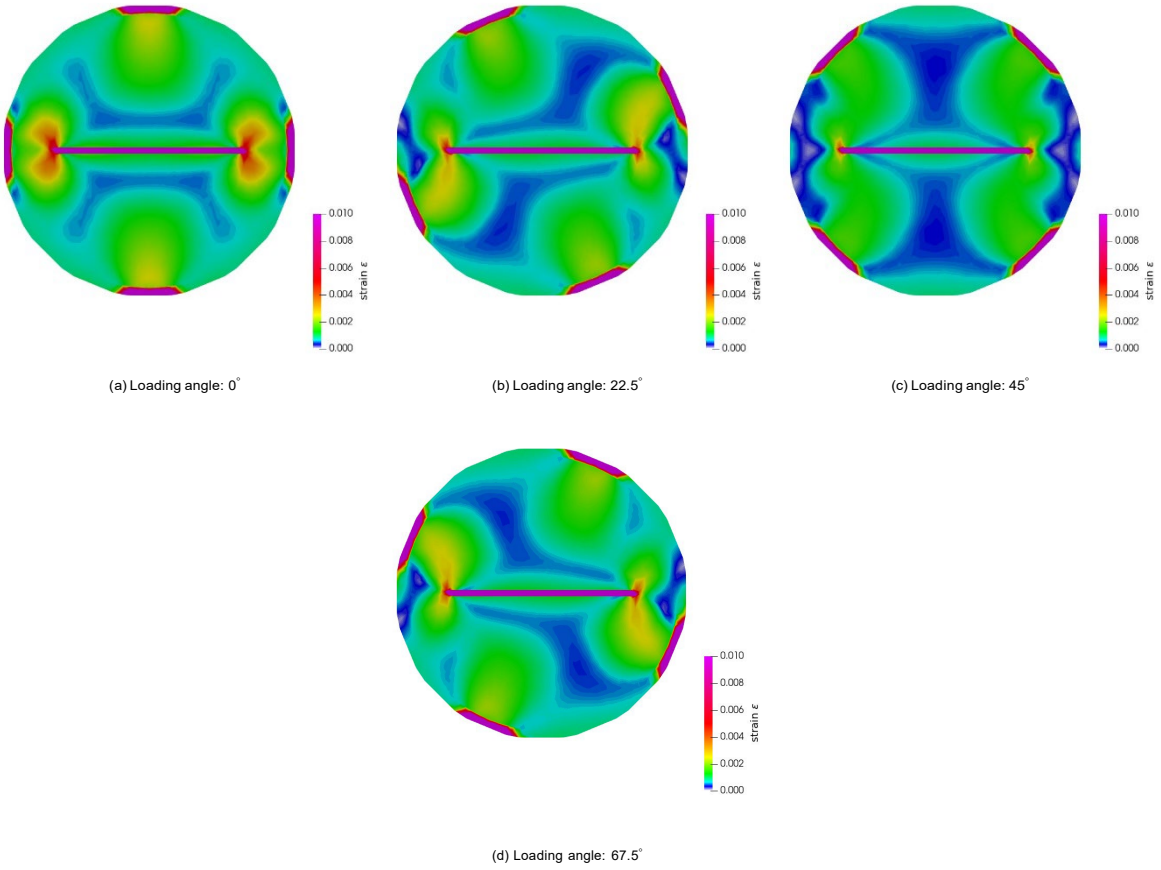

(a) Loading angle: 0° (b) Loading angle: 22.5° (c) Loading angle: 45°

(d) Loading angle: 67.5°

Figure 19 - Strain profile for 2D specimens include a pressurised two-wings fracture (HM3a).

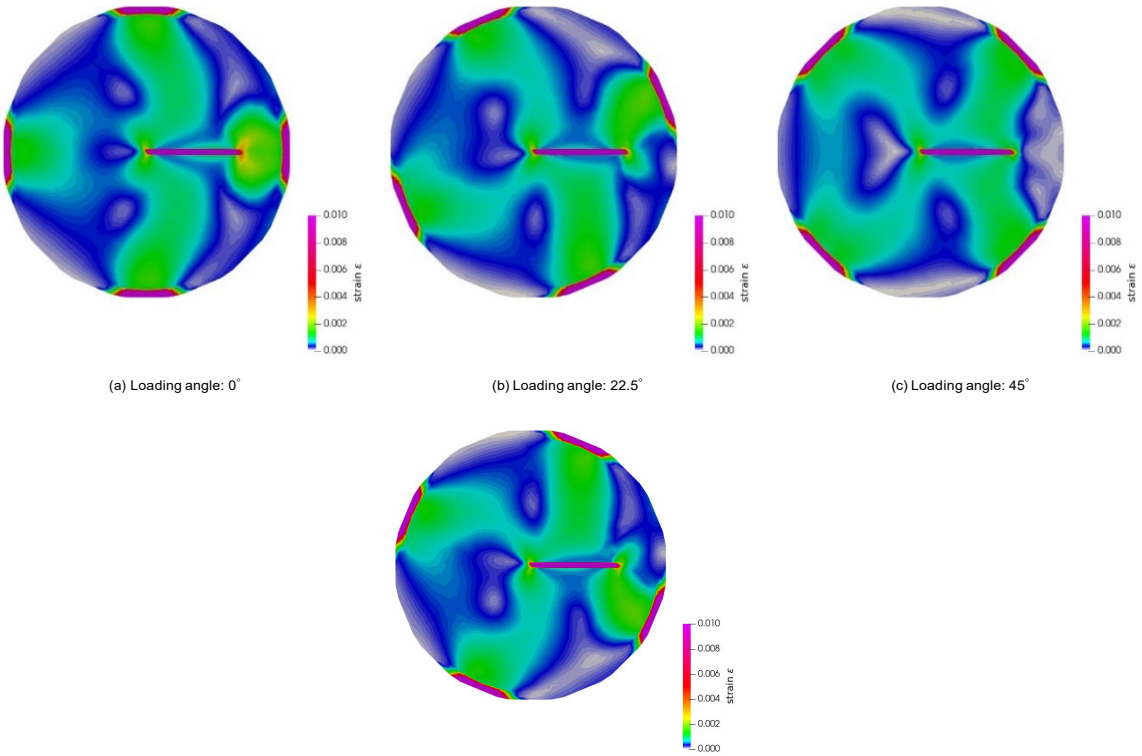

(a) Loading angle: 0°

(b) Loading angle: 22.5°

(c) Loading angle: 45°

(d) Loading angle: 67.5°

Figure 20 - Strain profile for 2D specimens include a pressurised one-wing fracture (HM 3b).

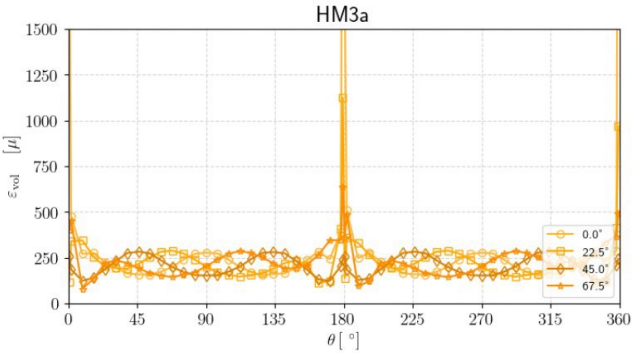

(a) $HM3a$: one-wing fracture

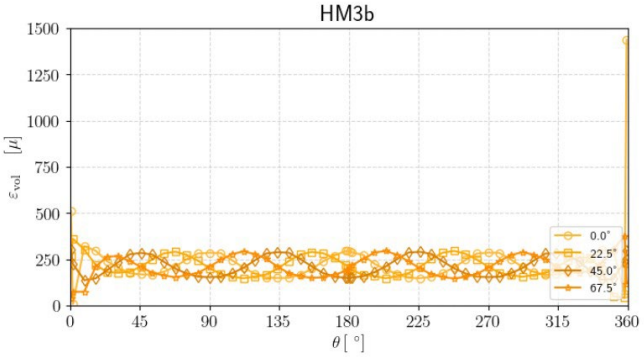

(b) $HM3b$: two-wings fracture

Figure 21 - Volumetric strain versus angle for fractured samples (HM3a and HM3b).

2.2.2 Hydraulic Fracturing (HM4)

In the final set of 2D benchmarks, we aim to simulate hydraulic fracturing under various boundary conditions. The fluid is injected at the center of an inclined fracture to capture the hydraulic fracturing process (Figure 22). To examine the influence of polyaxial stress boundary conditions on fracture propagation, we define three different scenarios, as summarized in Table 5. The material properties and fluid properties used in the simulations are presented in Table 4. These parameters play a crucial role in determining the behavior of the fractured sample and the fluid flow within the fracture. By exploring these benchmarks, we can gain valuable insights into the mechanics of hydraulic fracturing and its response to different polyaxial stress boundary conditions.

Figure 23, Figure 24, *Figure 25* depict snapshots of the phase field, pressure, and strain for various loading scenarios. In Figure 23 (Scenario I), the minimum stress applied in the y-direction leads to fracture propagation deviating towards the horizontal direction. Conversely, in Scenario II, where the minimum stress is applied in the x-direction, Figure 24 illustrates hydraulic fracturing deviating towards the vertical direction. Furthermore, in Scenario III, where the far-field stresses perpendicular and parallel to the fracture are identical, fractures persist in propagating diagonally (*Figure 25*).

Properties	**Values**	**Unit**
E	3.85×10^{9}	Pa
v	0.4	-
K	5×10^{-18}	m^2
ϕ	0.0	-
μ	10^{-8}	Pa·s
G_c	6.8	N/m
c_f	0	0
Q_0	2×10^{-3}	m^2/s

Table 4 - Material and Fluid Properties

Scenario	**Loading Conditions**	
I	PEEs 1 & 1a	2 MPa
	PEEs 5 & 5a	0.5 MPa
II	PEEs 1 & 1a	0.5 MPa
	PEEs 5 & 5a	2 MPa
III	PEEs 7 & 7a	1 MPa
	PEEs 3 & 3a	1 MPa
	DSSs	zero

Table 5 - Loading Conditions for Different Angles

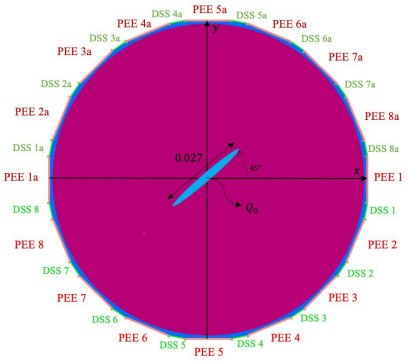

Figure 22 - Geometry and location of PEEs and DSSs.

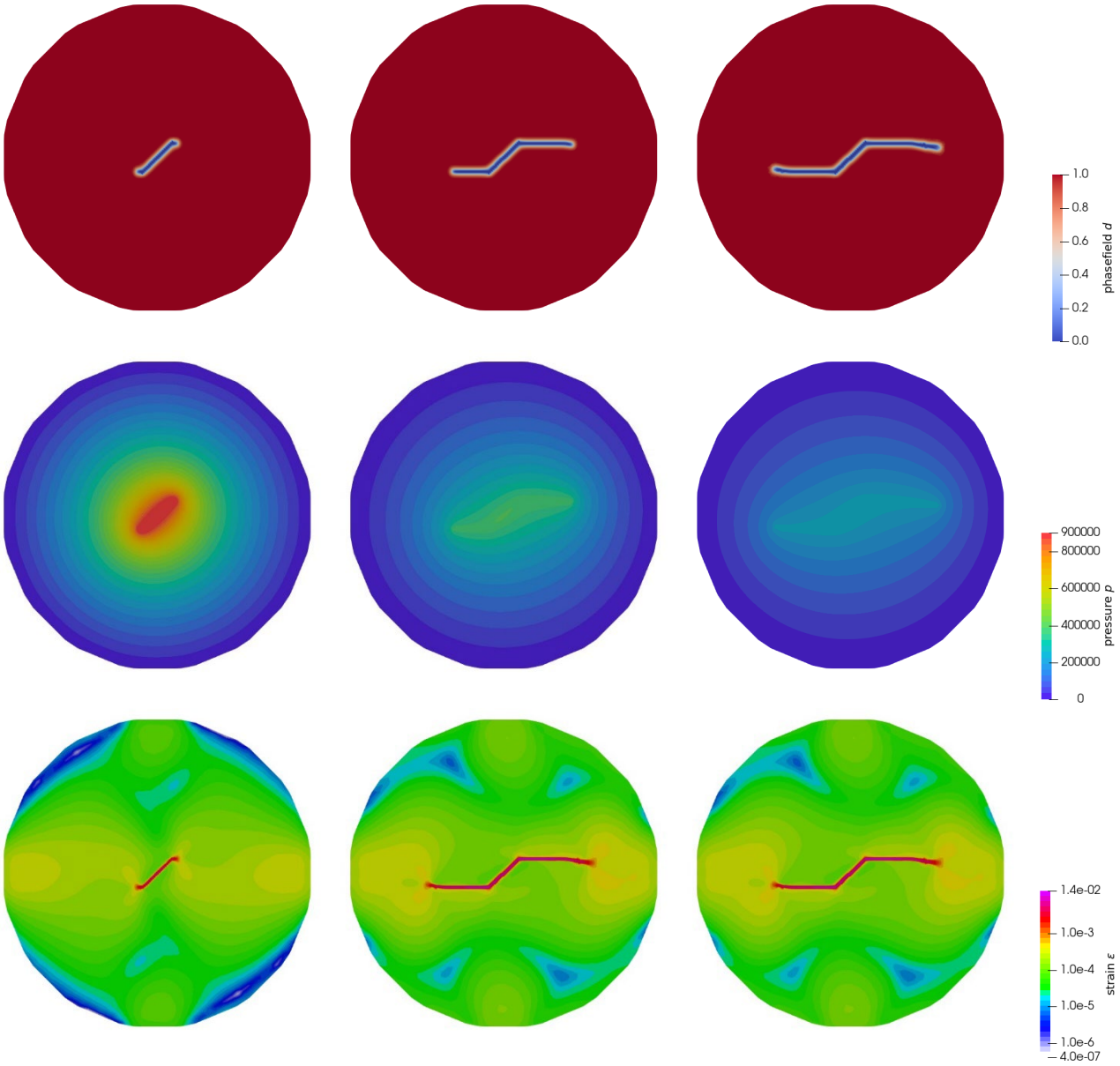

Figure 23 - Resulting fields for benchmark HM4 Scenario I, for different time steps

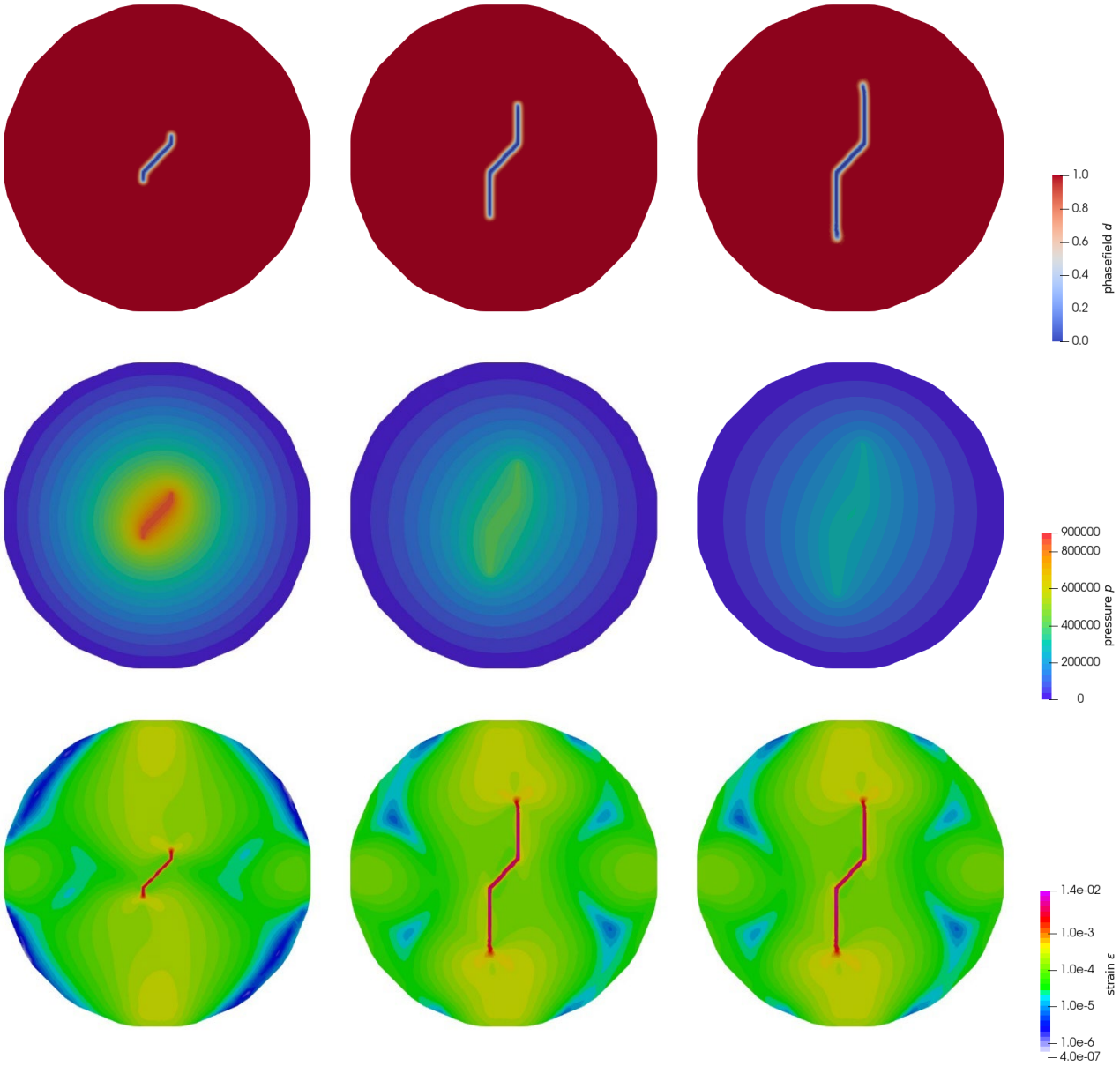

Figure 24 - Resulting fields for benchmark HM4 Scenario II, for different time steps

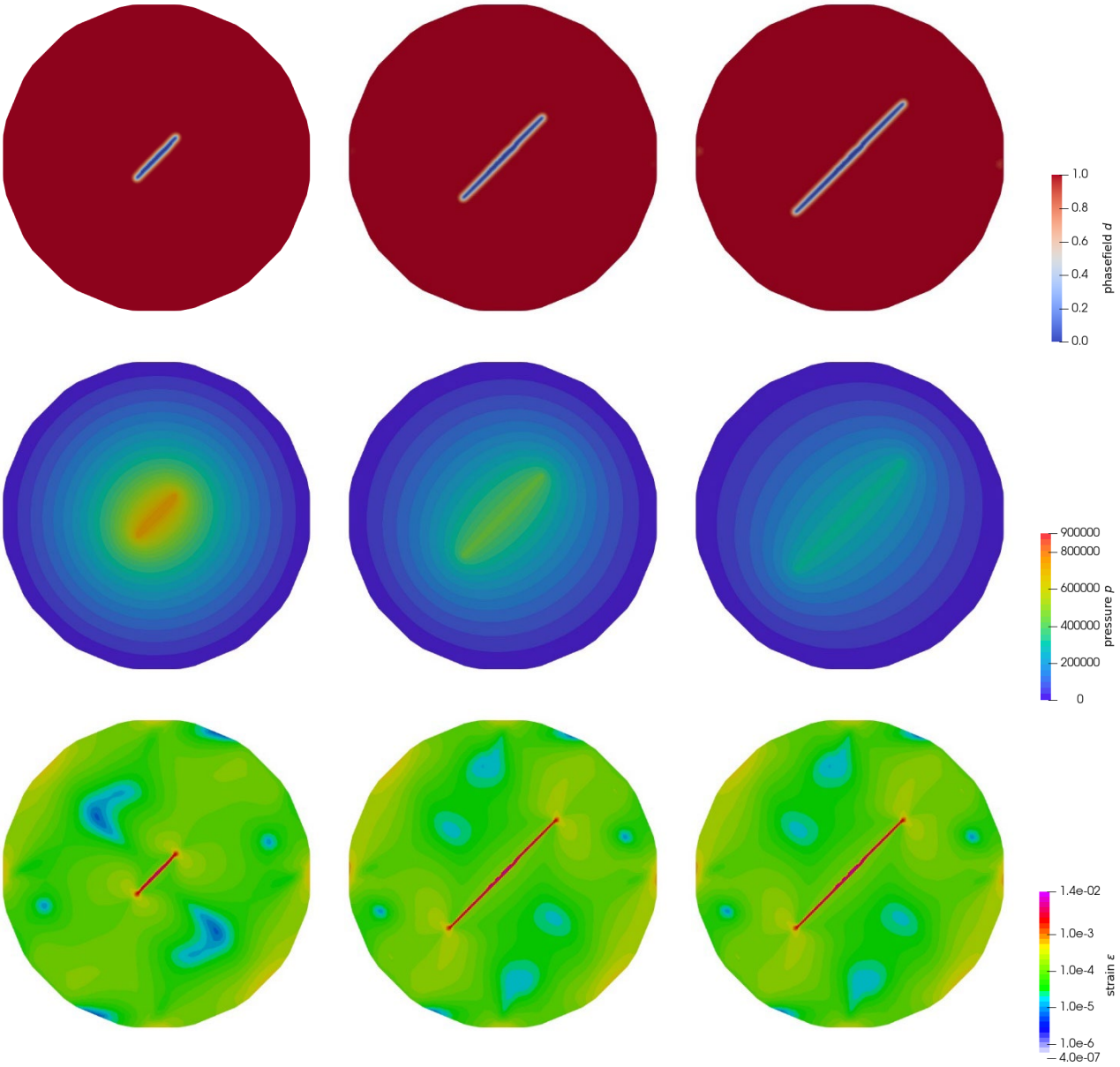

Figure 25 - Resulting fields for benchmark HM4 Scenario III, for different time steps

2.3 OGS JupyterLab

As part of the work for the WP DONUT, general contributions to the community were made, e.g. the extension of the benchmark collection for THM fracture mechanics (*Figure 26*).

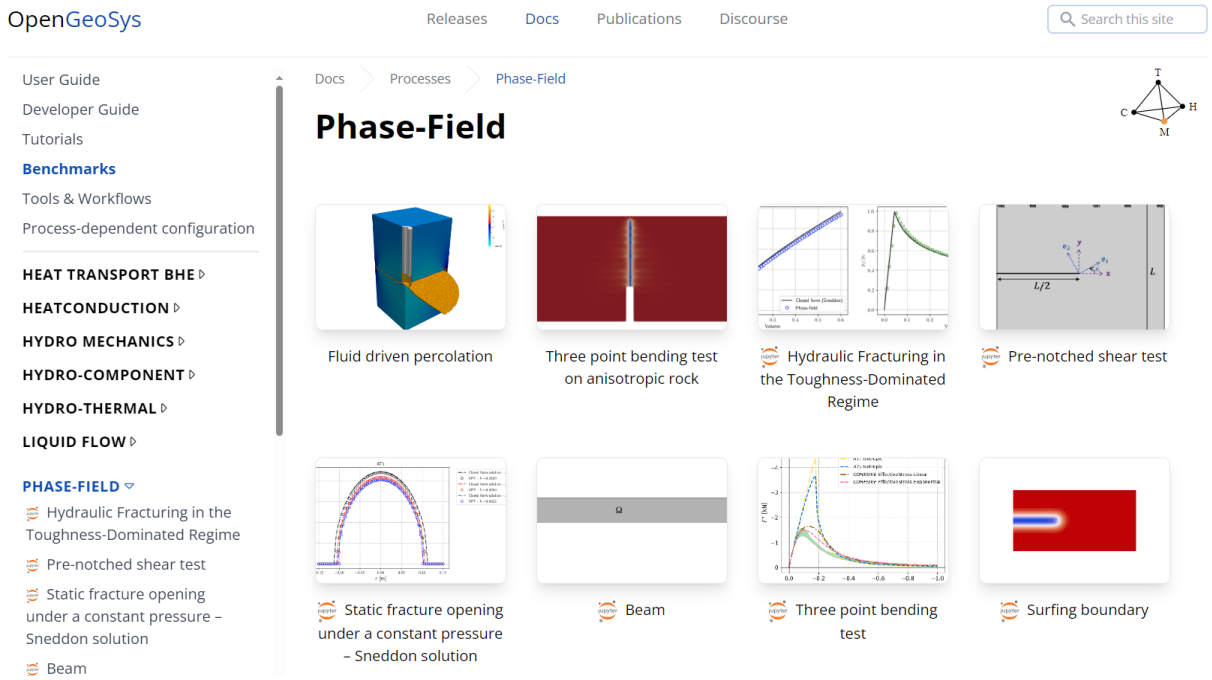

Figure 26 – OpenGeoSys benchmark gallery for fracture mechanics (https://www.opengeosys.org/docs/benchmarks/phase-field/)

3. GREAT cell experiments

Based on fracture models presented in the previous section, experimental analysis has been conducted based on the GREAT cell experiments at the University of Edinburgh.

The GREAT cell, *Figure 27*, provides the capability to load hydraulically connected fractures in rock samples under a controlled triaxial stress field, and to change that stress field during the experiment enabling the investigation of the impact of normal and shear stress on fracture permeability. The sample size is 200 mm diameter x 200 mm height, and strain is measured along the middle circumference of the cylinder. Additionally fluid sampling during the experiments and later analysis facilitates the investigation of changes in water chemistry as a consequence of different dynamic loading states.

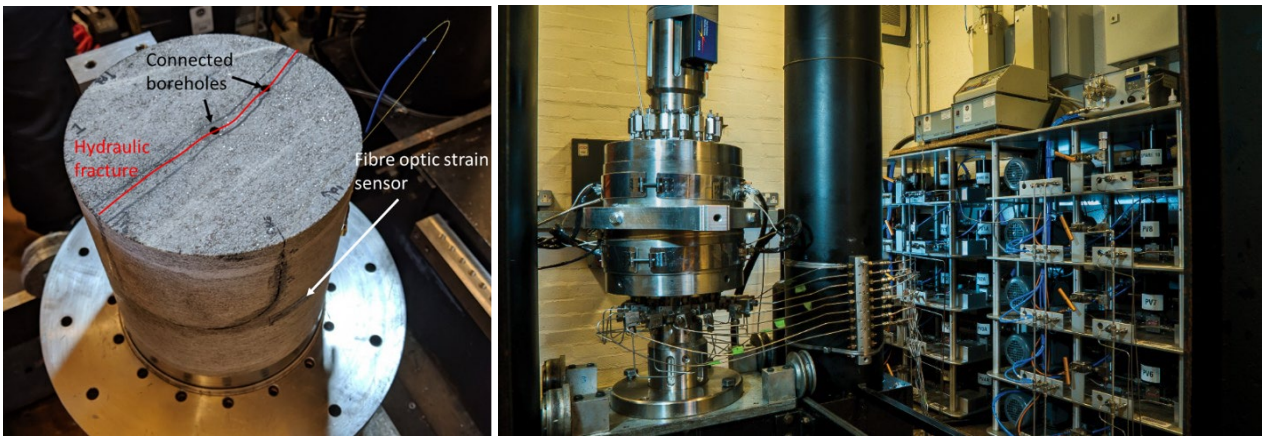

Figure 27 - GREAT cell sample and apparatus

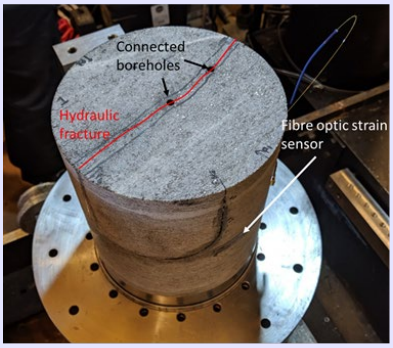

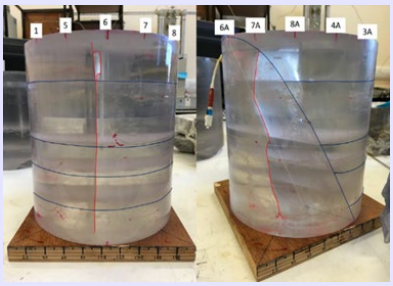

Samples and experiments

The GREAT cell experiments are dealing with various sample materials: he polymer material was used to develop the experimental procedure and as data set for model benchmark

- Polymer (M1) McDermott et al. (2018)
- Polyester resin with partial fracture, axisymmetric and triaxial conditions (HM1)
- Polyester resin with full fracture, axisymmetric and triaxial conditions (HM2)
- Polyester resin Fraser-Harris et al. (2020)
- Greywacke
- Freiberger Gneis Frühwirt et al. (2019), Fraser-Harris et al. (2023)

Parameter	Unit	Containing Sheaf	Resin	Greywacke	Gneis (Freiberg)*
Young's modulus, E,	(GPa)	0.1	3.85	26.85	83.9//57.1
Poisson's ratio, v	(-)	0.4	0.4	0.27	0.21//0.19
Tensile strength	(MPa)	-	17.96-25.08	17.01-16.67	16.8//6.2
Permeability, k	(m s^{-2})	-	-	2.58×10^{-19}	10^{-18}//< 10^{-19}

Table 6 - Overview of material properties for the GREAT cell samples

Sources: Fraser Harris et al. 2020 (Resin sample and Greywacke), personal communication (2019) for Gneiss (Freiberg), Thomas Fruehwirt, Lehrstuhl für Gebirgs- und Felsmechanik/Felsbau am Institut für Geotechnik der TU Bergakademie Freiberg.

The primary aim of this section is to explore how samples respond to changes in a triaxial stress field's values and orientations through near-field mechanical deformation. We examine three sample types (*Figure 28*): an intact sample, a sample containing an internal fracture (partially fractured sample), and a sample with a vertical fracture positioned in the middle (fully fractured sample). As our focus is on investigating mechanical deformation, we prohibit fracture propagation within the fractured sample. In the numerical models (OGS), we treat the fracture as static by assigning it a high fracture toughness.

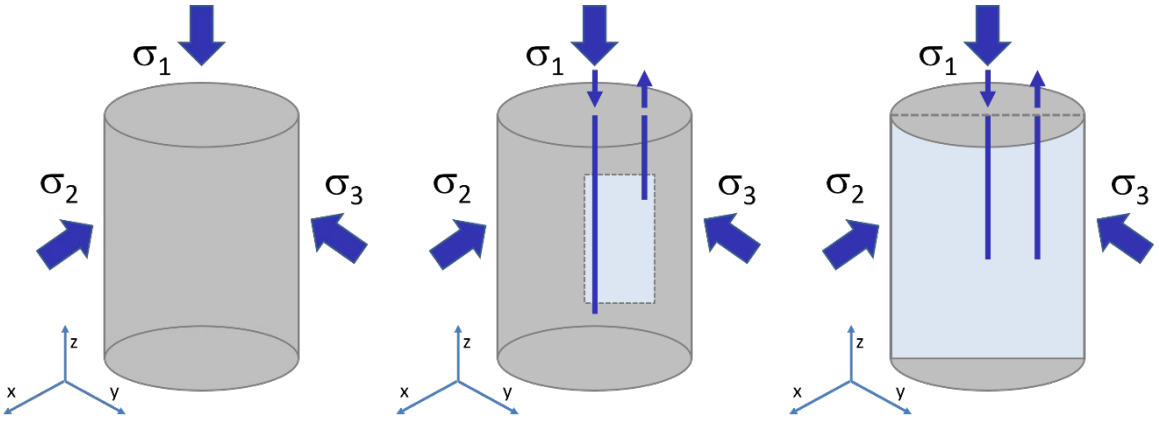

Figure 28 - Experiment types conducted on synthetic samples (polymer and polyester resin) McDermott et al. (2018)

3.1 Intact sample (M1)

The strain profile of both loading scenarios in 2D and 3D are shown in *Figure 29*, *Figure 30*, *Figure 31*, the volumetric strain results from 2D simulations are compared to three-dimensional simulations under varying axial loads. In addition to the case detailed with an axial load of 10 MPa along the z-axis, three-dimensional simulations are performed with axial loading (4, 6, and 10 MPa) as well as with no axial load. The findings suggest that in true tri-axial loading conditions, the three-dimensional simulation with a 4 MPa axial load accurately replicates the response seen in the 2D plane strain scenario. Conversely, in the axisymmetric loading test, the 6 MPa axial load aligns more closely with the 2D plane strain response. This highlights that while 2D plane strain simulations qualitatively capture the essence of the real 3D cases, they may not provide accurate quantitative representations.

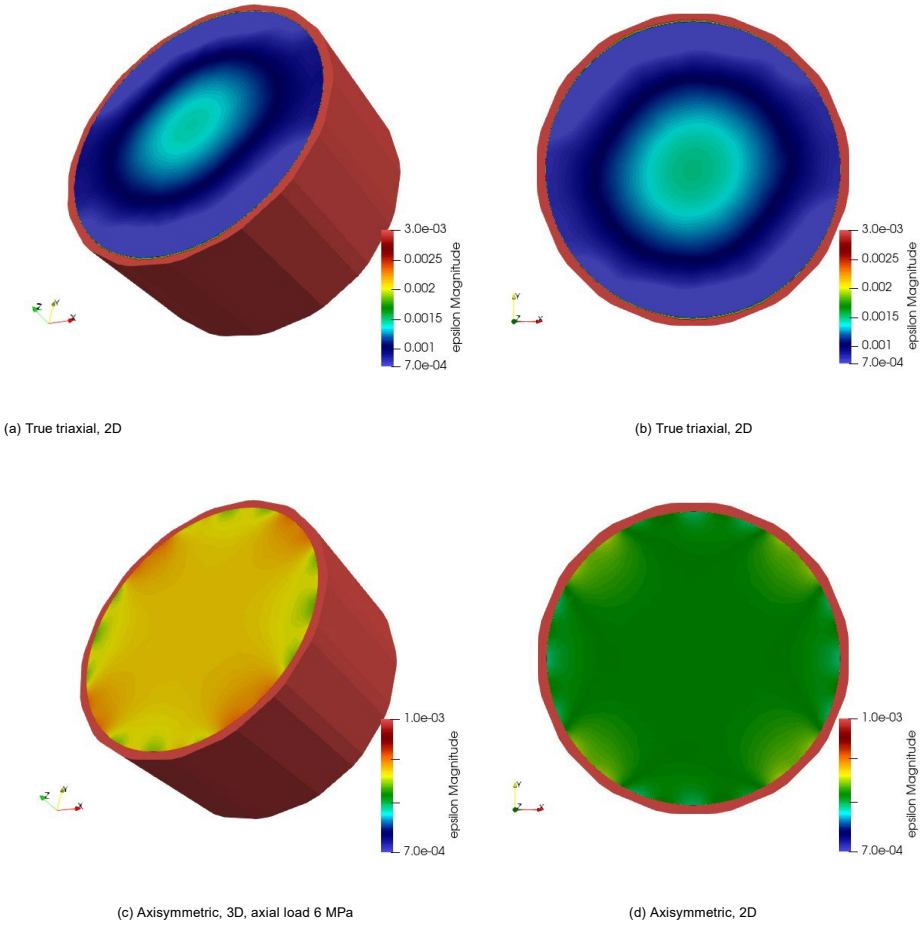

Figure 29 - The results of the strain field for the 2D/3D benchmark exercise M1 are shown, with loading scenarios. It's important to note the distinct strain ranges; the strain value at the sheath is much higher than the visualization range. Figures d and b are the same as those in Section 2.1. They are included here for comparison with 3D results

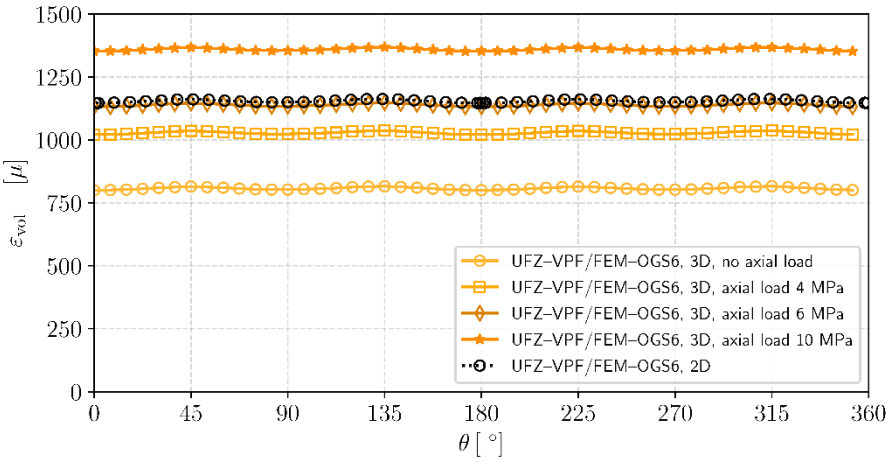

Figure 30 - Comparing volumetric strain at different angles for 2D and 3D cases in the M 1 benchmark under True-Tri-Axial loading

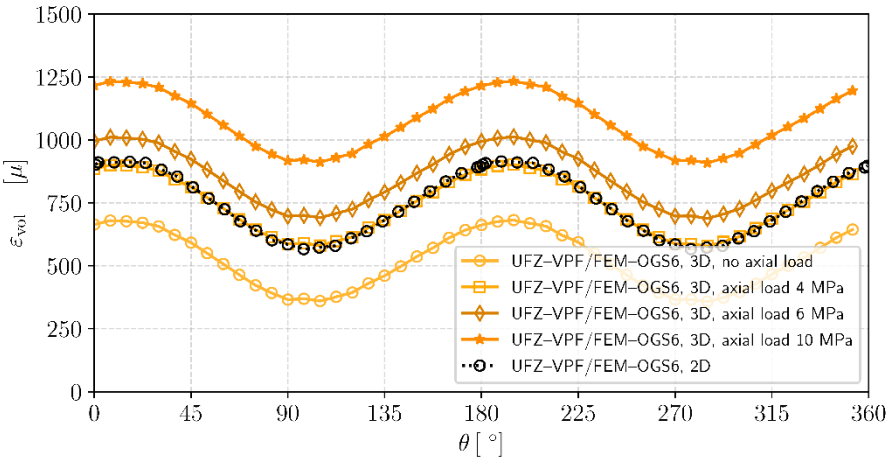

Figure 31 - Comparing volumetric strain at different angles for 2D and 3D cases in the M 1 benchmark under axi-symmetrical loading

We compared our results for volumetric strain with those from other numerical methods and found good agreement under both axisymmetric and triaxial loading conditions (Figure 32 and Figure 33).

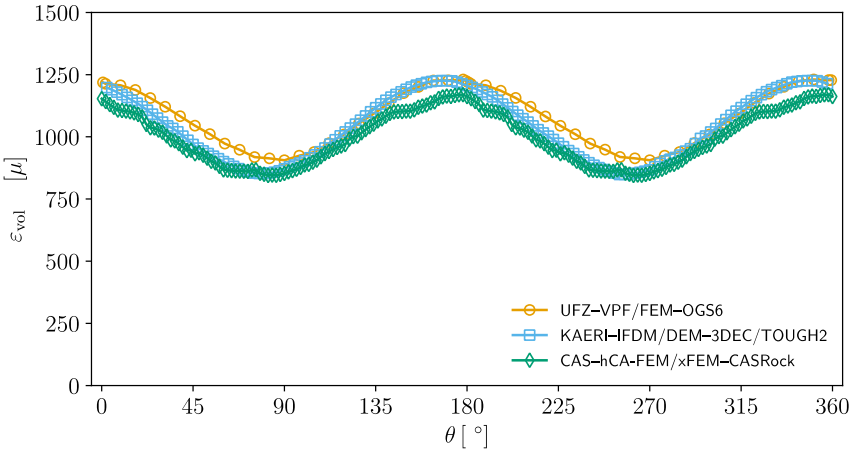

Figure 32 - Comparing volumetric strain at different angles for 3D cases in the M 1 benchmark under True-Tri-Axial loading.

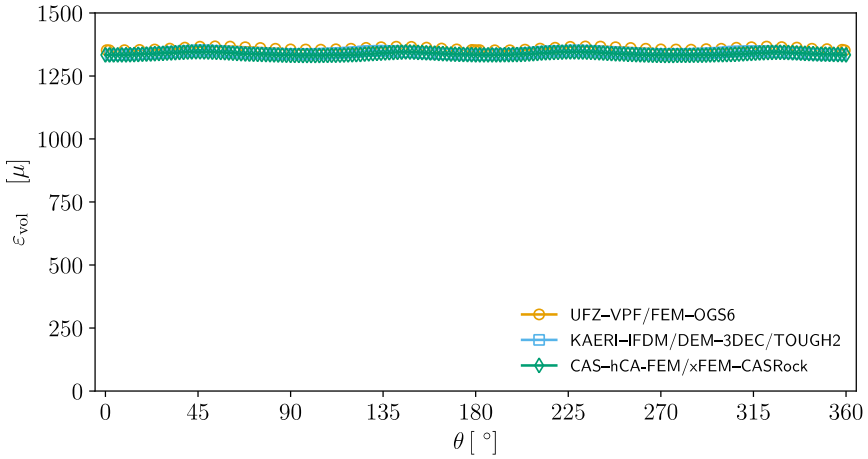

Figure 33 - Comparing volumetric strain at different angles for 3D cases in the M 1 benchmark under axi-symmetrical loading

Furthermore, for the partially fractured sample (*Figure 28*b) the mechanical responses were investigated due to load conditions listed in Table 7. *Figure 34*show the circumferential strain at the sample surface for two different fracture orientations compared to the experimental results, McDermott et al. (2018).

. In comparison to the intact sample the train values are larger for the fractured resin material (M2). Concerning the rock materials, greywacke and gneis, the cyclic strain behavior is much less pronounced

Angle PEE1 to σ_2	**PEEs**	**1 & 1a**	**2 & 2a**	**3 & 3a**	**4 & 4a**	**5 & 5a**	**6 & 6a**	**7 & 7a**	**8 & 8a**
33.75°		7.7	8.7	8.7	7.7	7.3	6.3	6.3	6.6

Table 7 Loading Conditions for partially fractured sample (reference: supplemental materials within, McDermott et al. (2018)

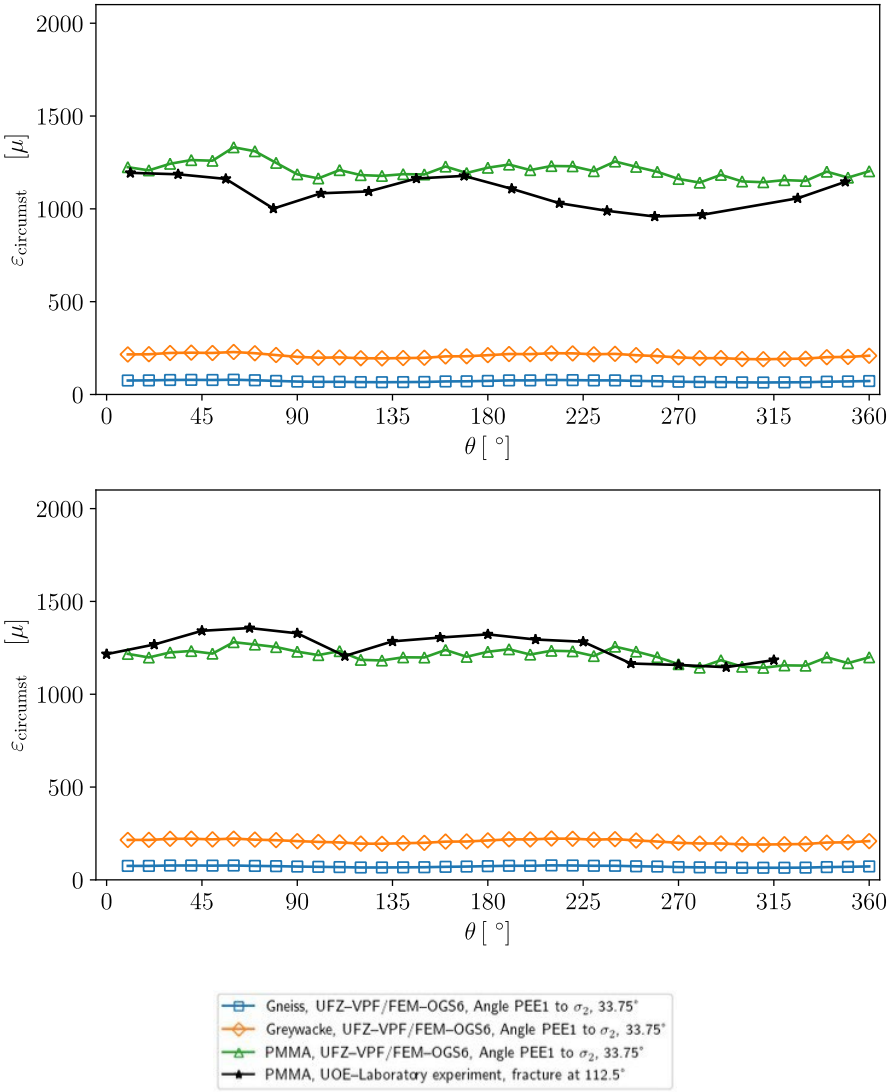

Figure 34 Circumferential strains at $(x, y, z) \in \mathbb{R}^3$ defined by $x^2 + y^2 - 0.09^2 < 10^{-6}$ and $z - 0.1 < 10^{-6}$,for mechanical (M2) compared for different materials, resin, greywacke and gneis, for two different fracture orientations.

3.2 Partially fractured sample (HM2)

We consider the lower-dimensional interface element (LIE) method (Watanabe et al. 2012) for the simulation the hydro-mechanical process in the fracture sample. In the LIE, the displacement difference between two sides of the surfaces is defined as a fracture relative displacement w, which is defined in the local system as *Figure 35* shows the numerical model for the simulation by the LIE method.

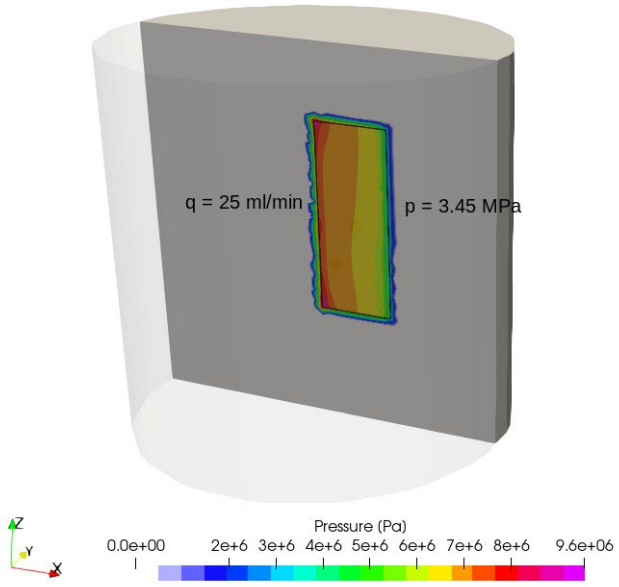

Figure 35 - OGS#LIE model for the hydro-mechanical flow tests.

As shown in *Figure 32*, the injection rate of 25 ml/min and the downstream pressure of 3.45 MPa are applied on the two vertical fracture interfaces, respectively. For the numerical simulation the injection rate is treated as the uniformly Neumann boundary condition with a value

$$q = 25\,\text{ml/ml/H} = 0.41667 \cdot 10^{-6}\,\text{m}^3/0.1\,\text{m}$$

with H = 0.1 m the fracture height. The domain is discretized into a conformable mesh with 328,785 tetraheda for the matrix, and 402 triangles for the fracture. The initial fracture aperture is assumed to be 10^{-5} m. The load conditions are the same as that given in Table 8. Simulations with high joint stiffness $k_{nn} = 100\,\text{GPa/m}, k_{tt} = 100\,\text{GPa/m}$, and with low joint stiffness $k_{nn} = 50\,\text{GPa/m}, k_{tt} = 50\,\text{GPa/m}$, are carried out. *Figure 33* shows the simulated permeability against the simulated normal stress on the fracture with high joint stiffness. While, with the low joint stiffness, the simulated fracture permeability becomes larger as what expected. This can be seen in *Figure 36*.

Marker	Angle PEE1 to σ_2	**PEEs**							
		1 & 1a	**2 & 2a**	**3 & 3a**	**4 & 4a**	**5 & 5a**	**6 & 6a**	**7 & 7a**	**8 & 8a**
B	0°	3.0	4.3	5.6	7.0	7.0	5.6	4.3	3.0
C	22.5°	4.3	5.6	7.0	7.0	5.6	4.3	3.0	3.0
D	45.0°	5.6	7.0	7.0	5.6	4.3	3.0	3.0	4.3
E	67.5°	7.0	7.0	5.6	4.3	3.0	3.0	4.3	5.6
F	90°	7.0	5.6	4.3	3.0	3.0	4.3	5.6	7.0

DSSs: average of loads of adjacent PEEs. The load for each PEE is given in MPa.

Table 8 Load conditions for HM2 simulation ($\sigma_1 = 10$ MPa).

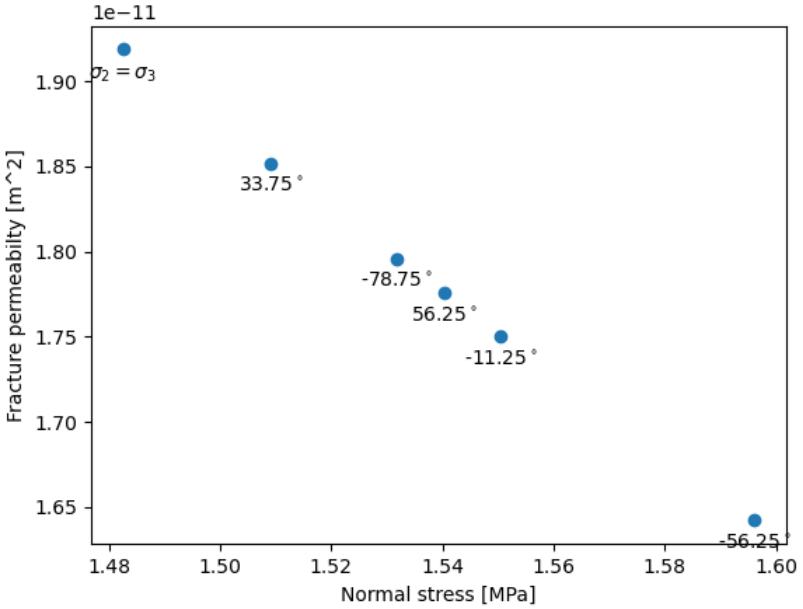

Figure 36 - OGS#LIE simulation: permeability obtained with high joint stiffness.

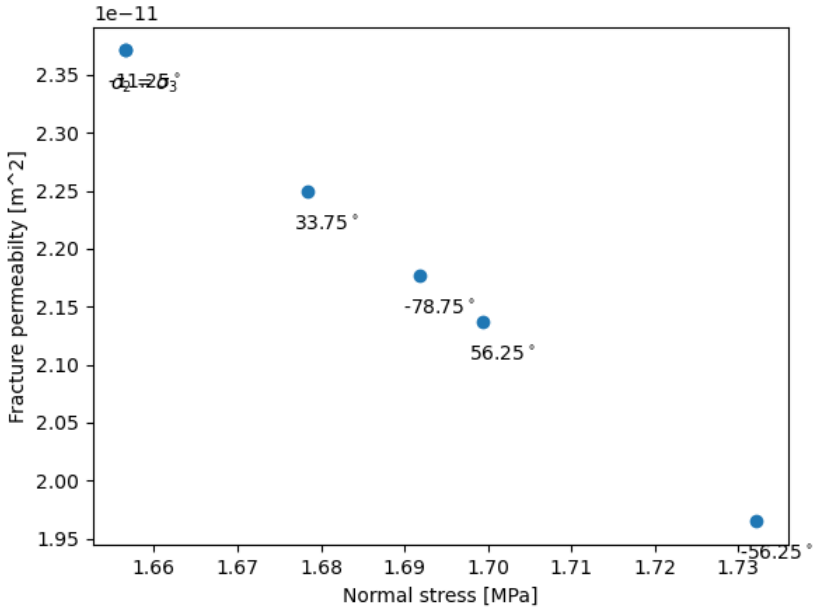

. Figure 37 - OGS#LIE simulation: permeability obtained with low joint stiffness.

Figure 38 shows the distribution of permeability and normal stress in the fracture under one load case. *Figure 39* shows the distribution of stress and strain in the matrix under one load case.

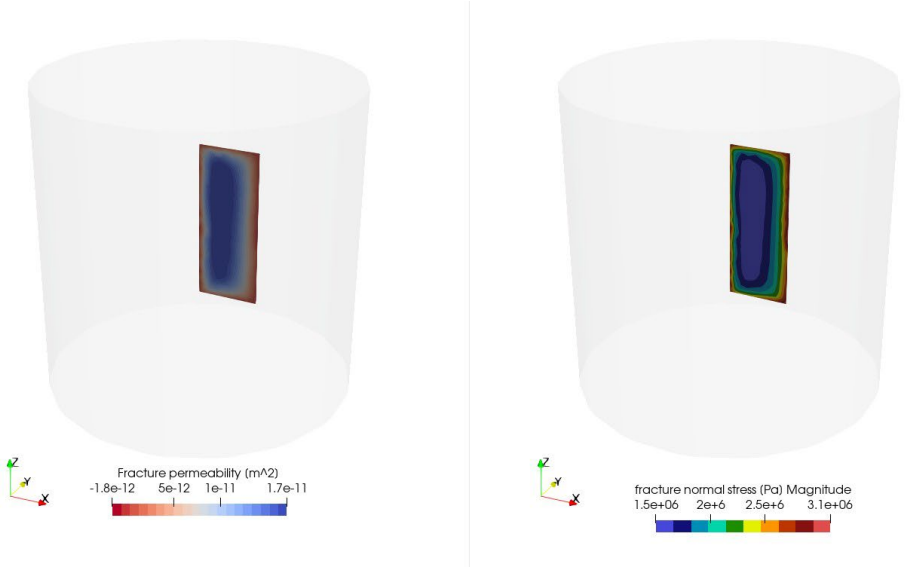

Figure 38 - OGS#LIE simulation: permeability and normal stress distribution in the fracture.

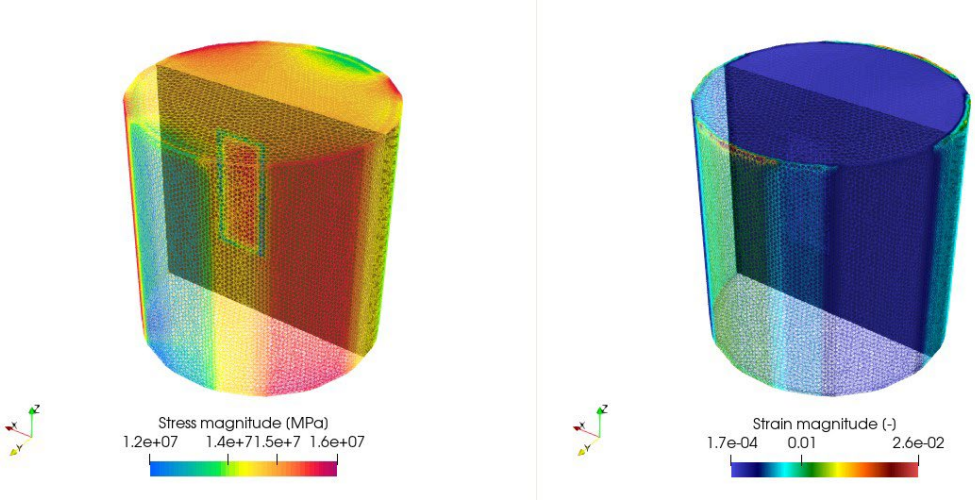

Figure 39 - OGS#LIE simulation: stress and strain distribution in the matrix.

4. Scale Transitions for coupled processes

In the frame of WP DONUT UFZ was pursuing the development and implementation of new numerical methods in OpenGeoSys (OGS-6) to perform multi-scale fracture simulations for THM processes as well as induced by chemical reactions. For simulation of reactive transport processes in strongly heterogeneous media a new numerical scheme has been developed, implemented and applied to FZJ experiments (Lu et al. 2022, Poonoosamy et al. (2022)). The experimental benchmark of FZJ is being used to test the VPF for chemo-mechanical processes.

The main concept for multi-scale simulation relies on the variational phase-field (VPF) method, which is available for THM processes, already, and will be extended for reactive transport processes and chemo-mechanics, respectively (in close cooperation with WP MAGIC). The VPF method for coupled processes has been successfully tested against other approaches and is being applied for experimental analysis of Opalinus clay and crystalline rock samples, respectively. The *Figure 40* shows the upscaling concept which has been realized and demonstrated for the CD-A experiment in Mont Terri.

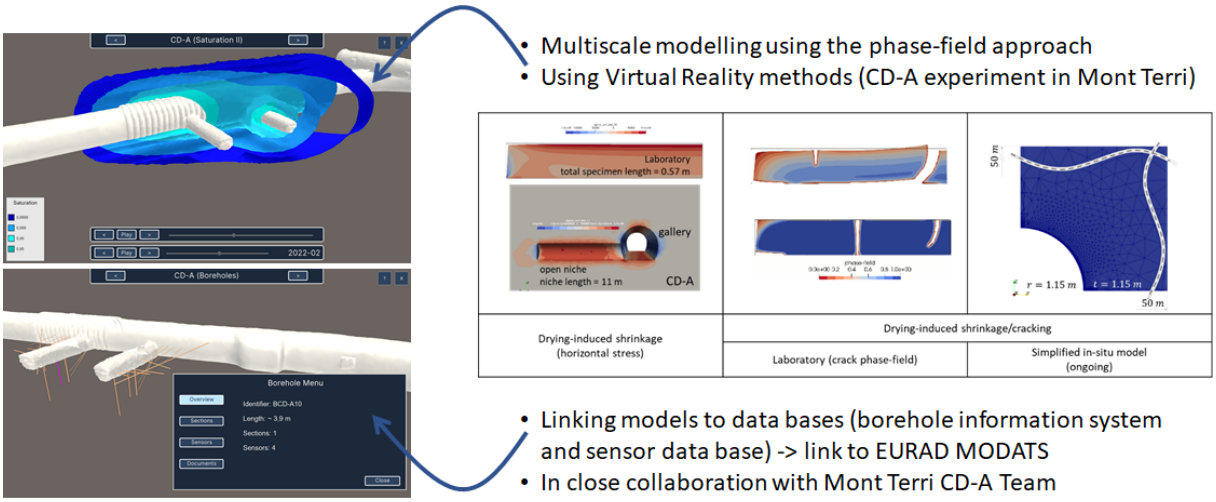

Figure 40 – Scale transition concept and applications to the CD-A experiment in the Underground Research Laboratory URL Mont Terri

The VPF methods have their strengths in scale-independent modelling of fracture processes. On the right are examples of modelling dry cracks at the laboratory scale. The simulation results agree well with the experimental observations. The VPF method could also be successfully used for modelling the CD-A experiment at URL Mont Terri. Thereby, the crack density in the open niche of the experiment could be well modelled (Cajuhi et al. 2023, Ziefle et al. 2022). Furthermore, the simulation results were integrated in the actual context of the URL using virtual reality methods (left side). Furthermore, experimental data can also be accessed interactively via the visual information system. This not only helps in interpreting the data and models and can be used for planning new experiments (Graebling et al. 2022). The VPF method was further developed for anisotropic constitutive models and can thus better reflect the anisotropic geomechanical conditions in Mont Terri (Ziaei-Rad et al. 2023). A summary of the methodological principles and applications of the VPF method in different host rock formations can be found in Kolditz et al. (2023).

5. Summary and Outlook

Despite increasing application of phase-field models for fracture, crack opening recovery has not been carefully investigated. However, since quantitative identification of crack opening is crucial in estimating fracture hydraulic conductivity, here we focused on the quantitative verification of the two most commonly used approaches under different scenarios.

Although the line integral is based on a more robust theoretical background, its actual implementation requires some adaptations in crack normal computation and special treatment near the crack tips. Therefore, we have proposed a practically tractable line integral algorithm instead.

The other proposed method on the level-set function lacked a robust justification for the ad-hoc parameter required in the function. We proposed a value for the parameter to define the level-set from the one-dimensional analysis and verified it under various situations together with the line integral approach.

The major milestone from this study is that we established approaches to recover crack opening, which in practice is in the order of micro meter and is impractical to explicitly discretize over the size of a fracture which spans in meters. On-going efforts are to expand this diffused approach to interface failure and incorporate the crack opening in a tighter coupling with hydro-mechanics followed by hydro-chemo-mechanics coupling in order to predict fracture propagation due to precipitation/dissolution reactions.

Code source

The OpenGeoSys platform has been further developed and applied to EURAD DONUT.

OpenGeoSys (OGS) is a scientific open source project for the development of numerical methods for the simulation of thermo-hydro-mechanical-chemical (THMC) processes in porous and fractured media. Current version is OpenGeoSys-6 which is documented on this page. For information about OpenGeoSys-5, see its dedicated section. OGS has been successfully applied in the fields of regional, contaminant and coastal hydrology, fundamental and geothermal energy systems, geotechnical engineering, energy storage, CO2 sequestration/storage and nuclear waste management and disposal.

Website: https://www.opengeosys.org/

Software repository: https://gitlab.opengeosys.org/

References: https://www.opengeosys.org/publications/

References

Bourdin, B., Francfort, G.A. and Marigo, J.J., 2000. Numerical experiments in revisited brittle fracture. *Journal of the Mechanics and Physics of Solids*, *48*(4), pp.797-826.

Bourdin, B., Chukwudozie, C.P. and Yoshioka, K., 2012, January. A variational approach to the numerical simulation of hydraulic fracturing. In *SPE Annual Technical Conference and Exhibition*. Society of Petroleum EngineersBuchwald, J., Chaudhry, A.A., Yoshioka, K., Kolditz, O., Attinger, S., Nagel, T. (2020): DoE-based history matching for probabilistic uncertainty quantification of thermo-hydro-mechanical processes around heat sources in clay rocks. Int. J. Rock Mech. Min. Sci. 134 , art. 104481

Buchwald, J., Kaiser, S., Kolditz, O., Nagel, T. (2021): Improved predictions of thermal fluid pressurization in hydro-thermal models based on consistent incorporation of thermo-mechanical effects in anisotropic porous media. Int. J. Heat Mass Transf. 172 , art. 121127

Buchwald, J., Kolditz, O., Nagel, T. (2023): Improved DoE-based history matching for probabilistic integrity analysis – a case study of the FE-experiment at Mt. Terri. Reliability Engineering and System Safety, submitted.

Cajuhi, T., Haghighat, N., Maßmann, J., Mollaali, M., Sattari, A.S., Ziaei-Rad, V., Ziefle, G., Nagel, T., Wuttke, F., Yoshioka, K. (2023): Hydro-mechanical effects and cracking in Opalinus clay. In: Kolditz, O., Yoshioka, K., Cajuhi, T., Günther, R.-M., Steeb, H., Wuttke, F., Nagel, T. (eds.) GeomInt—Discontinuities in geosystems from lab to field scale, SpringerBriefs in Earth System Sciences, Springer International Publishing, Cham, p. 7 – 46, https://doi.org/10.1007/978-3-031-26493-1_2

Fraser-Harris, A., Lightbody, A., Edlmann, K., Elphick, S., Couples, G., Sauter, M., McDermott, C., (2020). Sampling and preparation of 200 mm diameter cylindrical rock samples for geomechanical experiments. International Journal of Rock Mechanics and Mining Sciences

Graebling, N., Şen, Ö.O., Bilke, L., Cajuhi, T., Naumov, D., Wang, W., Ziefle, G., Jaeggi, D., Maßmann, J., Scheuermann, G., Kolditz, O., Rink, K. (2022): Prototype of a Virtual Experiment Information System for the Mont Terri Underground Research Laboratory. Front. Earth Sci. 10 , art. 946627

Kolditz, O., Yoshioka, K., Cajuhi, T., Günther, R.-M., Steeb, H., Wuttke, F., Nagel, T. (eds., 2023): GeomInt - Discontinuities in geosystems from lab to field scale SpringerBriefs in Earth System Sciences. Springer International Publishing, Cham, 98 pp.

Kolditz, O., Jacques, D., Claret, F., Bertrand, J., Churakov, S.V., Debayle, C., Diaconu, D., Fuzik, K., Garcia, D., Graebling, N., Grambow, B., Holt, E., Idiart, A., Leira, P., Montoya, V., Niederleithinger, E., Olin, M., Pfingsten, W., Prasianakis, N.I., Rink, K., Samper, J., Szöke, I., Szöke, R., Theodon, L., Wendling, J. (2023): Digitalisation for nuclear waste management: predisposal and disposal Environ. Earth Sci. 82 (1), art. 42

Lee, S., Wheeler, M.F. and Wick, T., 2017. Iterative coupling of flow, geomechanics and adaptive phase-field fracture including level-set crack width approaches. *Journal of Computational and Applied Mathematics*, *314*, pp.40-60.

McDermott, C.I., Fraser-Harris, A., Sauter, M., Couples, G.D., Edlmann, K., Kolditz, O., Lightbody, A., Somerville, J., Wang, W. (2018): New experimental equipment recreating geo-reservoir conditions in large, fractured, porous samples to investigate coupled thermal, hydraulic and polyaxial stress processes. Sci. Rep. 8 , art. 14549 10.1038/s41598-018-32753-z

Mollaali, M., Kolditz, O., Hu, M., Park, C.-H., Park, J.-W., McDermott, C.I., Chittenden, N., Bond, A., Yoon, J.S., Zhou, J., Pan, P.-Z., Liu, H., Hou, W., Lei, H., Zhang, L., Nagel, T., Barsch, M., Wang, W., Nguyen, S., Kwon, S., Lee, C., Yoshioka, K. (2023): Comparative verification of hydro-mechanical

fracture behavior: Task G of international research project DECOVALEX–2023. Int. J. Rock Mech. Min. Sci. 170 , art. 105530

Mollaali, M., Lu, R., Montoya, V., Kolditz, O., Yoshioka, K. (2023): Chemo-Hydro-Mechanical variational phase-field fracture model in cementitious systems. Presentation at the WP MAGIC annual workshop

Radeisen, E., Shao, H., Pitz, M., Hesser, J., Wang, W. (2023): Derivation of heterogeneous material distributions and their sensitivity to HM-coupled two-phase flow models exemplified with the LASGIT experiment. Environ. Earth Sci. 82 (14), art. 347

Yoshioka, K., Parisio, F., Naumov, D., Lu, R., Kolditz, O., Nagel, T. (2019): Comparative verification of discrete and smeared numerical approaches for the simulation of hydraulic fracturing. GEM - Int. J. Geomath. 10 (1), art. 13

Yoshioka, K.; Naumov, D.; Kolditz, O. (2020) On crack opening computation in variational phase-field models for fracture. Computer Methods in Applied Mechanics and Engineering. 369, 1, 113210

You, T., Yoshioka, K. (2023): On poroelastic strain energy degradation in the variational phase-field models for hydraulic fracture. Comput. Meth. Appl. Mech. Eng. 416 , art. 116305

Ziaei-Rad, V., Mollaali, M., Nagel, T., Kolditz, O., Yoshioka, K. (2023): Orthogonal decomposition of anisotropic constitutive models for the phase field approach to fracture. J. Mech. Phys. Solids 171 , art. 105143

Ziefle, G., Cajuhi, T., Graebling, N., Jaeggi, D., Kolditz, O., Kunz, H., Maßmann, J., Rink, K. (2022): Multi-disciplinary investigation of the hydraulic-mechanically driven convergence behavior: CD-A twin niches in the Mont Terri Rock Laboratory during the first year. Geomech. Energy Environ. 31 , art. 100325

Part D: Integral postprocessing of a 3D flow and transport model into a lumped-parameter model as an upscaling method

[1]Landa, J., [1]Hokr, M.

[1]Technical University of Liberec, Czech Republic

The project leading to this application has received funding from the European Union's Horizon 2020 research and innovation programme under grant agreement No 847593.

Abstract

A model of contaminant transport from a repository to the biosphere is one of the major needs of the safety assessment of the geological disposal of the spent nuclear fuel. This work developed a procedure which obtains characteristic data of the transport path by postprocessing the results of 3D flow and tracer transport models. Postprocessing is used to map the entire transport pathway, including the smallest tracer flows, and is therefore called the "integral method". The result is the characteristics of the storage system, such as: transport path length, flow time, total dilution, groundwater flow, longitudinal dispersivity, porosity, etc. These acquired characteristics can be used directly in safety analyses or to narrow the selection of candidate sites. Furthermore, these parameters are used to set up a model with lumped parameters, in this case created in the GoldSim SW environment. Even only one "Pipe" component, after being properly set up, shows almost identical results to the entire 3D model. Based on the results of the 3D model, it is therefore possible to set up a lumped parameter model which accurately simulates the transport path and can perform further calculations of a larger number of radionuclides in repeated runs e.g. with stochastic input data, which would be very laborious or not possible at all with the 3D models. The demonstration calculation uses model problems of 9 candidate site in Czechia, with provided data from previous project of the Radioactive Waste Repository Authority (SÚRAO) – because this work is not a part of the site selection process, the presented sites are anonymized.

Significance Statement

The derived method improves the efficiency of radionuclide transport simulations needed for the repository safety assessment and provides quantitative indicators for comparison of candidate sites as its results.

The idea is explained if considering two generic classes of models: 3D models are motivated to comprise as much of information as possible and be as precise as possible, representing spatial distribution of quantities, but are data and computationally demanding. Contrary, the lumped-parameter models are oriented on simplicity and computational efficiency, which is especially of interest for stochastic computations with many runs – these are represented by quantities defined by a single number for the whole domain (a “pipe” between an inlet and an outlet).

The method processes the results of the 3D model into lumped parameters which serve both as inputs for a simpler model run and as indicators for site comparisons.

Although the lumped-parameter models have been commonly used for the safety assessment in the past, we have shown that such model can be defined by a rigorous procedure from the real hydrogeological configuration projected into the 3D model, in larger extent than with the formerly used particle tracking approaches or even generic conceptualisation.

Table of content

List of figures

List of Tables

Glossary

DGR	deep geological repository
LPM	lumped parameter model
SA	safety assessment
SÚRAO	Radioactive Waste Repository Authority

1. Introduction

The lumped parameter model (LPM) is a term for representing a system as a whole, by a small number of parameters and interaction through e.g. “input” and “output”, typically as ordinary differential equations, as opposite to distributed parameter models, with partial differential equations, which are typical cases of groundwater flow and solute transport models with realistic aquifer geometry and geological heterogeneity, boundary conditions, solved by numerical methods. An example of LPM in contaminant transport and safety assessment context is the compartment concept in GoldSim software (Goldsim, 2018) – the basic “Pipe” object represents 1D channel with advection, diffusion, and other interactions, which homogeneous (lumped) parameters, evaluated by analytical solution. A similar approach is applied in (Chopra et al., 2015).

The purpose of this work is to introduce a procedure to derive a set of lumped parameters (of the geosphere as one of the DGR barriers) from a 3D flow and transport model containing the available hydrogeological knowledge of a particular repository site (*Figure 41*). This would be more general than (SKB, 2015): More potentially relevant parameters are obtained which can have the meaning of either safety/performance indicators, or inputs to “pipe” model of contaminant transport for quick evaluation. This procedure defines the LPM as an upscaling of the original 3D model and contribute to justification of the compartment-like models for SA, which could not be available with the concept of (SKB, 2015) where the processes of dispersion and retention are added to the compartment model separately.

While the concept and technical procedure is generic, the demonstration of use and verification is done with two particular software codes, as representative examples. Flow123d (Březina et al 2021) software, in-house developed open-source code, is used for calculations of 3D models. For derived LPM, the commercial GoldSim software environment is used, with its “pipe” object.

The method is demonstrated on data from Czech DGR candidate site. Although the data were provided directly from the site models elaborated for SÚRAO, the national authority (Říha et al, 2018, Milický et al, 2018), this study is not a part of the official site selection process. Therefore, the sites are used anonymously. The presented indicator values and site ranking have only a meaning of method demonstration and testing.

2. Modelling procedure

2.1 3D model – input data specification

The concept of work assumes, that a standard 3D numerical model of the DGR site is built, including all the hydrogeological and other related data. It includes the use of the digital terrain model, specification of geological heterogeneity (rock type blocks or layers, faults as 2D planar subdomains), definition of the boundary conditions eventually defining the infiltration and drainage areas, river positions, precipitation distribution etc. The interface between the repository volume and the geosphere must be defined in the model mesh or geometry. The models adopted from (Murakami and Ahn, 2011, Milický et al, 2018) represent DGRs in granite and are typically several kilometres large with meshes containing 1-2 million of elements (*Figure 42*).

The examples of Czech candidate sites in Flow123d software are built as follows: The boundaries in the plan view are defined along water divides. The top surface is defined by a digital terrain model with a resolution of 10m. The bottom boundary is defined at 1000 m depth (with respect to the lowest point of the surface). Depth-dependent hydraulic conductivity and porosity are used. Faults are included in the models as 2D vertical structures with assigned transmissivity and porosity. The repository is included in the domain in the 500 m depth as a block of size/dimensions 1.8 km × 1.6 km × 50 m. Zero water and contaminant flow are prescribed on the lateral and bottom boundaries. The top boundary is distinguished

between recharge and discharge boundaries: selected element sides are defined as rivers with prescribed water levels at the surface, while the flow rate of 95-100 mm/a corresponding to a defined share of precipitation is prescribed on the remaining area. Subareas belonging to individual river basins are assigned. Zero contaminant (tracer) concentration is prescribed in the initial condition and in the recharge flow. In the repository volume, constant tracer concentration is prescribed (details below).

We chose three stable chemical elements as tracers: non-sorbing I, medium-sorbing Se, highly sorbing Cs and one non-sorbing radioactive nuclide ^{93}Mo with a half-life of 4000 a. Linear sorption is considered both in the 3D model and in the LPM (K_d concept), the K_d values are 0.0005 m^3/kg for Se and 0.01 m^3/kg for Cs.

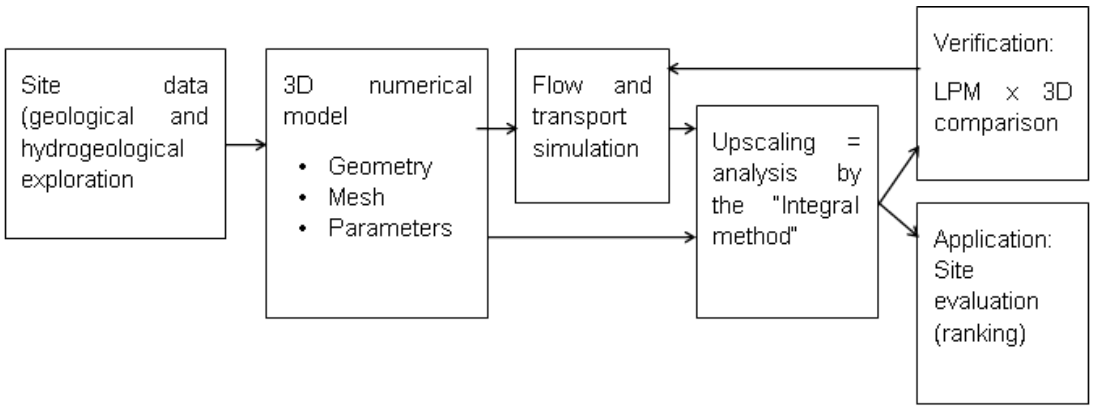

Figure 41 – Workflow of the developed method, with two final steps: the lower is the intended use of the method and presented in section 4 as an example, the upper is only considered as a part of this work for justification and done once.

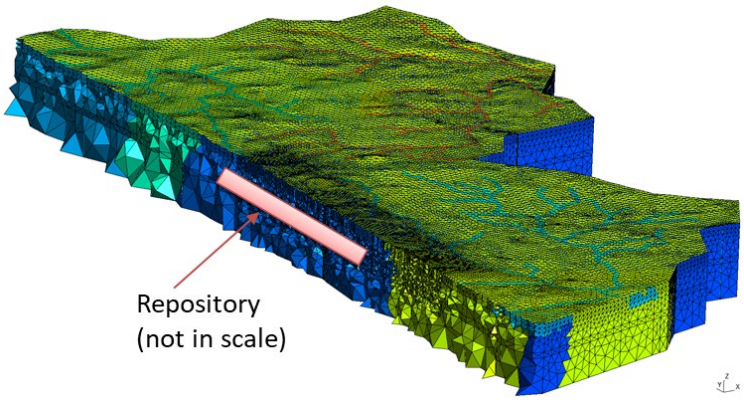

Figure 42 – Example of used site 3D model with meshing (vertical section across the repository area).

2.2 Lumped parameter calculation

The GoldSim component “Pipe" is considered as the LPM case. It represents a fictitious channel of homogeneous permeable medium with defined input and output equivalent to the 1D advection-diffusion equation solution, together with a “junction” at the input, evaluating the prescribed difference of the inflow and outflow rates as dilution with water of zero tracer concentration.

Here, the main parameters, procedures, and related conditions and assumptions are summarized:

- "Geosphere" inflow area. Considering the repository volume is a part of the model domain, the interface repository/geosphere is supposed to be defined in the model input. The area is composed of the element sides between the repository subdomain and the geosphere subdomain with water flux in the respective direction. The procedure could be affected by the backflow described in section 2. A compensation factor of the ratio between the total tracer outflow from the model (asymptotic in time) and the total tracer outflow from the repository (including the backflow), is used for correction.
- Water inflow into the "geosphere" – calculated as a sum of fluxes through the respective element sides, considering an eventual correction for the back-flow.
- Length of the transport pathway. It is calculated by back-tracking the tracer in the mesh. Starting from each outflow contaminated element, a neighbour element with highest tracer flux from is considered the up-stream in the path and the distance of the gravity centres is added to the length. Then the average of all paths is made, weighted by fluxes in the respective outflow elements.
- Contaminated outflow area – sum of element sides based on the above threshold choice.
- Outflow rate of contaminated water – sum of the fluxes through the "contaminated outflow area".
- Volume, porosity of the "path" – sum of element volumes except the back-flow cases, minimum and maximum values along the path.
- Dilution factor is postprocessed as the ratio of the outflow to the inflow values above.

The second part of the parameter set is based on processing of the breakthrough curve, time evolution of the average concentration across the outflow area. The representative tracer travel time between input (repository) and output (biosphere) can be represented by the mean transit time, the first moment of the breakthrough curve, a response to the Dirac tracer input pulse. The dispersion can be related to the second moment of the breakthrough curve *c(t)* – the variance – and consequently, the longitudinal dispersivity is derived.

3. Example of candidate site ordering

For an example of evaluation and selection of a suitable location, we have selected 11 parameters (in general other sets are possible depending on the opinion of an evaluator):

1. inflow – i.e. the flow of groundwater from the repository space into "the "geosphere"
2. dilution on the outflow element with the maximum tracer concentration
3. dilution on the outflow element with the maximum tracer flux
4. mean dilution on the outflow elements in the "contaminated outflow area" (0.99999 share of the total tracer flux)
5. flow time to the outflow element with the maximum concentration
6. flow time to the outflow element with the maximum tracer flux
7. mean flow on the outflow elements in the "contaminated outflow area"
8. flow length to the outflow element with maximum tracer concentration
9. flow length to the outflow element with the maximum flux of the tracer
10. minimum flow length over all elements with a tracer flux, i.e. included in the "contaminated outflow area"
11. mean flow length over the outflow elements in the "contaminated out-flow area"

These are directly given by the values explained above as results of the 3D model upscaling – the integral method. The list represents four quantities which have three variants of values depending on choice of a single outflow element in the numerical discretisation of the 3D model. For indicator 1 (inflow into the geosphere), the lower it is, the more suitable the site is. For all other selected indicators, the higher they are, the more suitable the site.

Table 9 .shows the values of the selected indicators for all 9 tested sites (denoted as I1-I9, representing anonymously the Czech candidate sites) as well as the evaluation according to both selected variants. In this case, the site I1 is the best (best according to the more relevant variant 2) and also the site I3 which is based well according to both evaluation variants. Site I9 is completely unsuitable, sites I6 and I2 also appear to be unsuitable.

However, this assessment should only be taken as an example, the actual site selection must be made by a team of experts, taking into account other indicators and circumstances that cannot be included in these calculations.

id	inflow [m^3/a]	dilution [-]		transport time [a]		length pathway [m]			evaluation			
		max conc. elm.	mean of all elms.	max conc. elm.	mean of all elms.	max conc. elm.	min. length elm.	mean of all elms.	variant 1		variant 2	
									sum indic.	order	sum indic.	order
	1)	2)	4)	5)	7)	8)	10)	11)				
I1	792	545	4 205	11 589	25 478	1 194	995	2 597	37	3	63	1
I2	2 116	15	531	2 059	4 725	1 670	728	2 674	69	6	164	8
I3	1 637	589	4 695	15 785	16 646	4 647	1 012	4 414	25	1	65	2
I4	1 648	69	2 742	14 217	17 406	4 323	650	3 609	51	5	112	5
I5	1 143	153	4 162	49 095	20 071	7 142	762	3 813	29	2	68	3
I6	2 085	44	1 538	1 105	13 096	855	663	2 220	80	8	154	7
I7	4 599	5	202	4 087	4 960	1 604	723	1 734	84	9	201	9
I8	2 369	245	1 416	5 844	18 495	2 490	1 013	3 971	46	4	142	6
I9	729	69	914	11 438	14 788	740	491	1 381	74	7	111	4

Table 9 – *Example of two variants (weight choice explained in the text) of the site evaluation resulting to the order of suitability (selected indicators shown due to limited space: 1,2,4,5,7,8,10,11).*

4. Verification by 3D model and LPM comparison

To demonstrate how efficient if the integral method to estimate the LPM parameters and how well the resulting LPM represent the “real” flow and transport process, both kinds of models are compared in this section. The temporal evolution of the contaminant outflow is used as the compared quantity – model fit criterion. We compare three model results:

- 3D model (Flow123d results as the example)
- LPM with the parameters calculated by the integral method (section 2.2)
- LPM with optimized parameters based on the defined criterion (GoldSim processed)

Optimisation confirms how good the “prediction” is, i.e. checks the relevance of the LPM parameters calculated from integral processing of the 3D model inputs and results. If the optimized LPM, i.e. with parameters minimizing the criterion, provides significantly better fit, it indicates not so efficient method for the upscaling (integral method), and vice versa.

4.1 Example of one sample site processing

The resulting values of the optimized parameters, including the values of the optimization criterion are listed in Table 10. The resulting breakthrough curves of the tracers are shown in *Figure 43*. It can be seen here that even a single optimized component "Pipe" shows results almost identical to the results of the whole 3D model. In this case, however, it should be noted that the defined transport path has an unrealistically large cross-section, of the order of several thousand square km (that is about 1000 times larger than the model area). This is due to the fact that the entire "Pipe" component comprises the flow rate equal to the "outflow" (flow of groundwater from the geo-sphere to the biosphere) which is orders of magnitude larger than a realistic inflow. In order to comply with the transport time, the model leads to a large cross section.

LPM parameter	units	postprocessing	optimized
flow length	m	2596.62	
cross section	km^2	3724	5516
longitudinal dispersivity	m	4707.32	5161.38
porosity of the filling medium	%	0.8774	
Inflow	m^3/a	791.92	
Outflow	m^3/a	3329904	
Dilution	-	4205	
transport time	a	25478	37741
value of relative optimization criterion	%	0.2	0.007

Table 10– *Parameters obtained by the postprocessing and by the optimization, used to set one "Pipe" component. The last row represents the evaluation of fit between the LPM and the 3D model.*

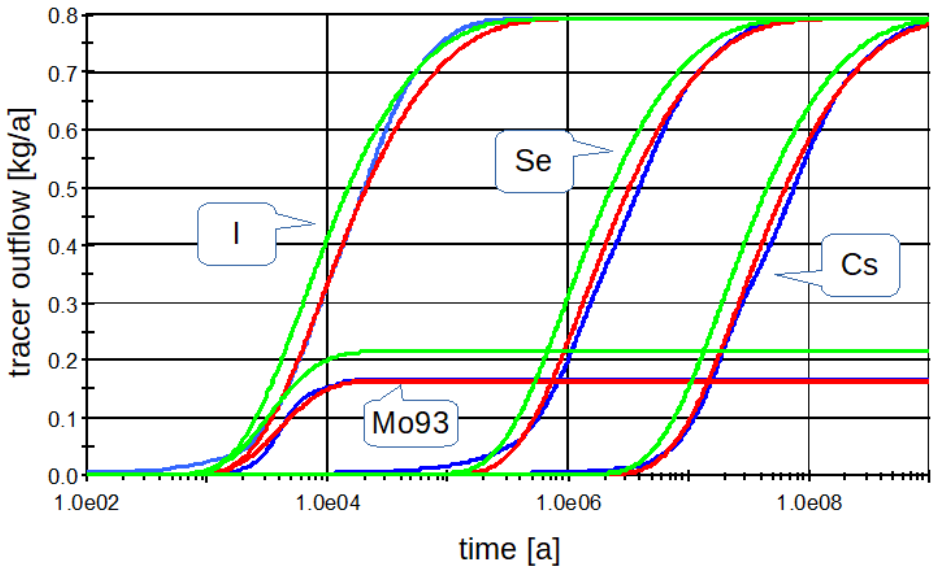

Figure 43 – Comparison of tracer fluxes at site I1 from the Flow123d model (blue curves), from one "Pipe" component set from the postprocessing data (green curves), and from the optimized "Pipe" component (red curves)

4.2 Results of single-pipe model for all sites

The parameters for the "Pipe" were determined for both the non-sorbing tracer (iodine) and as the average of the three stable tracers (iodine, selenium and cesium, referred to as "stable" in *Figure 44*). Furthermore, optimization was performed using GoldSim for the parameters "transport time" and "dispersivity" (referred to as "opt" in the legend). The resulting transport times are slightly lower from the data of the non-sorbing tracer than according to the averages of all three stable tracers. With the help of optimization, the transport times are even higher.

It can therefore be said that the LPM can be set as described above so that it gives values that are sufficiently close to the results of the 3D model, and, if we use the optimized parameters, the difference is small comparable to e.g. numerical errors in the 3D model.

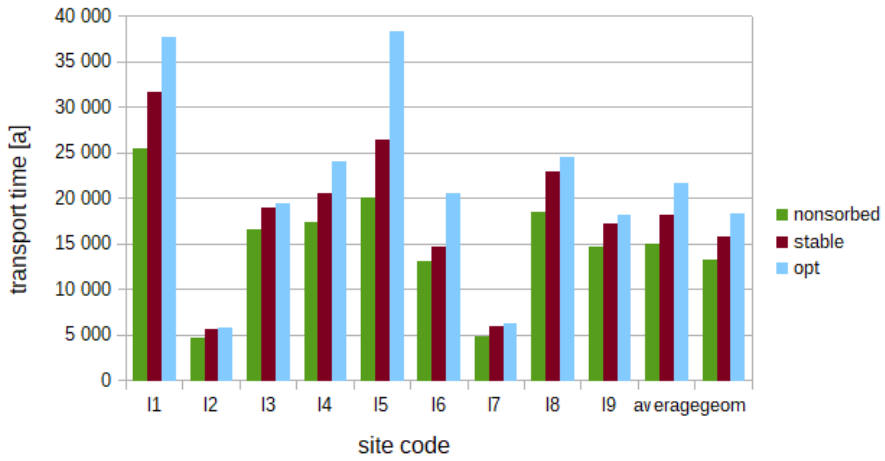

Figure 44 – Tracer travel times for test sites for non-sorbing tracer, average of stable tracers ("stable") and for optimized parameters ("opt"); there are also arithmetic ("average") and geometric ("geom") averages of all sites.

4.3 Results of more complex variants

To get a more physically realistic model, we consider cases with more degrees of freedom. The first case is that the transport path is divided into two parts serially, represented by two model Pipes. The first pipe has the same inflow rate and outflow rate, equal to “inflow to the geo-sphere”, the second pipe has the inflow rate equal to first pipe outflow and the outflow rate equal to the “outflow rate of contaminated water”, i.e. it includes the dilution. To determine the two independent porosity values, one degree of freedom would remain if only the total (average) porosity of the path was available.

It can be said that the variant with the total mean porosity according to the non-sorbing tracer has a slightly worse criterion than the variant with the min-max porosities. Basic optimization, where the dispersivities were optimized for both cascade Pipes independently, does not have a significantly better result than a case when the optimized dispersivity was the same for both Pipes. The worsening of fit compared to the single-pipe model with less parameters is an effect of adding new constraints that ensure both the pipes to have more realistic parameters.

The second case is a model with the three cascade Pipe components so that even more characteristics of the transport path could agree to realistic values, i.e. the flow length, the travel time, the total middle porosity, and the total volume. The relationship for the calculation of the cross section of the middle “Pipe” is based on the assumption that in the first approximation, the transport path has a shape of two consecutive truncated cones with a common base. The constraint equations compose a system of three algebraic equations for three unknown lengths of the individual pipe. It improves the fit but in some cases this procedure results to non-physical values of the parameters.

The third case is a model with parallel pipes, which is motivated by needs of the safety assessment to find the place or area with the highest contamination or to observe the flow into several streams, two or more river basins (catchments), with different concentration or contaminant flux.

Code source

The code is not published. The formulas are published as supplementary material of the paper (Landa and Hokr, 2022). Other codes are used as optional part of the method:

Flow123d https://flow123d.github.io

GoldSim – commercial code https://www.goldsim.com/

References

GoldSim Technology Group LLC, GoldSim Contaminant Transport Module, User's Guide, vol. Contaminant Transport Module Version 7.1, June 2018.

Chopra, M.; Nair, R. N.; Sunny, F.; Sharma, D. N., Migration of radionuclides from a high-level radioactive waste repository in deep geological formations, Environmental Earth Sciences, vol. 73, pp. 1757-1768, 2015.

SKB, Radionuclide transport and dose calculations for the safety assessment SR-PSU, Revised edition,

Murakami, H.; Ahn, J., Development of compartment models with Markov-chain processes for radionuclide transport in repository region, Annals of Nuclear Energy, vol. 38, no. 2-3, pp. 511-519, February-March 2011.

Březina, J.; Stebel, J.; Exner, P.; Flanderka, D.,: Flow123d. http://flow123d.github.com, 2021

Říha J., Uhlík J., Grecká M., Baier J., Černý M., Gvoždík L., Havlová V., Královcová J., Maryška J., Milický M., Polák M., Trpkošová D.,Transport models. Final Report, SÚRAO TZ 324/2018/ENG, 105 p., 2018.

Milický M., Uhlík J, Gvoždík L., Polák M., Černý M., Baier J., Jankovec J., Královcová J., Grecká M., Rukavičková L., Final Detailed 3D Groundwater Flow Models of Potential Deep Repository Sites, Final Report, SURAO TZ 323/2018/ENG, 196 p., 2018.

Landa J., Hokr, M., Contaminant transport from a deep geological repository: lumped parameters derived from 3D hydrogeological model, Energies 2022, 15(18), 6602; https://doi.org/10.3390/en15186602.